Zeitschrift: IABSE reports of the working commissions = Rapports des commissions de travail AIPC = IVBH Berichte der Arbeitskommissionen

Band: 11 (1971)

Rubrik: Introductory reports

RAPPORTS INTRODUCTIFS / EINFÜHRUNGSBERICHTE / INTRODUCTORY REPORTS

Zum Einfluss von verzinkungsabhängigem Vorbeulen auf die Tragfähigkeit von Vollwandträgern

The Influence of Initial Buckling Due to Galvanization on the Ultimate Strength of Plate Girders

L'influence du voilement initial dû à la galvanisation sur la résistance à la ruine des poutres à âme pleine

BÜRGERMEISTER H. STEUP
Prof. Dr.-Ing. habil. Dr.-Ing. habil.
Dresden, DDR

1) Allgemeines

Mit Rücksicht auf eine vereinfachte Herstellungstechnologie werden Vollwandträger teils ohne regelmäßige Anordnung stabilisierender Quersteifen ausgeführt. Solche Lösungen sind besonders gebräuchlich bei Trägern des Leichtbaues mit geringeren Stegblechhöhen. Lediglich im Bereich des Auflagers wird zur Vorbeugung gegen das Krüppeln in stärkerem Maße eine Querversteifung ausgeführt Derartige Träger ohne nennenswerte Querversteifung sind stabilitätsmäßig eingehender zu betrachten, wobei insbesondere durch Verzinkungsvorgänge mit Wärmeeinwirkung zu relativ größeren Vorbeulungen führen können.

2) Beanspruchung von Vollwandträgern durch thermisch bedingte Nachwirkungen

Vollwandträger mit konventionellem Korrosionsschutz sind bei geschweißter Ausführung mit Schweißeigenspannungen behaftet, die einen reduzierenden Einfluß auf die Tragfähigkeit des Systems besitzen. Im Falle sorgfältiger Ausführung der Schweißnähte bei durchdachtem Schweißfolgeplan bleiben die ungewollten Deformationen aus den aktivierten Schweißeigenspannungen gering. Um die Fertigungstoleranzen hinsichtlich der Schweißvorgänge einzuengen, wird nach dem Standard TGL 13510 (Stahlbauten - Herstellung und Abnahme) das Maß der zulässigen Vorbeulungen, als Amplituden gemessen, auf 4 mm begrenzt.
Es ist offensichtlich, daß eine derartig pauschale Festlegung den variablen Einflüssen von Abmessung und Belastung nur in gröberer Weise Rechnung trägt. Hierbei bleibt auch der unterschiedliche Grad von Einspannungsverhältnissen des Stegbleches ohne Einfluß auf die reduzierende Wirkung solcher Vorbeulungen.
Bei dem Korrosionsschutz modernerer Art werden zunehmend auch Vollwandträger größerer Abmessungen tauchverzinkt,wobei nunmehr durch den Verzinkungsvorgang bedingte Vorbeulen größerer Amplituden in Erscheinung treten. Während bei Systemen kleinerer Steg-

höhe (etwa $h_{St} < 50$ cm) die auftretenden Vorbeulungen den vorgeschriebenen Grenzwert bei der Mehrzahl von Trägern nicht erreichen, werden bei größeren Steghöhen oftmals zu große Werte dann beobachtet, wenn das System nicht periodisch querversteift ist.

3) Vorbeulenverteilung bei einem tauchverzinkten Vollwandträger

Bei tauchverzinkten Walzträgern wenigstens mittlerer Steghöhen treten Deformationen durch thermische Effekte (Walzeigenspannungen - Eigenspannungen aus Tauchverzinkung) kaum wahrnehmbar in Erscheinung. Im Gegensatz hierzu werden bei zusammengeschweißten Trägern mit nicht zu starken Stegblechen (Plattenschlankheit etwa oberhalb 80) Vorbeulungen deutlich wahrgenommen. Bild 1 zeigt eine Vorbeulenverteilung für einen längeren Vollwandträger ohne innere Querversteifungen periodischer Art mit den Stegabmessungen 1000 x 10 mm und den Flanschen 300 x 20 mm . Der annähernd periodische Aufbau der Vorbeulungen hinsichtlich des Beulenrasters läßt vermuten, daß eine Eigendruckspannung etwa entsprechend einer mittleren gleichförmigen Achsialbeanspruchung in den einzelnen Abschnitten zur Deformation geführt hat. Auch die verwandten Vorbeulformen einer Reihe in den Abmessungen gleichartiger Vollwandträger sowie verkleinerter Modellträger zeigen deutlich eine gleichartige Entwicklung.

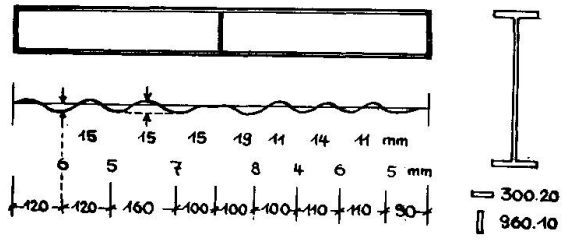

Bild 1

4) Die Wechselbeziehungen Eigenspannungen - Vorbeulungen

Unter Wirkung von Eigendruckspannungen beanspruchte Bereiche eines Systems versuchen sich dem Zwang zur Kompression durch Ausbeulen zu entziehen, wobei der Wechsel vom labilen zum stabilen überkritischen Zustand durch die Steifigkeit des Systems unter Beachtung der Randbedingungen erfolgt. In der Differentialgleichung des Problems sind die Terme mit Eigenspannungsanteilen denen der aus der äußeren Belastung herrührenden Membranspannungen gleichwertig.
Liegen bei gedrungenen Blechen die Beulspannungen in der Nähe der Proportionalitäts-bzw. Fließgrenze, so werden Vorbeulungen bei kleinen Eigenspannungswerten im Verhältnis zur Fließgrenze kaum sichtbar sein. Bilden sich unter dem Zwang der Eigenspannungen Beulfiguren des überkritischen Bereiches aus, so führt dies zu einer Reduktion der örtlichen Membranspannungen infolge der Verkürzung der zu den Beulwellen gehörigen Projektionslängen. Ein gleichzeitiges Auftreten von Eigenspannungen und Beulungen ist also nur beschränkt möglich, das Stegblech entspannt sich selbst.

Das infolge ursprünglicher Eigenspannungseffekte vorgebeulte System stellt aber einen neuen Ausgangszustand für weitere Belastungsaufnahme dar und bestimmt das weitere Tragverhalten in Abhängigkeit der Zuordnung von Vorbeulungen und überkritisch wirksamen Idealbeulen, d.h. bei Vernachlässigung von Vorbeuleffekten.

Sind bei Stegblechen gedrungener Abmessungen nicht aktivierte

Eigenspannungen ohne sichtbare Vorbeulungen wirksam, so nimmt die Eigenspannungsverteilung Einfluß auf das Beulverhalten bei Eintragung äußerer Lasten. Die Berücksichtigung einer üblichen Eigenspannungsverteilung mit ausgeprägten Zugspannungen im Bereich der Schweißnaht zwischen Steg und Gurt intensiviert die Druckspannungen im mittleren Stegblechbereich und wirkt sich daher stabilitätserniedrigend besonders bei Eintragung gleichförmig verteilter Druckkräfte aus. Der Effekt tritt merklich zurück, wenn anstelle gleichförmiger Druckkräfte über den Querschnitt linear veränderliche Kräfte infolge Biegung auftreten.

5) Zwängungen infolge der Wärmebehandlung durch Tauchverzinken

Nach Eintauchen der Trägerelemente in das Verzinkungsbad und Erwärmung auf etwa 450° C wird zunächst eine geringe Kompensation der durch den Schweißvorgang bedingten Eigenspannungen erzielt. (Eine vollständige Spannungs- und Gefügenormalisierung erfolgt bekanntlich erst bei etwa 920° C , ein Spannungsausgleich kann jedoch schon bei etwa 600° C erreicht werden)

Sofern die Abkühlung der Träger bei längerer Zeitdauer gleichmässig erfolgt, könnte dieser eigenspannungsmäßig verbesserte Zustand beibehalten werden. Da die meist verwendeten Technologien zumindest bei Systemen größerer Abmessungen eine derart verlangsamte Abkühlung der wärmekapazitiveren Flansche und der leichter wärmeabgebenden Stegbleche nicht zulassen, kommt es zu Verspannungen. Das rascher abkühlende Stegblech bewirkt plastische Stauchungen der Flansche, welche schließlich bei Abkühlung des Gesamtsystems eine zusammendrückende Wirkung auf den Steg ausüben. Diese Phasen sind in Bild 2 schematisch veranschaulicht.

Die über Randschubkräfte vor allem der Randzonen an den Trägerenden bewirkte Zusammendrückung des Steges bewirkt eine Faltung, die etwa der eines in der Achsenrichtung gedrückten Stegbleches entspricht.

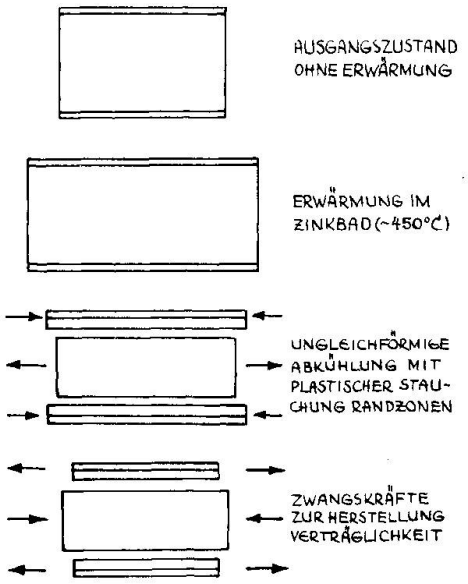

Bild 2

Für den letztgenannten Fall ist die Rasterteilung der Beulfelder bei Annahme gelenkig gelagerter Ränder a/b = 1 und bei Annahme voller Einspannungen 0,67. Gegenüber dem Beulfall mit k = 4 sind wegen der notwendigen stetigen Eigenspannungsverteilung über den Querschnitt die Kontaktzonen des Stegbleches am Flansch noch zugbeansprucht. Im übrigen wird das resultierende Eigenspannungsbild auch aus den schweißbedingten Zwängungen mit ausgeprägten Zugspannungen im Nahtbereich bestimmt. Eine Veränderlichkeit der Eigenspannungen in der Trägerlängsachse kann bei jeweils konstanten Abkühlungszeitintervallen der Stegzone und Flanschzonen bis auf den Randstörungsbereich an den Trägerenden nicht in Erscheinung treten, da auf Grund der Gleichgewichts- und Verträglichkeitsbeziehungen ein Spannungsausgleich der resultierenden Zug- und Druckkräfte nur an den Rändern des Trägers, etwa im Sinne von Endscheiben erfolgt. Dies hat nun zur Folge, daß bei nichtausgebeultem Zustand im inneren Bereich zwi-

schen Steg- und Flanschzonen keine Schubkräfte übertragen werden. Eine theoretisch zufriedenstellende Behandlung des Problems der Eigenspannungsverteilung liegt u.W.noch nicht vor.

Die Verteilung der aus Zwängungen herrührenden Kräfte im einfachsten Fall zweier elastisch dehnbarer aber biegestarrer schubfest verbundener Stäbe zeigt Bild 3.

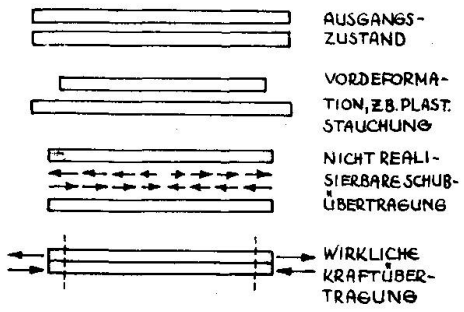

Bild 3

6) Bewertung der Vorbeulungen

Der Vorbeulungseinfluß infolge der Verzinkungseffekte auf das Beulverhalten wird ungünstig sein, wenn eine dominierende Axialbeanspruchung wie etwa bei Rahmenstielen vorliegt. Die Affinität zwischen Vorbeul- und Beulfigur des nicht vordeformierten Grundsystems mit relativ starker Übereinstimmung bewirkt eine Erhöhung der Druckspannungsintensität in den Randzonen des Stegbleches. Bei Voraussetzung scharniergelagerter Ränder entsprechend NAVIERschen Randbedingungen sind diese Verhältnisse hinreichend erforscht und können z.B. durch die mittragenden Breiten formuliert werden.

Im Falle $v_{o,max} / t = 1$ ergibt sich bspw. für die zu einer mittleren Nennspannung führenden Überschreitung $\xi = 1,5$ der fiktiven beulkritischen Spannung σ_k bei Annahme normalspannungsfreier Längsränder das Verhältnis der mittragenden Breite zur Stegblechbreite $b_m / b = 0,53$. Dies bedingt eine Erhöhung der Randspannung um 89 % . Nun sind aber die Gurtungen selbst an der Kraftübertragung beteiligt und bedingen infolge ihrer Kapazität hinsichtlich der Kraftaufnahme eine Zunahme der mittragenden Breite in Abhängigkeit des Gurtaufwandes $f_g = F_g / bt$. Der reziproke Wert des Verhältnisses b_m / b kann als Multiplikator der Randnennspannungen betrachtet werden, welcher die erhöhte Randspannung im Gurt σ_r erzeugt, wobei gilt

$$\frac{b_m}{b} = \frac{\xi \cdot \sigma_k}{\sigma_r} \qquad c = \frac{\sigma_r}{\xi \cdot \sigma_k}$$

Für das ebene Blech kann die erhöhte mittragende Breite bzw. der reduzierte Spannungsmultiplikator c in Abhängigkeit des Gurtaufwandes f_g der Art angesetzt werden

$$c_{red} = 1 + (c - 1) . \beta_g$$

Dabei genügt der Gurteinflußparameter β_g einer Approximation entsprechend

$$\beta_g = 1 / (1 + 2,5 f_g + 1,27 f_g^2)$$

Bei spezieller Berücksichtigung des Vorbeuleneinflusses, zunächst unter Außerachtlassung einer Gurtflächenreduktion wird in verwandter Form

$$c'_{red} = 1 + (c - 1) . \beta_v$$

Eine Annäherung für die Umlagerung der Randspannungen ist mit der Beziehung gegeben

$$\sigma_{red} = 1 + (c - 1) . \beta_g . \beta_v$$

Mit dem Gurtaufwand $f_g = 0,6$ und damit bei Reduktion $\beta_g = 0,34$ wird im vorliegenden Falle des vorgebeulten Trägers erhalten

$$\sigma_r = 1,5 \cdot 0,76 \cdot (1 + 0,89 \cdot 0,34) = 1,48 \text{ Mp/cm}^2 .$$

Die überhöhten Randdruckspannungen werden zu einem Teil durch die wirksamen Eigenspannungen reduziert, jedoch ist zu beachten, daß mit der Entspannung der thermisch bedingten Zwängungen auch die Reaktionszugkräfte in den Randzonen nachlassen. Man wird also vorteilhafterweise auf eine günstige Entlastung der Randbereiche verzichten.

Ist die äußere Belastung vom Fall des mittleren Druckes abweichend, so ist der spannungserhöhende Effekt der zur Achse symmetrischen Vorbeulungen auf Grund beschränkter Affinität zur fiktiven Beulfigur des vorbeulenfreien Zustandes geringer. Bei Orthogonalität der Vorbeulungen kann das System sogar stabilisiert werden. Da die festigkeitsmäßige Beanspruchung solcher Systeme angesichts der relativ höheren Stabilitätsgrenze weitergehend ist, wird man die verzinkungsbedingten Vorbeulungen unter der Bedingung in Kauf nehmen, daß eine zusätzliche Stabilitätsreserve im Spannungsnachweis der Theorie I. bzw. II.Ordnung gegeben ist und darüber hinaus ein vorzeitiges Versagen des für das Stegverhalten fundamentalen Gurtes durch Kippung ausgeschlossen bleibt.

Einer Lockerung der Toleranzbeschränkungen von Vorbeulungen sollte bei steifenlosen Trägern mit Rücksicht auf die angestrebte Vollauslastung und die noch nicht genauer zu erfassende Gefahr von periodischen Deformationswechseln bezüglich der Materialfestigkeit bis zum Abschluß weiterer Untersuchungen nicht zugestimmt werden.

ZUSAMMENFASSUNG

Verzinkte Träger ohne Quersteifen weisen oftmals periodische Vorbeulungen auf, die nach den bislang üblichen Toleranzbeschränkungen unzulässig sind. Es wird eine Bewertung derartiger Imperfektionen vorgenommen, wobei ungeachtet der überkritischen Tragreserven einer Lockerung derartiger Vorschreibungen nur dann zugestimmt wird, wenn die versteifende Gurtung einen erhöhten Sicherheitsspielraum gegen festigkeits- und stabilitätsmässiges Versagen aufweist.

RESUME

Les poutres sans raidisseurs transversaux présentent souvent, après galvanisation, des déformations périodiques qui dépassent les tolérances usuelles. Les auteurs évaluent l'influence de ce cloquage initial; malgré les réserves de résistance post-critiques. un dépassement des tolérances ne peut être accepté que lorsque les membrures présentent une marge de sécurité élevée par rapport à la résistance et à la stabilité.

SUMMARY

Galvanized girders without web stiffeners show often periodical buckles that overstep the usual tolerance limits. Such insufficiancies are examined in the present paper. In spite of the post-critical load reserves an overstepping of these limits will only be accepted if the stiffening flanges show a higher margin of security against resistance and stability dependant break-down.

Analyse du comportement des plaques minces raidies dans le domaine des grands déplacements

Untersuchung des Verhaltens ausgesteifter dünner Bleche im Bereich grosser Verformungen

Analysis of the Behavior of Thin Stiffened Plates in the Large Displacements Range

H. GACHON
Professeur à l'Ecole Nationale Supérieure
d'Arts et Métiers
Paris, France

I - INTRODUCTION

Le présent mémoire développe une méthode d'analyse approchée, par éléments finis, du champ de déplacement des structures très déformables.

Cette méthode trouve, en particulier, son application dans l'étude du comportement non linéaire des plaques minces raidies utilisées sous forme de panneaux constituant les parois de structures légères ou de poutres de grande portée (âme mince élancée, plaque orthotrope, ...).

Cette méthode convient bien à l'analyse du champ de déplacement car, d'une part, elle prend parfaitement bien en compte les conditions aux limites de chargement, de liaisons et d'appuis et, d'autre part, elle est développée de manière à assurer une bonne continuité, non seulement des déplacements, mais aussi des déformations donc des contraintes dans toute la structure.

Les raidisseurs associés à la plaque mince peuvent être orientés suivant des directions parallèles, orthogonales ou obliques (cas des membrures obliques des poutres de hauteur variable) et disposés symétriquement ou non par rapport au plan moyen de la plaque. Ils sont à parois minces et à section droite ouverte ou fermée. Ils sont traités dans certains cas dans le domaine des déplacements finis.

L'introduction d'une déformée initiale de faible courbure aussi bien pour la plaque que pour les raidisseurs et d'un état de contraintes propre dans la plaque permet de compléter la prise en compte des données initiales dans le but d'une bonne simulation du comportement réel de la structure.

Nous avons admis, dans une première étape, une loi de comportement élastique du matériau, nous réservant la possibilité dans une seconde étape de prolonger l'étude dans le domaine plastique.

La méthode des "éléments finis" est développée à partir du théorème des travaux virtuels. Le modèle mathématique ainsi défini est traité sur calculateur numérique automatique - I B M 360-75 - et conduit à l'établissement d'un système non linéaire d'équations exprimant une application de l'espace des déplacements dans l'espace des chargements. La dimension de ces espaces correspond au nombre de degrésde liberté du modèle mathématique adopté. Ce système est résolu par "incrémentation" de la charge, ce qui conduit à mettre en évidence la matrice de raideur tangente de la structure.

Nous présentons ci-après :

- L'équation fondamentale du travail de déformation dans un champ de déplacement virtuel infinitésimal à partir d'un état actuel caractérisé par un champ de déplacement fini, en coordonnées de Lagrange.
- Le choix du champ de déplacement cinématiquement admissible et son application aux plaques minces raidies.
- L'établissement et la méthode de résolution du système d'équations définissant l'application de l'espace des déplacements dans l'espace des chargements du modèle mathématique adopté.
- Un organigramme général du programme développé sur ordinateur - I B M 360-75 - dans le système I C E S (Integrated Civil Engineering System) développé au M I T.

II - TRAVAIL DE DEFORMATION EN DEPLACEMENTS FINIS

(Coordonnées Cartesiennes - Définition de LAGRANGE)

- Etat initial : coordonnées x_i°
- Etat actuel : coordonnées $x_i = x_i^\circ + u_i$

- Transformation virtuelle infinitésimale cinématiquement admissible : δu_i
- Travail de déformation dans la transformation virtuelle

$$\delta \mathcal{C} = \int_{V^\circ} S_{ij} \cdot \delta E_{ij} \cdot DV^\circ$$

avec :

- $\overline{\overline{E}}$: tenseur de la déformation de GREEN

$$E_{ij} = \frac{1}{2}\left[\frac{\partial u_i}{\partial x_j^\circ} + \frac{\partial u_j}{\partial x_i^\circ} + \frac{\partial u_\alpha}{\partial x_i^\circ}\frac{\partial u_\alpha}{\partial x_j^\circ}\right]$$

- $\overline{\overline{S}}$: tenseur de la contrainte de KIRCHHOFF

$$S_{ij} = J \cdot \frac{\partial x_i^\circ}{\partial x_k} \cdot \frac{\partial x_j^\circ}{\partial x_\ell} \cdot \sigma_{k\ell}$$

($\sigma_{k\ell}$:tenseur d'EULER)

- J : Jacobien de la transformation (u_i)

$$J = \det\left|\frac{\partial x_i}{\partial x_j^\circ}\right| = \frac{\rho^\circ}{\rho}$$

- En déformation infinitésimale $J = 1$

et en élasticité :

$$S_{ij} = G_{ijmn} \cdot E_{mn}$$

III - TENSEURS GENERALISES DE LA DEFORMATION ET DE LA CONTRAINTE DANS LES PLAQUES MINCES, EN ELASTICITE

$$(E_{ij})_m \begin{cases} \bar{E}_{xx} = \dfrac{\partial u}{\partial x^\circ} + \dfrac{1}{2}\left(\dfrac{\partial w}{\partial x^\circ}\right)^2 + \dfrac{\partial w^\circ}{\partial x^\circ}\cdot\dfrac{\partial w}{\partial x^\circ} \\ \bar{E}_{yy} = \dfrac{\partial v}{\partial x^\circ} + \dfrac{1}{2}\left(\dfrac{\partial w}{\partial y^\circ}\right)^2 + \dfrac{\partial w^\circ}{\partial y^\circ}\cdot\dfrac{\partial w}{\partial y^\circ} \\ \bar{E}_{xy} = \dfrac{1}{2}\left(\dfrac{\partial u}{\partial y^\circ} + \dfrac{\partial v}{\partial x^\circ} + \dfrac{\partial w}{\partial x^\circ}\cdot\dfrac{\partial w}{\partial y^\circ} + \dfrac{\partial w^\circ}{\partial x^\circ}\cdot\dfrac{\partial w}{\partial y^\circ} + \dfrac{\partial w^\circ}{\partial y^\circ}\cdot\dfrac{\partial w}{\partial x^\circ}\right) = \bar{E}_{yx} \end{cases}$$

$$(\chi_{ij}) \begin{cases} \chi_{xx} = \dfrac{\partial^2 w}{\partial x^{\circ 2}} \\ \chi_{yy} = \dfrac{\partial^2 w}{\partial y^{\circ 2}} \\ \chi_{xy} = \dfrac{\partial^2 w}{\partial x^\circ \partial y^\circ} = \chi_{yx} \end{cases}$$

$$(S_{ij})_m \begin{cases} N_{xx} = \dfrac{E.h}{1-\nu^2}\cdot\left(\bar{E}_{xx} + \nu.\bar{E}_{yy}\right) + N^\circ_{xx} \\ N_{yy} = \dfrac{E.h}{1-\nu^2}\cdot\left(\bar{E}_{yy} + \nu.\bar{E}_{xx}\right) + N^\circ_{yy} \\ N_{xy} = \dfrac{E\,h}{1-\nu^2}\cdot\dfrac{1-\nu}{2}\cdot\bar{E}_{xy} + N^\circ_{xy} \end{cases}$$

$$(S_{ij})_f \begin{cases} M_{xx} = D.(\chi_{xx} + \nu.\chi_{yy}) \\ M_{yy} = D.(\chi_{yy} + \nu.\chi_{xx}) \\ M_{xy} = D.(1-\nu).\chi_{xy} \end{cases} \qquad D = \frac{E.h^3}{12(1-\nu^2)}$$

- Travail de déformation dans une transformation virtuelle (δu_i)

$$(\delta \mathcal{C})_{plaque} = \int_{S^\circ} (N_{ij}.\delta\bar{E}_{ij} + M_{ij}.\delta\chi_{ij}).dx^\circ.dy^\circ$$

IV - CHAMP DE DEPLACEMENT DANS UN RAIDISSEUR

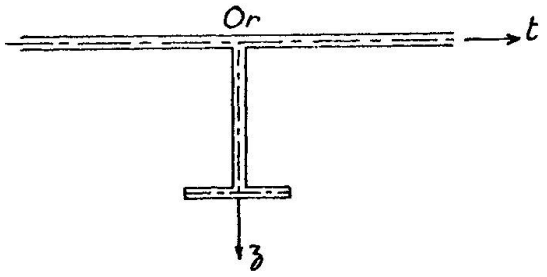

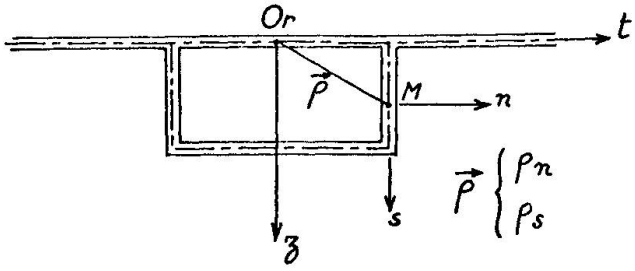

- En O suivant Ox , Oy , Oz $\quad u \quad , v \quad , w$

  suivant Or , Ot , Oz $\quad u_r \quad , u_t \quad , w \quad , \theta$

- En M suivant M_t , M_z

$$. \; u_t(r,s) = u_t(r) - \theta(r).\, z(s)$$
$$. \; w(r,s) = w(r) + \theta(r).\, t(s)$$

suivant M_s , M_n

$$u_s(r,s) = u_t(r).\frac{dt(s)}{ds} + w(r).\frac{dz(s)}{ds} + \theta(r).\rho_n(s)$$

$$u_n(r,s) = u_t(r).\frac{dz(s)}{ds} - w(r).\frac{dt(s)}{ds} - \theta(r).\rho_s(s)$$

suivant M_r :

$$u_r(r,s) = u_r(r) - \frac{\partial u_t(r)}{\partial r}.\, t(s) - \frac{\partial w(r)}{\partial r}.\, z(s) - \frac{\partial \theta(r)}{\partial r}.\, \Omega(s)$$

avec

$$\Omega(s) = \omega(s) - \frac{\omega_o}{\Gamma_o}.\,\Gamma(s)$$

$$\cdot \; \omega(s) = \int_0^s \rho_n(s).\, ds \qquad \Gamma(s) = \int_0^s \frac{ds}{e}$$

$$\left.\begin{aligned} \omega_o &= \oint \rho_n(s).\, ds \\ \Gamma_o &= \oint \frac{ds}{e} \end{aligned}\right\} \text{ en section droite fermée}$$

V - CHAMP DE DEFORMATION ET DE CONTRAINTE DANS UN RAIDISSEUR EN ELASTICITE

$$(E_{ij})_m \begin{cases} E_{rr}(r,s) = \dfrac{\partial u_r(r)}{\partial r} - \dfrac{\partial^2 u_t(r)}{\partial r^2}\cdot t(s) - \dfrac{\partial^2 w(r)}{\partial r^2}\cdot z(s) - \dfrac{\partial^2 \theta(r)}{\partial r^2}\cdot \Omega(s) \\ \quad + \dfrac{1}{2}\left[\dfrac{\partial w(r)}{\partial r} + \dfrac{\partial \theta(r)}{\partial r}\cdot t(s)\right]^2 + \dfrac{1}{2}\cdot\left[\dfrac{\partial u_t(r)}{\partial r} - \dfrac{\partial \theta(r)}{\partial r}\cdot z(s)\right]^2 \\ \quad + \left[\dfrac{\partial w^\circ(r)}{\partial r} + \dfrac{\partial \theta^\circ(r)}{\partial r}\cdot t(s)\right]\left[\dfrac{\partial w(r)}{\partial r} + \dfrac{\partial \theta(r)}{\partial r}\cdot t(s)\right] + \left[\dfrac{\partial u_t^\circ(r)}{\partial r} - \dfrac{\partial \theta^\circ(r)}{\partial r}\cdot z(s)\right]\left[\dfrac{\partial u_t(r)}{\partial r} - \dfrac{\partial \theta(r)}{\partial r}\cdot z(s)\right] \\ \cdot \left[E_{rs}(r,s)\right]_{torsion} = \dfrac{\omega_o}{\Gamma_o}\cdot\dfrac{d\theta(r)}{dr} \quad \text{(section droite fermée en torsion uniforme)} \end{cases}$$

$$(S_{ij})_m \begin{cases} S_{rr}(r,s) = E\ E_{rr}(r,s) \\ S_{rs}(r,s) = \dfrac{E}{2(1+\nu)}\ E_{rs}(r,s) \end{cases}$$

Travail de déformation dans une transformation virtuelle (δu_i)

$$(\delta \mathcal{C})_{raidisseur} = E \left\{ \int_0^c \left[\int_0^\ell \left[E_{rr}\cdot \delta E_{rr} + \frac{e^2}{12}\cdot\frac{d^2u_n}{dr^2}\cdot\delta\left(\frac{d^2u_n}{dr^2}\right)\right] e\,ds \right.\right.$$
$$\left.\left. + \frac{1}{2(1+\nu)}\cdot\left(\frac{\omega_o^2}{\Gamma_o} + J\right)\cdot\frac{d\theta}{dr}\ \delta\left(\frac{d\theta}{dr}\right) dr \right] \right\}$$

avec $J = \dfrac{1}{3}\cdot\int_0^\ell e^3\,ds$

VI - EQUATION FONDAMENTALE DE L'EQUILIBRE

(Théorème des Travaux Virtuels)

- La transformation virtuelle δu_i est cinématiquement admissible -

$$\int_{V^\circ} S_{ij} \cdot \delta E_{ij} \cdot dV^\circ = \int_{V^\circ} \rho^\circ F_i^\circ \cdot \delta u_i \cdot dV^\circ + \int_{S^\circ} T_i^\circ \cdot \delta u_i \cdot dS^\circ$$

F_i° : force massique rapportée à l'état initial

T_i° : force de contact par unité de surface, rapportée à l'état initial

Dans le cas des plaques raidies

$$(\delta \mathcal{C})_{plaque} + (\delta \mathcal{C})_{raidisseurs} = \int_{S^\circ} p_i^\circ \cdot \delta u_i \cdot dx^\circ \cdot dy^\circ$$

p_i° : force active rapportée au plan moyen de la plaque dans son état initial.

VII - FORMULATION MATRICIELLE DU CHAMP DE DEPLACEMENT DANS UN ELEMENT DU MAILLAGE

- Champ de déplacement dans l'état actuel :

$$u_i^k(x^\circ) = \left\{\widetilde{\varphi(x^\circ)}\right\}_i \cdot [A]^k \cdot \{D\}$$

- Transformation virtuelle cinématiquement admissible :

$$\delta u_i^k(x^\circ) = \left\{\widetilde{\varphi(x^\circ)}\right\}_i \cdot [A]^k \cdot \left\{\frac{\partial D}{\partial D_\ell}\right\}$$

où :

$$D_\ell \in [A]^k\{D\} = \{D\}^k \subset \{D\}$$

VIII - CHAMP DE DEFORMATION DE FLEXION-TORSION

$\cdot f_1(\xi) = 1 - 3\xi^2 + 2\xi^3 \qquad (f_1^{IV}(\xi) = 0)$

$\cdot g_1(\xi) = 3\xi^2 - 2\xi^3 \qquad (g_1^{IV}(\xi) = 0)$

$\cdot f_2(\xi) = \xi - 2\xi^2 + \xi^3 \qquad (f_2^{IV}(\xi) = 0)$

$\cdot g_2(\xi) = -\xi^2 + \xi^3 \qquad (g_2^{IV}(\xi) = 0)$

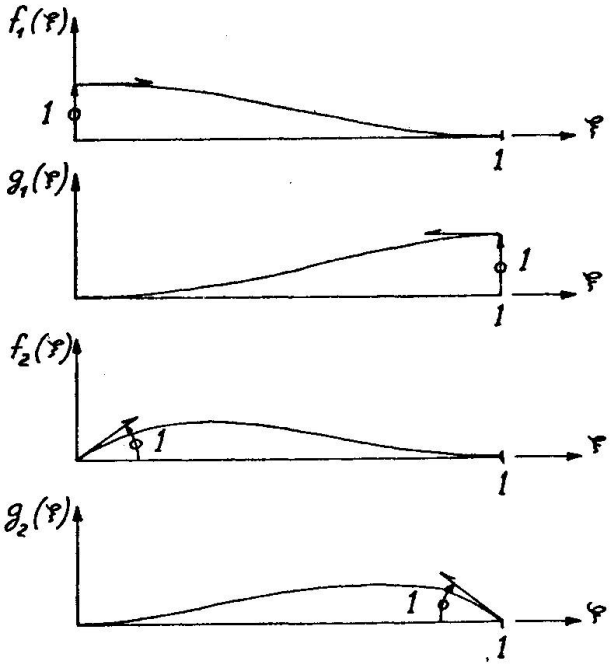

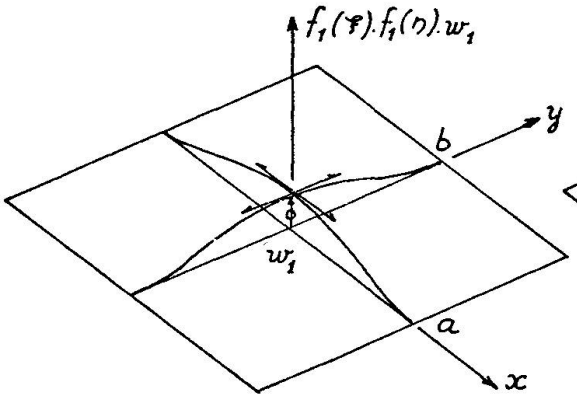

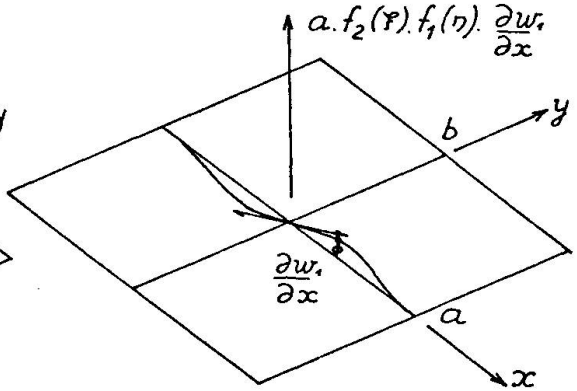

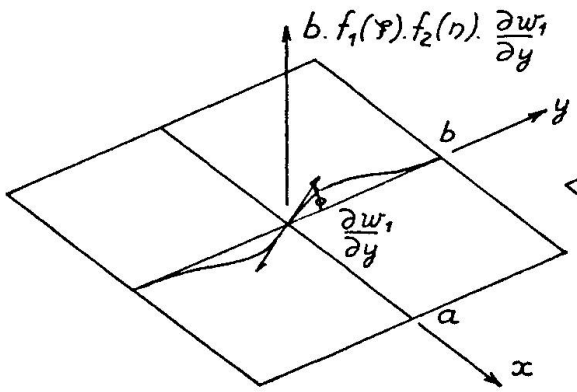

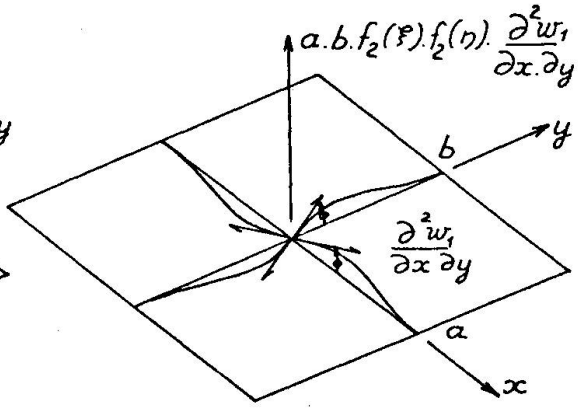

avec $\xi = \frac{x}{a}$ et $\eta = \frac{y}{b}$

IX - CHAMP DE DEPLACEMENT DANS UN ELEMENT DE PLAQUE

$$u_i^k(x^\circ, y^\circ) = \{\widetilde{\varphi(x^\circ, y^\circ)}\} \cdot \{D_i\}^k \qquad (i = 1, 2, 3)$$

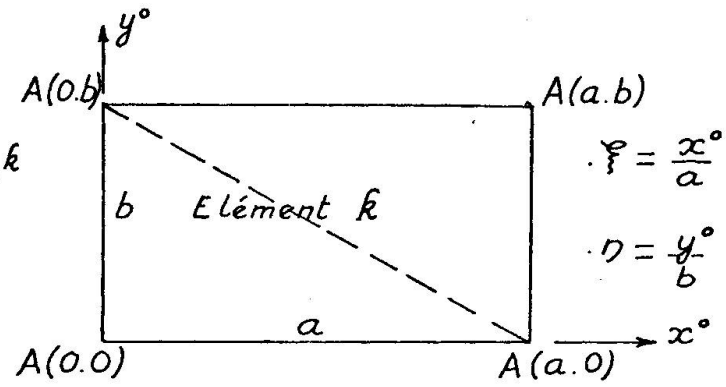

$$\xi = \frac{x^\circ}{a}$$

$$\eta = \frac{y^\circ}{b}$$

$$u_i^k(x, y) = \left\{ \widetilde{\begin{array}{l} f_1(\xi).f_1(\eta) \\ a.f_2(\xi).f_1(\eta) \\ b.f_1(\xi).f_2(\eta) \\ a.b.f_2(\xi).f_2(\eta) \\ g_1(\xi).f_1(\eta) \\ a.g_2(\xi).f_1(\eta) \\ b.g_1(\xi).f_2(\eta) \\ a.b.g_2(\xi).f_2(\eta) \\ g_1(\xi).g_1(\eta) \\ a.g_2(\xi).g_1(\eta) \\ b.g_1(\xi).g_2(\eta) \\ a.b.g_2(\xi).g_2(\eta) \\ f_1(\xi).g_1(\eta) \\ a.f_2(\xi).g_1(\eta) \\ b.f_1(\xi).g_2(\eta) \\ a.b.f_2(\xi).g_2(\eta) \end{array}} \right\} \cdot \left\{ \begin{array}{l} \left\{ \begin{array}{l} u_i \\ u_{i,x} \\ u_{i,y} \\ u_{i,xy} \end{array} \right\} 0.0 \\ \left\{ \begin{array}{l} u_i \\ u_{i,x} \\ u_{i,y} \\ u_{i,xy} \end{array} \right\} a.0 \\ \left\{ \begin{array}{l} u_i \\ u_{i,x} \\ u_{i,y} \\ u_{i,xy} \end{array} \right\} a.b \\ \left\{ \begin{array}{l} u_i \\ u_{i,x} \\ u_{i,y} \\ u_{i,xy} \end{array} \right\} 0.b \end{array} \right\}^k .$$

$$(i = 1.2.3)$$

X - CHAMP DE DEPLACEMENT DANS UN RADISSEUR (r).

$$\{\Delta_1\}_O = \begin{Bmatrix} u_r(0) \\ u_{r,r}(0) \end{Bmatrix} \qquad \{\Delta_1\}_C = \begin{Bmatrix} u_r(c) \\ u_{r,r}(c) \end{Bmatrix}$$

$$\{\Delta_2\}_O = \begin{Bmatrix} u_t(0) \\ u_{t,r}(0) \end{Bmatrix} \qquad \{\Delta_2\}_C = \begin{Bmatrix} u_t(c) \\ u_{t,r}(c) \end{Bmatrix}$$

$$\{\Delta_3\}_O = \begin{Bmatrix} w(0) \\ w_{,r}(0) \end{Bmatrix} \qquad \{\Delta_3\}_C = \begin{Bmatrix} w(c) \\ w_{,r}(c) \end{Bmatrix}$$

$$\{\Delta_4\}_O = \begin{Bmatrix} \theta(0) \\ \theta_{,r}(0) \end{Bmatrix} \qquad \{\Delta_4\}_C = \begin{Bmatrix} \theta(c) \\ \theta_{,r}(c) \end{Bmatrix}$$

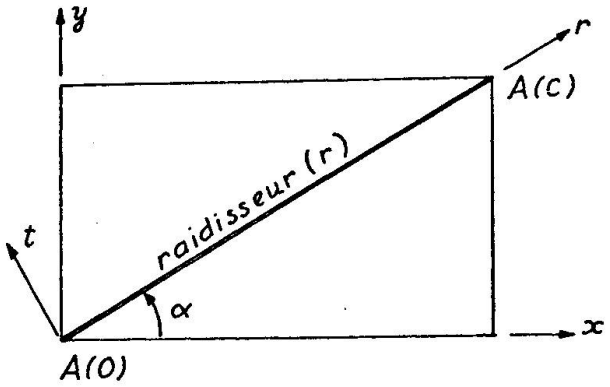

Posons $\{\Delta_i\}^r = \begin{Bmatrix} \{\Delta_i\}_O \\ \{\Delta_i\}_C \end{Bmatrix}$ composantes de déplacement de $A(0)$ et $A(C)$ dans (r, t, z)

- Champ de déplacement dans le système (r, t, z)

$$u_i^r(r) = \{\widetilde{\rho(r)}\}\{\Delta_i\}^r \qquad (u_i \equiv u_r, u_t, w, \theta)$$

$$\{\widetilde{\rho(r)}\} = | f_1(\rho), c.f_2(\rho), g_1(\rho), c.g_2(\rho) | \qquad (\rho = \frac{r}{c})$$

- Matrices de passage :

$$\cdot \{\Delta_1\}_{O \text{ ou } C} = [T_r] \cdot \begin{Bmatrix} \{D_1\} \\ \{D_2\} \end{Bmatrix}_{O \text{ ou } C}$$

$$\cdot \{\Delta_2\}_{O \text{ ou } C} = [T_t] \cdot \begin{Bmatrix} \{D_1\} \\ \{D_2\} \end{Bmatrix}_{O \text{ ou } C}$$

$$\cdot \{\Delta_3\}_{O \text{ ou } C} = [T_w] \cdot \{D_3\}_{O \text{ ou } C}$$

$$\cdot \{\Delta_4\}_{O \text{ ou } C} = [T_\theta] \cdot \{D_3\}_{O \text{ ou } C}$$

avec $\{D_i\}_O = \begin{Bmatrix} u_i(0) \\ u_{i,x}(0) \\ u_{i,y}(0) \\ u_{i,xy}(0) \end{Bmatrix}$ $(i = 1.2.3)$

Composantes de déplacement de $A(0)$ dans (x, y, z)

XI - RESOLUTION DU SYSTEME NON LINEAIRE

$$F(D) = P$$

Developpons :

$$\left[[K_0] + [K_1(D)] + [K_2(D^2)]\right] \{D\} = \{P\}$$

ou

$$[K(D)]\{D\} = \{P\}$$

- Méthode de résolution selon NEWTON -

$$F(D^{(n)}) + \frac{\partial F(D^{(n)})}{\partial D_i} \Delta D_i^{(n+1)} = P$$

$$\left\{\left[\frac{\partial K}{\partial D_i}\right]^n \{D\}^n + [K]^n \left\{\frac{\partial D}{\partial D_i}\right\}^n\right\} \Delta D_i^{n+1} = \{P\} - [K(D)]^n \{D\}^n$$

$$\left(\frac{\partial K_{\ell j} \cdot D_j}{\partial D_i} + K_{\ell i}\right)^n \Delta D_i^{n+1} \quad \text{avec} \quad (\Delta D_i^{n+1} \to 0)_{n+1 \to \infty}$$

$$R_{\ell i} \quad \text{avec} \quad R_{\ell i} = R_{i\ell} \in [R]$$

$$[R(D)]^n \{\Delta D\}^{n+1} = \{P\} - [K(D)]^n \{D\}^n$$

- Méthode de résolution par petits accroissements de charge

$$[R(D)]^n \{\Delta D\}^{n+1} = \{\Delta P\}^{n+1}$$

$[R(D)]^n$: matrice de raideur tangente de la structure dans un état $(P, D)^n$

XII - PROPRIETES DE LA MATRICE DE RAIDEUR TANGENTE

1 - La matrice $[R]$ est symétrique réelle : $[R]_{ii} = \widetilde{[R]}_{ii}$, $[R]_{ij} = \widetilde{[R]}_{ji}$

$$\begin{bmatrix} \cdots & \cdots & \cdots & \cdots \\ [R]_{ii} & [R]_{ij} & [R]_{ik} & [R]_{il} \\ [R]_{ji} & [R]_{jj} & [R]_{jk} & [R]_{jl} \\ [R]_{ki} & [R]_{kj} & [R]_{kk} & [R]_{kl} \\ [R]_{li} & [R]_{lj} & [R]_{lk} & [R]_{ll} \\ \cdots & \cdots & \cdots & \cdots \end{bmatrix} \begin{Bmatrix} \vdots \\ \{\Delta D\}_i \\ \{\Delta D\}_j \\ \{\Delta D\}_k \\ \{\Delta D\}_l \\ \vdots \end{Bmatrix} = \begin{Bmatrix} \vdots \\ \{\Delta P\}_i \\ \{\Delta P\}_j \\ \{\Delta P\}_k \\ \{\Delta P\}_l \\ \vdots \end{Bmatrix}$$

2 - Critère général de stabilité :

$$\{\widetilde{\Delta D^*}\}\,[R]\,\{\Delta D^*\} > 0 \qquad \forall\ \overrightarrow{\Delta D^*} \qquad \longrightarrow \qquad \det [R] > 0$$

ou plus précisément, les valeurs propres $\lambda_i > 0$, $\forall i$.

La matrice $[R]$ est définie positive -

3 - Seuil de bifurcation d'une plaque idéale : $\det [R]_{ww} = 0$

$$\begin{bmatrix} [R]_{uu} & [R]_{uv} & [R]_{uw} \\ [R]_{vu} & [R]_{vv} & [R]_{vw} \\ [R]_{wu} & [R]_{wv} & [R]_{ww} \end{bmatrix} \begin{Bmatrix} \{\Delta D\}_u \\ \{\Delta D\}_v \\ \{\Delta D\}_w \end{Bmatrix} = \begin{Bmatrix} \{\Delta P\}_u \\ \{\Delta P\}_v \\ \{\Delta P\}_w \end{Bmatrix}$$

XIII - ORGANIGRAMME GENERAL

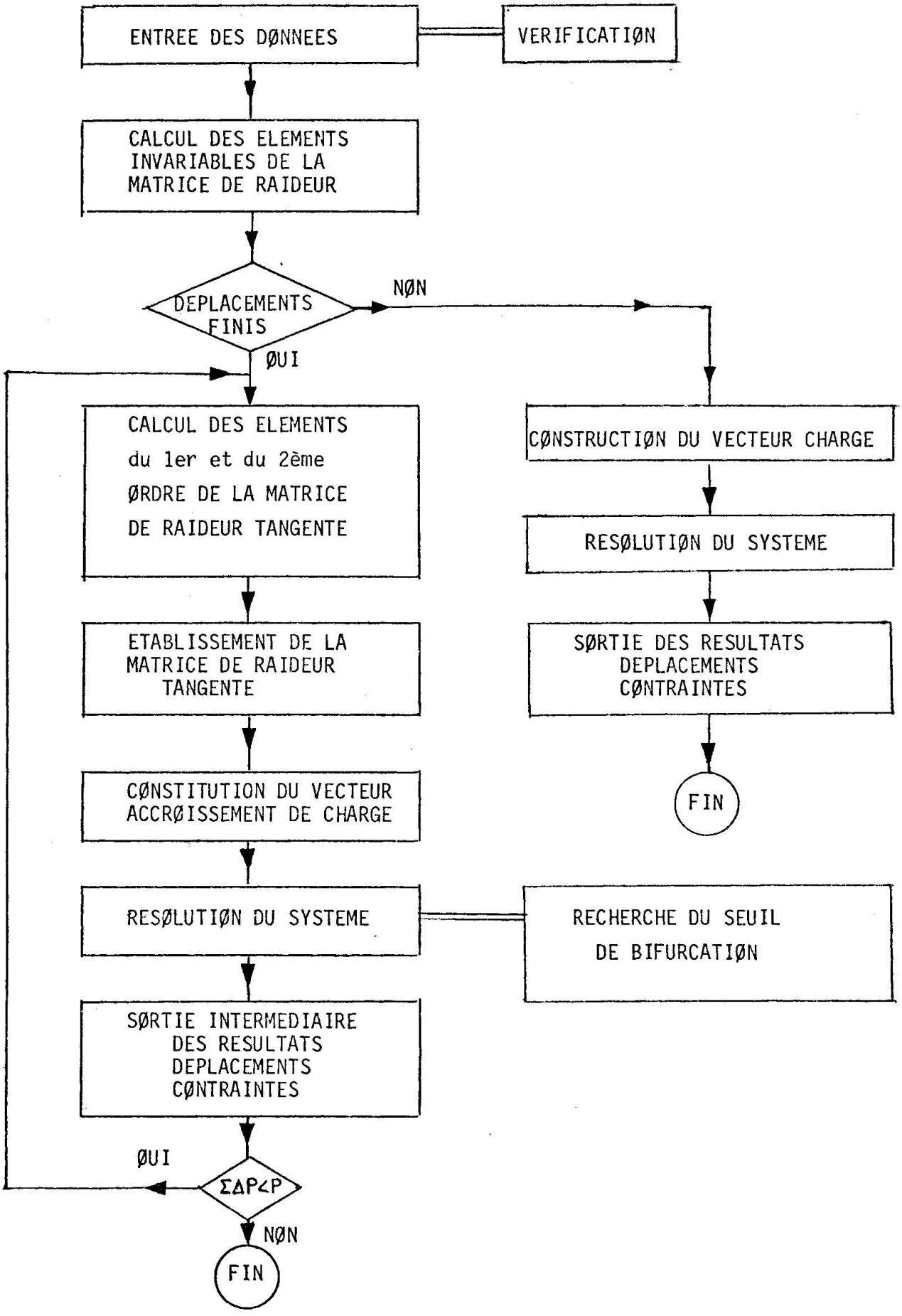

CONCLUSION

Cette méthode de calcul s'avère satisfaisante sur le plan théorique et permet une bonne approche de l'étude du comportement des structures à plaques minces raidies dans le domaine des petits déplacements et dans celui des déplacements finis.

La définition du champ de déplacement dans le modèle mathématique adopté est suffisamment complète pour permettre un maillage de faible densité de la structure, sans altérer de manière sensible la solution. Une moins bonne définition aurait conduit, pour une même précision, à un modèle mathématique différent, présentant un maillage plus dense et un nombre de degré de liberté plus élevé. Dans la solution adoptée, la constitution de la matrice de raideur tangente demande plus de temps, car chacun des éléments est une combinaison de termes constants, de termes du premier degré et de termes du second degré du déplacement dans l'état actuel. La triangularisation de la matrice s'effectue sans difficulté et avec une bonne précision étant donné sa dimension relativement faible.

Le nombre de petits accroissements qu'il convient de donner à la charge pour décrire les différents états de la structure dépend de sa réponse.
La non linéarité de cette réponse dépend de deux facteurs :

- les déplacements sont finis,
- la loi de comportement du matériau n'est pas linéaire.

Cette étude permet de rendre compte, dans une structure donnée, de l'état de déformation à toutes les étapes de chargement et de suivre, par conséquent, une loi de chargement quelconque. Nous pouvons donc adopter un critère de dimensionnement basé soit sur la contrainte limite, soit sur la déformation limite.

Il est à noter qu'une certaine forme d'instabilité est observée expérimentalement et se manifeste à certains niveaux de chargement par un claquement traduisant le passage brutal du panneau d'une configuration d'équilibre instable à une autre configuration d'équilibre stable cette fois et nettement différente de la précédente. Ce phénomène se produit toujours pour un niveau de chargement situé au delà du seuil de bifurcation et il est lié essentiellement à l'état

de déformation initiale du panneau. En effet, un panneau tend, dans son état ultime, vers une configuration indépendante de son état de déformation initiale. Si celles-ci sont d'allure nettement différentes, le panneau, au cours du chargement, doit franchir un certain seuil dit de "claquement" qui marque une profonde modification de la configuration actuelle du panneau, pour lui donner l'allure de la configuration ultime vers laquelle il tend. La difficulté de rendre compte théoriquement d'un pareil phénomène est liée à une ignorance de sa cause essentielle, c'est-à-dire de l'état initial de déformation et aussi sans doute de l'état de contrainte propre de la structure.

L'incidence que peut avoir l'apparition du phénomène de "claquement" sur la résistance locale d'un panneau est sans doute très sensible dans le cas d'un chargement repété de la structure. En effet, dans la zone où cette instabilité de forme se produit, l'effet de fatigue est plus accentué car il correspond à une action cyclique alternée des déformations.

Nous pensons développer, en élasticité, une méthode de résolution des systèmes non linéaires selon Newton, ce qui nous permettra de rechercher, sans suivre la loi de chargement, un état de déformation correspondant à un niveau de chargement donné.

Nous avons réalisé, pour tester la méthode, des essais de chargement suivant des lois bien établies, comportant un nombre limité de cycles de chargement, engendrant dans diverses structures à parois minces des types de sollicitations variées.

Nous projetons, dans un avenir très proche, de poursuivre cette recherche en développant un programme d'essais de fatigue sur un large échantillonnage de structures.

La réalisation complète du programme de calcul, sur ordinateur IBM 360-75, a été prise en charge par le C.T.I.C.M. (Centre Technique Industriel de la Construction Métallique). Ce programme réalisé par Monsieur Barraco, Ingénieur de Recherche, est actuellement au stade expérimental et doit être développé prochainement dans le domaine plastique et dans l'étude des petits mouvements autour d'une position d'équilibre déformée.

Nous présenterons dans une annexe à ce mémoire, l'étude comparée des résultats des essais en laboratoire et de la simulation sur ordinateur, portant sur diverses structures ayant servi de tests à la méthode.

- BIBLIOGRAPHIE -

1 - Ouvrages fondamentaux

- Y.C. FUNG, Foundations of solid mechanics
  - Prentice-Hall.
- P. GERMAIN, Mécanique des milieux continus
  - Masson & Cie - Paris
- J. MANDEL, Mécanique des milieux continus
  - Gauthier-Villars - Paris.
- OLSZAC, Recent trends in the developpement of theory of plasticity
  - Pergamon Press.
- J.H. ARGYRIS, Energy theorems and strutural analysis
  - Butterworths - Londres 1960.

2 - Ouvrages spécialisés

- J.H. ARGYRIS, S. KELSEY et H. KAMEL, Matrix methods of structural analysis
  - Agardograph n° 72, Pergamon Press - N.Y. 1964.
- HOLAND et BELL, Finite element method in structural analysis
  - Tapir 1969.
- O.C. ZIENKIEWICZ, The finite element method in structural and continuum mechanics
  - Mc. Graw-Hill 1967.

3 - Congrès et Conférences

- Engineering Plasticity (Cambridge University Press),
  - . J.N. GOODIER, Dynamic buckling of rectangular plates in surtained plastic compression flow.
  - . Ch. MASSONNET, General theory of elasto-plastic menbrane-plates
    - edited by J. HEYMAN & F.A. LECKIE.
- Finite element techniques in solids mechanics (University of Southampton Department of Civil Engineering - 15,17 April 1970).

4 - Publications dans des revues ou des collections

- J. COAN, Large deflection theory for plates with small initial curvature loaded in edge compression
  - Journal of App. Mech. 1959.
- J. DJUBEK, Solution of the non linear problem of the deformation of webs
  - Mém. A.I.P.C. 1963.
- ZIAD M. ELIAS, Duality in finite element methods - Proceedings of A.S.C.E.
  - vol. 94 - EM 4 - august 1968.

- H.D. HIBBITT, P.V. MARCAL et J.R. RICE, A finite element formulation for problems of large strain and large displacement
  - Int. Jour. of solids & strutures - August 1970,vol.6, n° 8.
- ROBERT H. MALLET et PEDRO D. MARCAL, Finite element analysis of non linear structures - Proceedings of the A.S.C.E.
  - vol. 94 - ST 9 - September 1968.
- Ch. MASSONNET, M.ŠKALOUD, J. DONEA, Comportement post-critique des plaques cisaillées raidies
  - A.I.P.C. 1968
- Ch. MASSONNET, Plaques er coques cylindriques orthotropes à nervures dissymétriques
  - A.I.P.C. - Zurich - 1959.
- DAVID W. MURRAY et EDWARD L. WILSON, Finite element large deflection analysis of plates
  - A.S.C.E. - vol. 95 - EM 1 - February 1969.
- K.C. ROCKEY et D.K. BAGGHI, Buckling of plate girder webs under partial edge loadings
  - Report n° W/SB/KCR/4 - University College Cardiff, Faculty of Applied Science, Depart. of Civil and Structural Enginnering
- G. SANDER, Application de la méthode des éléments finis à la flexion des plaques
  - Collection des publications n° 15-1969- Université de Liège, Faculté des Sciences Appliquées (thèse de Doctorat).
- WILLIAM Y.J. SHIEH, SENG-LIP LEE et RICHARD A. PARMALEE, Analysis of plate bending by triangular elements
  - A.S.C.E. - vol. 94 - EM 5 - October 1968.
- M. ŠKALOUD et J. DONEA, Voilement des âmes à tensions résiduelles
  - A.I.P.C. - vol. 23 - 1963.
- M. ŠKALOUD, Effet d'une courbure initiale sur le comportement post-critique d'une âme comprimée uniformément et renforcée par un raidisseur longitudinal.
  - Acier - n° 5 - 1965.
- SEMITH S. TEZCAN, B.C. MAHAPATRA et C.I. MATHEWS, Tangent stiffness matrices for finite elements
  - A.I.P.C. - 30 I - 1970.
- ALASTAIR C. WALKER, Rayleigh, Ritz method for plate flexure
  - A.S.C.E. - vol. 93 - EM 6, December 1967.
- O.C. ZIENKIEWICZ et Y.K. CHEUNG, The finite element method for analysis of elastic isotropic and orthotropic slabs
  - Proc. Inst. Civil Eng. - vol. 28 - 1964

RESUME

Le présent mémoire développe une méthode d'analyse approchée, par éléments finis des plaques raidies anisotropes, présentant un état de contraintes propres et une faible courbure initiale. Cette analyse s'applique au domaine des grands déplacements, aussi bien pour la plaque que pour les raidisseurs. Un programme a été établi et fonctionne sur - IBM 360-75. Il est actuellement au stade expérimental et sera développé prochainement dans le domaine plastique et dans l'étude des petits mouvements autour d'une position d'équilibre déformée. Divers tests expérimentaux de la méthode seront présentés en annexe.

ZUSAMMENFASSUNG

Diese Darlegung entwickelt eine Näherungsmethode mittels endlicher Elemente für die Analyse anisotroper, ausgesteifter dünner Platten mit Eigenspannungszustand und schwacher Vorkrümmung. Die Analyse findet Verwendung im Bereich der grossen Verschiebungen, sowohl der Platten als auch der Versteifungen. Ein elektronisches Programm wurde bereits aufgestellt und läuft gegenwärtig auf einer -IBM 360-75 - Rechenmaschine. Vorläufig wird es nur experimentell studiert; demnächst wird das Programm im plastischen Bereich und für die Untersuchung kleiner Schwingungen um eine verformte Gleichgewichtslage entwickelt. Im Anhang werden verschiedene Kontrollversuche dieser Methode angegeben.

SUMMARY

The present paper gives an approximate analytical method using the finite element technique, for thin anisotropic stiffened plates with residual stresses and small initial curvature. This analysis takes into account the large displacement of plates as well as stiffeners. A computer program has been set up and works on a - IBM 360-75. This program is used, at the present time, as an experimental tool; in a next future it will be performing in the plastic range and for the study of small movement around the deformed equilibrium position. Various experimental tests of the method will be presented in appendices.

Leere Seite
Blank page
Page vide

Comportement à l'effort tranchant dans le domaine des déplacements finis de panneaux d'une poutre en I

Verhalten von Stegblechfeldern von I-Trägern unter Schubbeanspruchung im Bereich endlicher Verschiebungen

Shear Behaviour in the Finite Displacements Range of I-Beam Panels

H. GACHON
Professeur à l'Ecole Nationale Supérieure
d'Arts et Métiers
Paris, France

I - INTRODUCTION

Dans le but de tester la méthode d'analyse et de simulation du comportement des plaques minces raidies dans le domaine des déplacements finis, nous avons réalisé en laboratoire une série d'essais sur diverses structures constituées de panneaux soumis à des conditions de charge et présentant des coefficients d'élancement et d'aspect variables.

Les essais que nous présentons dans ce qui suit portent sur une poutre à âme mince et à membrures symétriques. Cette poutre se compose de cinq panneaux de coefficient d'aspect distincte et d'élancement d'âme identique. Chacun des panneaux est sollicité différemment.

Le dimensionnement complet de la poutre a été fait par la méthode développée et mise au point par Messieurs BASLER et THURLIMANN à l'Université de LEHIG. C'est donc un dimensionnement défini à l'état limite et, dans ce cas particulier, dans le domaine dit "post-critique".

Les essais ont été réalisés au Laboratoire du C.E.B.T.P. à PARIS à l'initiative du C.T.I.C.M. Ils ont été développés de manière à faire passer successivement chaque panneau d'un état initial à l'état ultime caractérisé par l'amorce de l'écoulement. L'état initial était seulement défini par la mesure de la déformée de la plaque hors du plan moyen du panneau.

Le déroulement général du programme devait compter cinq étapes. A chaque étape correspondait l'essai d'un panneau. A l'issue de chaque étape le panneau essayé était consolidé à l'aide de raidisseurs transversaux boulonnés. Malheureusement, nous n'avons pu réaliser totalement notre programme, car la mise hors service de la poutre est survenue au cours de la quatrième étape par l'instabilité à la torsion de la membrure comprimée.

II - DESCRIPTION DE LA POUTRE - (Fig.1)

La poutre est à section droite en I, à membrures symétriques et à âme mince raidie par des raidisseurs transversaux. Sa portée est de 8,00m - la hauteur de l'âme est de 700 mm et son épaisseur est de 3 mm. Ce qui donne un élancement de $\frac{700}{3} \simeq 235$.

Les raidisseurs transversaux définissent cinq panneaux :

- Le panneau A (2100 x 700 en mm)
- Le panneau B (1300 x 700 en mm)
- Le panneau C (1100 x 700 en mm)
- Le panneau D (1500 x 700 en mm)
- Le panneau E (1500 x 700 en mm)

Les dimensions de ces panneaux ont été définies en fonction de l'état des sollicitations que nous voulions y développer (effort tranchant, effort tranchant + moment fléchissant, moment fléchissant).

La constitution de cette poutre a été réalisée par soudage. L'acier utilisé présente un palier de plasticité à environ 38 daN.mm2 . L'amorce du palier se produit à 2000μ déformations. La limite de linéarité observée est environ de 26 daN.mm2.

III - MODE OPERATOIRE - MESURES

Trois cas de charges distinctes ont été appliqués

- P_1 pour essayer le panneau A
- P_2 pour essayer les panneaux B, C, D
- $P_1 = P_2$ pour essayer le panneau E .

Avant chaque essai, la poutre a été soumise à un chargement cyclique de 0 à 5 tonnes de manière à assurer une bonne mise en place des différents systèmes d'appuis, de charges et de mesures.

Au cours de chaque essai, les charges ont été appliquées depuis 5 tonnes par cycles lents, d'amplitude progressivement croissante. Les mesures ont été faites systématiquement, à chaque cycle et pour chaque niveau extrême de charge (5t et Pt).

Ainsi, en adoptant un pas relativement faible de la charge P ou de l'accroissement de l'amplitude de chaque cycle de chargement et en notant à chaque retour à 5 tonnes les déformations rémanentes, nous avons pu mettre en évidence le seuil de reversibilité de chaque panneau dans l'état de chargement imposé.

De plus, nous avons noté au passage le point d'inflexion de la courbe de déformation hors du plan de l'âme en fonction de la charge appliquée, ce point correspondant au seuil de bifurcation de l'équilibre du panneau ou encore au seuil dit critique.

Et enfin, nous avons relevé le seuil d'écoulement de la charge ou le seuil de divergence de l'équilibre, seuil au delà duquel l'instabilité effective du panneau se produit. Il convient de remarquer que le chargement de chaque panneau n'a pas été poursuivi jusqu'à la ruine totale mais que nous nous sommes limités à l'observation de l'amorce du palier d'écoulement des déformations en fonction de la charge.

Les mesures ont portées :

- Sur l'analyse du champ de déformation sur chacune des faces de l'âme, des raidisseurs et des membrures.
- Sur l'étude du champ de déplacement vertical des membrures supérieure et inférieure de la poutre.
- Sur l'étude du champ de déplacement de l'âme suivant une direction perpendiculaire à son plan.

- Fig. 1 - POUTRE A AME MINCE ET MEMBRURES SYMETRIQUES

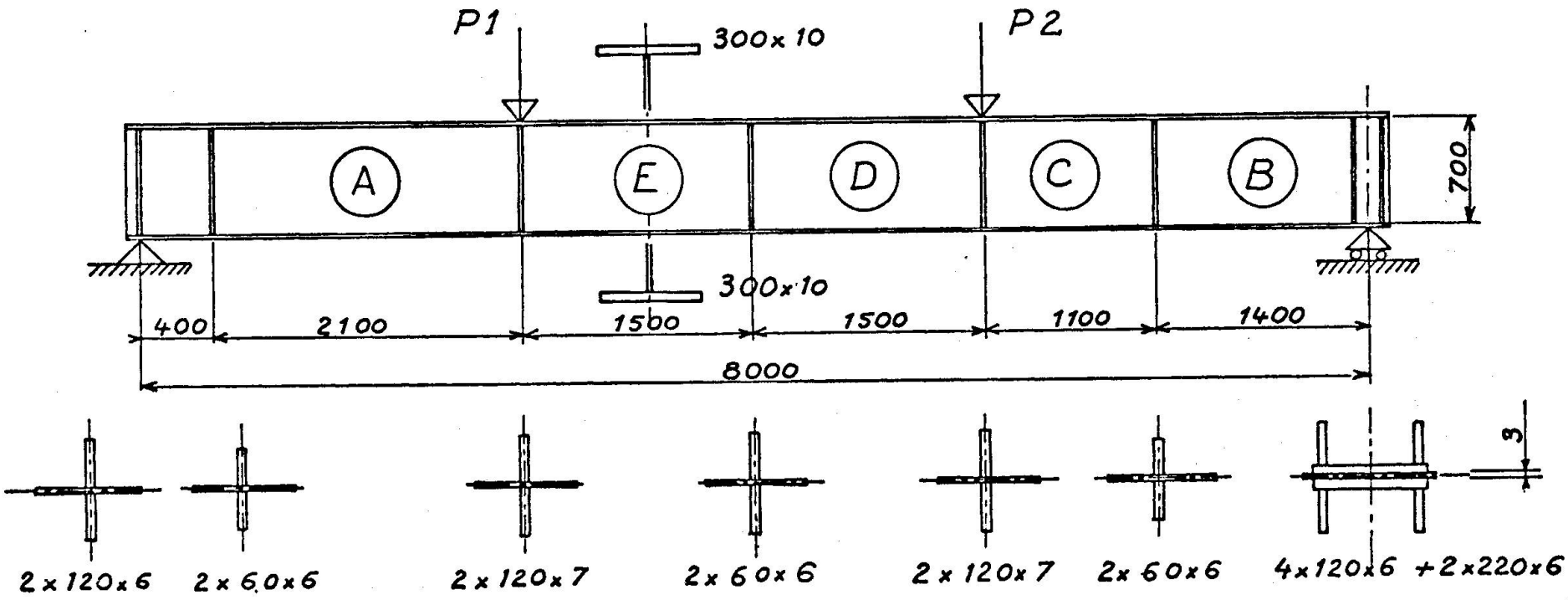

PANNEAUX ESSAYES	CHARGES ULTIMES CALCULEES (en tonnes)	CHARGES ULTIMES MESUREES (en tonnes)
. A	. P_1 = 21,7 (P_{cr} = 6.22)	. P_1 = 23 ($P_{rev.}$ = 16)
. B	. P_2 = 28,0 (P_{cr} = 6.75)	. P_2 = 30 ($P_{rev.}$ = 19)
. C	. P_2 = 33,4 (P_{cr} = 6.80)	. P_2 = 33 ($P_{rev.}$ = 20)
. D	. P_2 = 48,8	
. E	. $P_1 = P_2$ = 31,3	

Nous présentons, dans ce qui suit, sous forme de graphes, les principaux résultats observés sur les panneaux A, B et C.

IV - ETUDE DU PANNEAU A

Le panneau A est soumis :

. à un effort tranchant de $\frac{5.5}{8} P_1$

. et à un moment fléchissant variant de (0.4 à 2.5) $\frac{5.5}{8} P_1$

Il présente :

. un coefficient d'élancement $\frac{b}{h} = \frac{700}{3}$

. et un coefficient d'aspect $\frac{a}{b} = \frac{2100}{700} = 3$

La charge ultime calculée est de 21.7 T.
La charge mesurée au seuil d'écoulement est de 23 T.
Le seuil de reversibilité se situe à environ 16 T.
La charge critique calculée est de 6.22 T.
Le seuil de bifurcation mesurée se situe à environ 7 T.

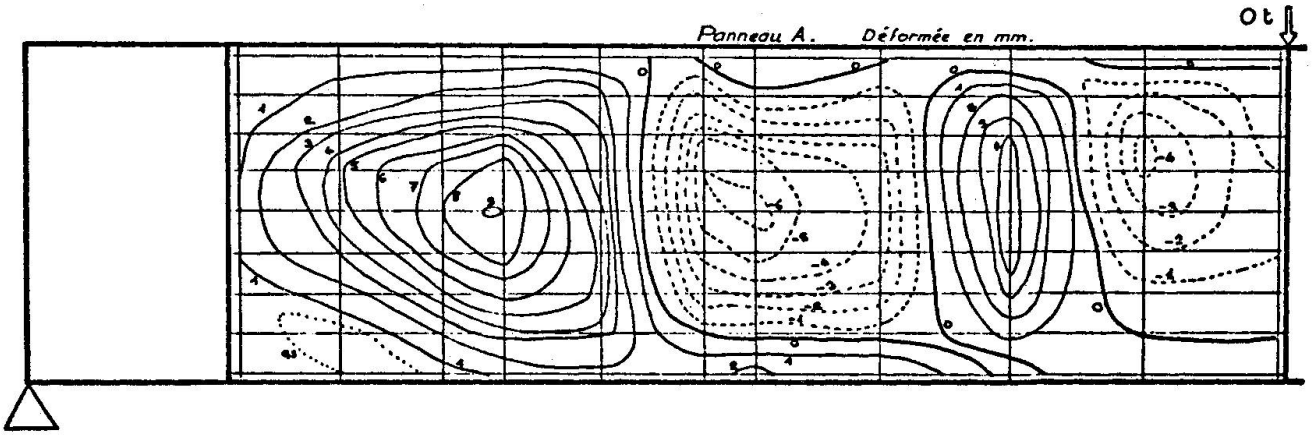

- Fig. 2 - DEFORMEE INITIALE DU PANNEAU A (en mm)

Nous remarquons une déformée initiale très importante puisqu'elle atteint en un point 3 fois l'épaisseur de l'âme. Néammoins ce panneau s'est comporté très normalement. Les différentes mesures qui y ont été faites marquent clairement les différents seuils que nous y attendions.

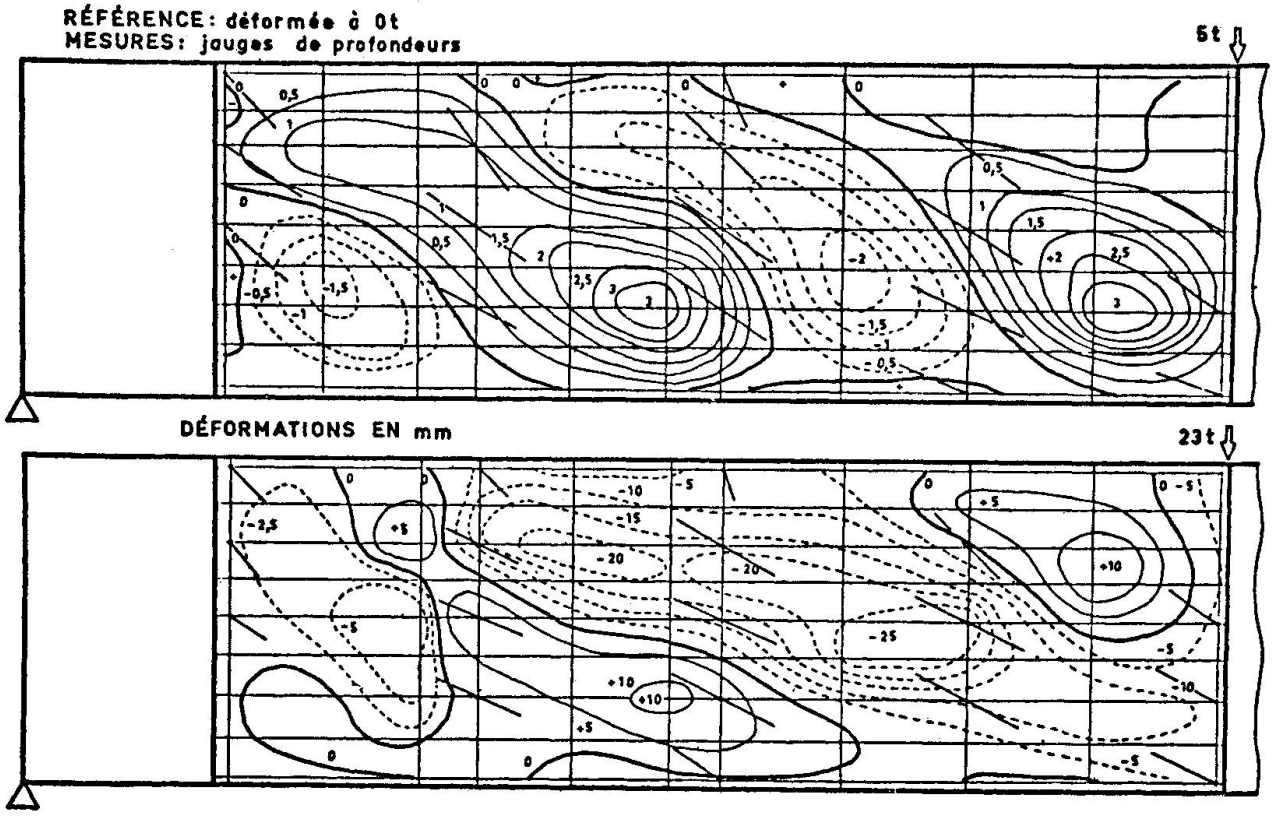

- Fig. 3 - DEFORMEE TOTALE SOUS CHARGE DU PANNEAU A - (en mm)

Ces courbes sont accompagnées du tracé de la direction de la contrainte principale supérieure de traction en différents points de la surface moyenne de l'âme. Nous remarquons l'excellente concordance des deux tracés dans la définition du champ diagonal de traction dans l'âme. Il est aussi interessant de noter qu'au seuil d'écoulement à 23t, l'inclinaison du champ diagonal, ne coincide pas avec la diagonale du panneau. Il apparait que, dans une première partie du panneau, le champ diagonal s'est développé suivant une inclinaison limite de pente $1/_{2.3}$ et dans la partie complémentaire ce champ a conservé une pente 1/1. En fait, il semble qu'on puisse affirmer, qu'en l'absence de raidisseurs transversaux le champ diagonal peut encore se développer, ce qui confirme la théorie de BERGMAN'S.

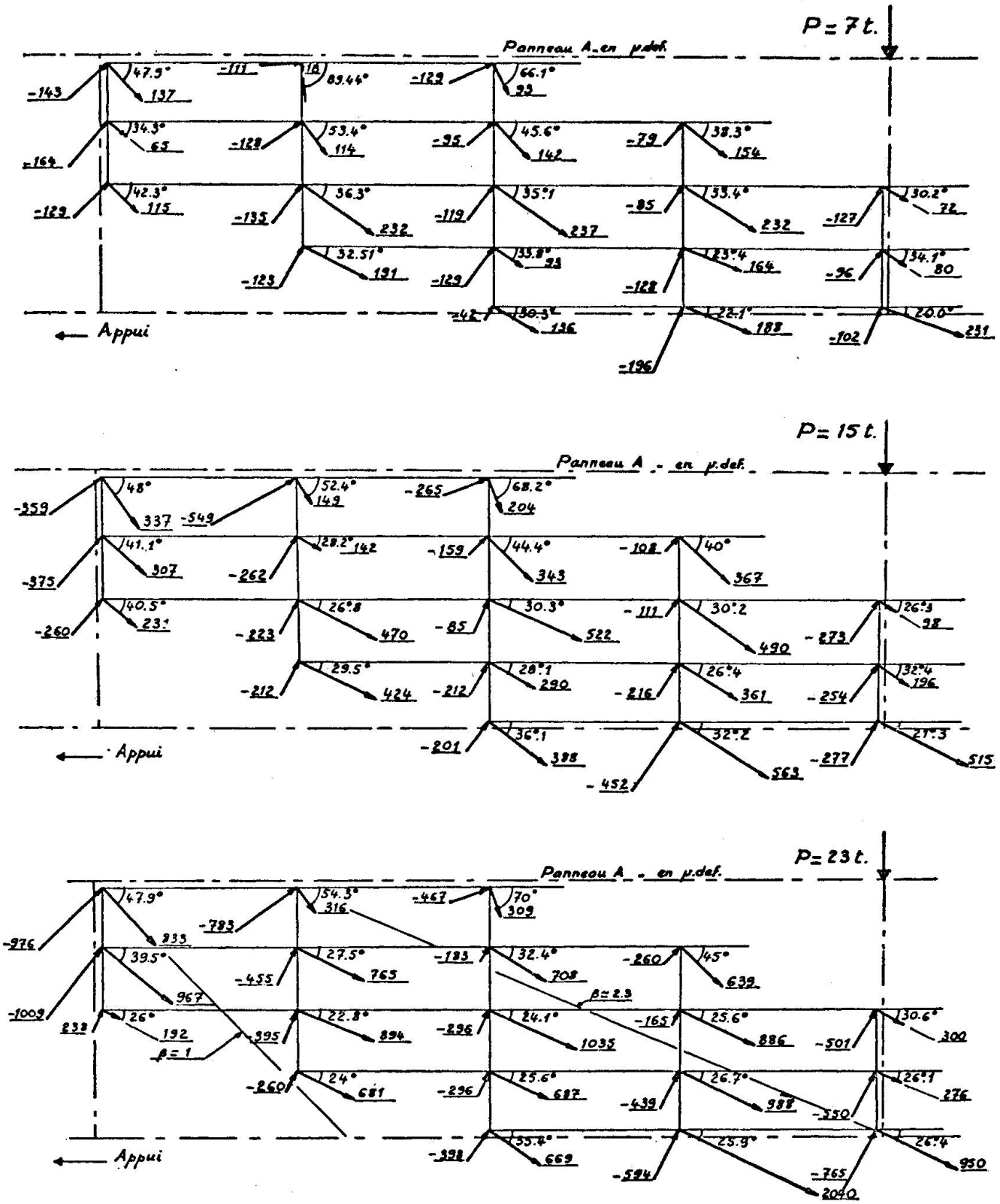

- Fig. 4 - CHAMP DE DEFORMATIONS DANS LA SURFACE MOYENNE DE L'AME DU PANNEAU A (en μ déformations)

. P = 7 t ≃ seuil de bifurcation, seuil critique

. P = 15 t ≃ seuil de reversibilité

. P = 23 t ≃ seuil d'écoulement

Le tracé du déplacement d'un point de l'âme, suivant une direction hors de son plan moyen, en fonction de la charge, montre bien les différents seuils de bifurcation et de reversibilité annoncés précedemment. Nous présentons ci-dessous - en Fig. 5 - une telle fonction.

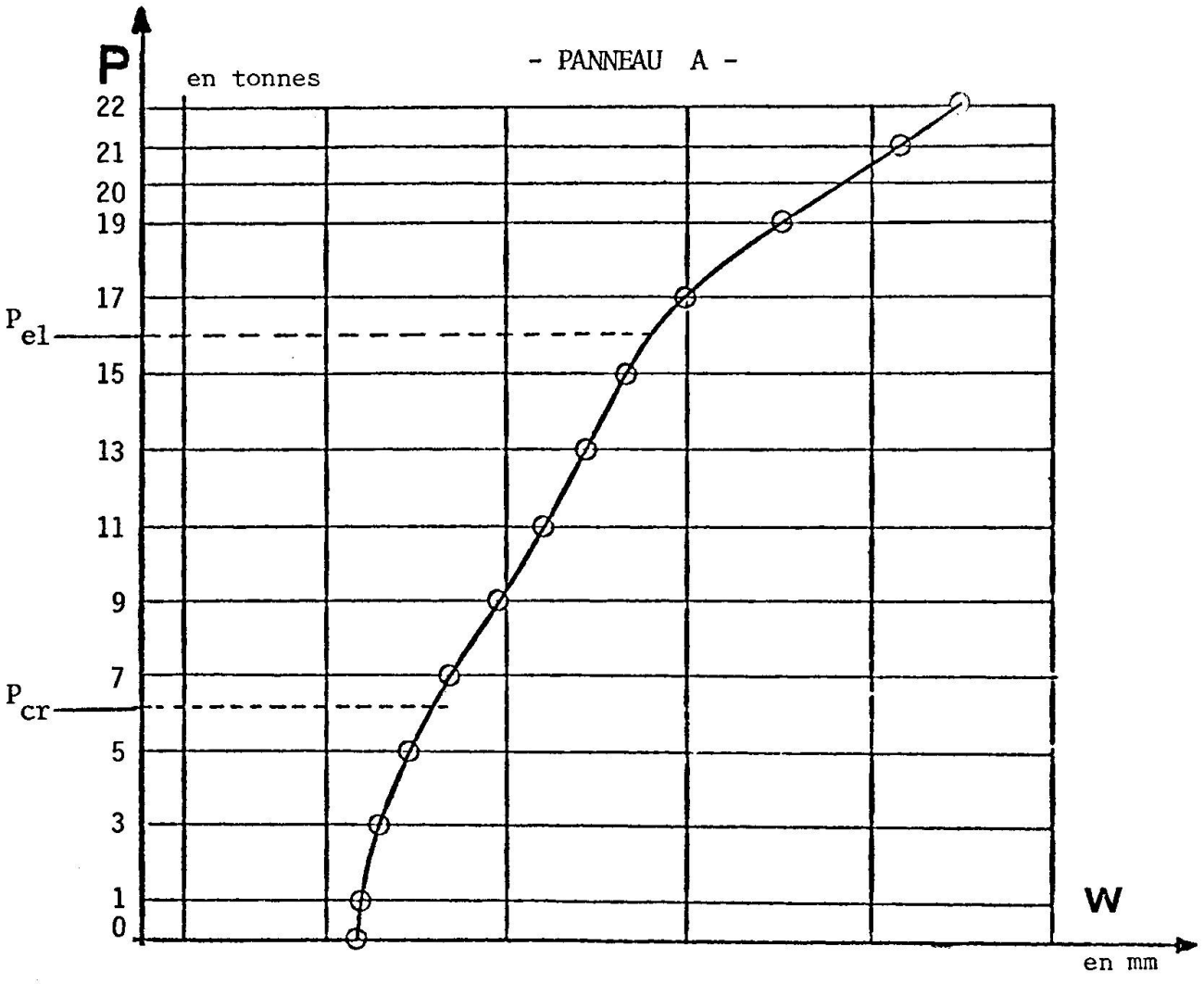

W : déformation hors du plan moyen, au centre du panneau

P_{cr} = 6,22 tonnes P_{el} = 16 tonnes

- Fig. 5 - DEPLACEMENT D'UN POINT DE L'AME HORS DU PLAN MOYEN DU PANNEAU A (en mm)

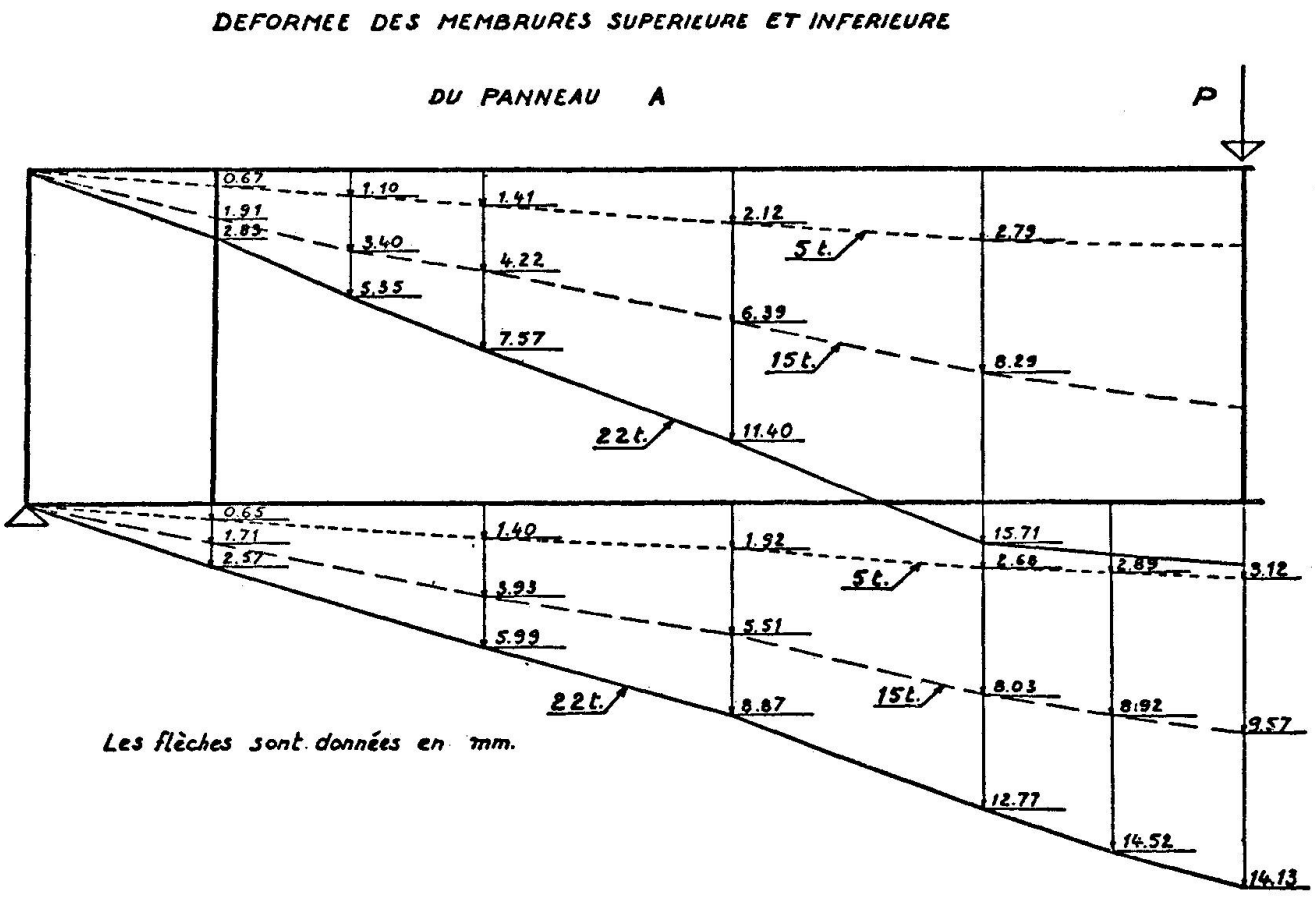

- Fig. 6 - DEFORMEE DES MEMBRURES SUPERIEURE ET INFERIEURE (en mm) (Panneau A)

V - ETUDE DU PANNEAU B

Le panneau B est soumis

. à un effort tranchant de $\frac{5.5}{8} P_2$

. et à un moment fléchissant variant de (0 à 1.4) $\frac{5.5}{8} P_2$

Il présente

. un coefficient d'élancement $\frac{b}{h} = \frac{700}{3}$

. et un coefficient d'aspect $\frac{a}{b} = \frac{1300}{700} = 1.85$

Les essais ont mis en évidence :

. Un seuil de bifurcation pour $P_2 \simeq$ 6 à 7 tonnes

. Un seuil de reversibilité pour $P_2 \simeq$ 17 à 19 tonnes

. Un seuil d'écoulement pour $P_2 \simeq$ 30 tonnes

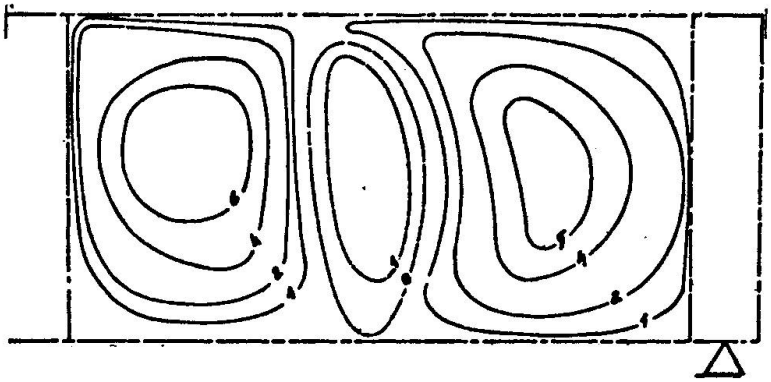

. DEFORMEE INITIALE

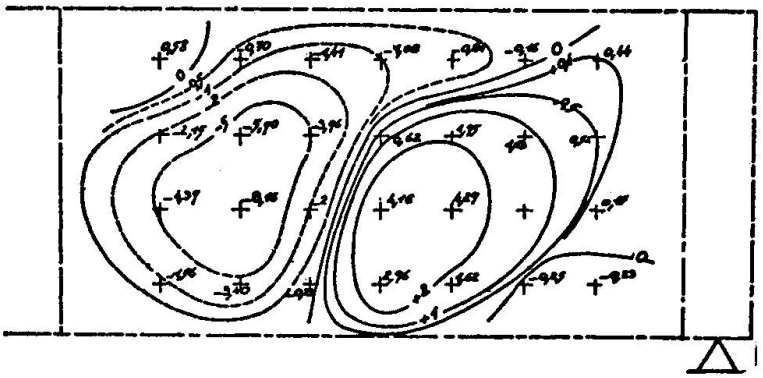

. CHARGE 6.1 T.

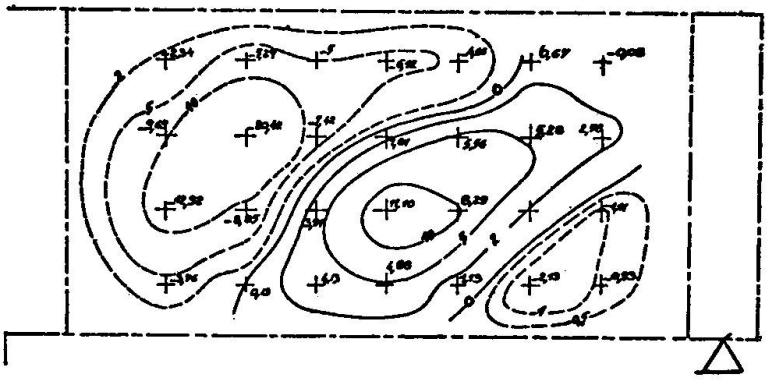

. CHARGE 20 T.

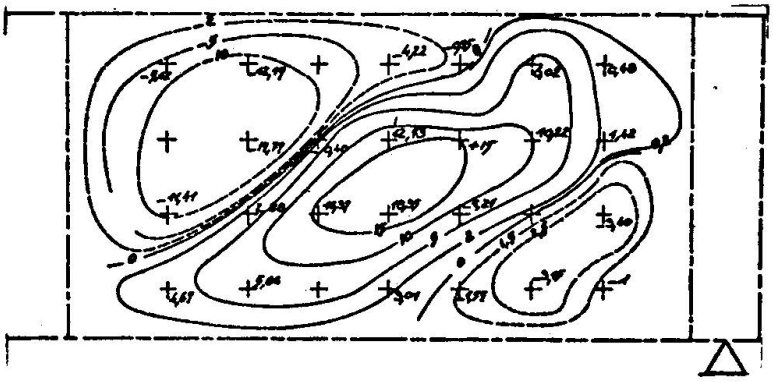

. CHARGE 30 T.

Fig. 7 - DEFORMEE DE L'AME HORS DU PLAN MOYEN DU PANNEAU B (en mm)

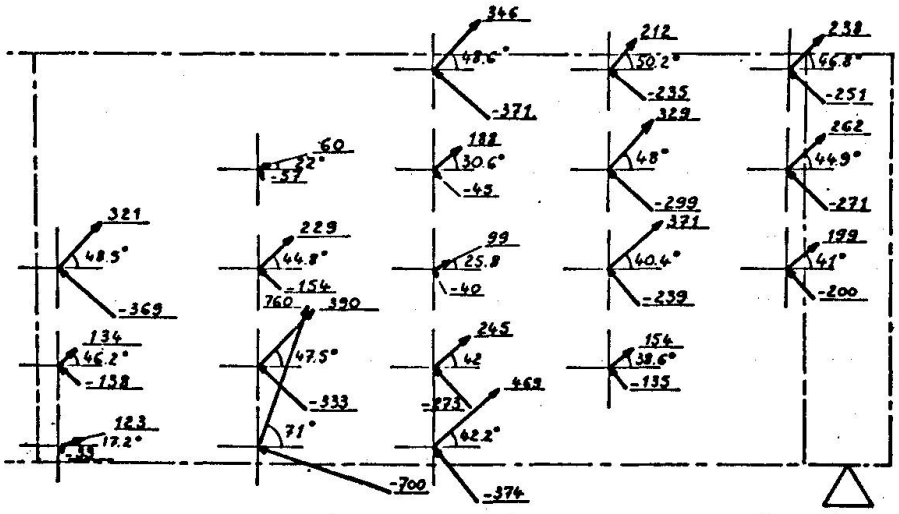

. CHARGE 6.1 T.

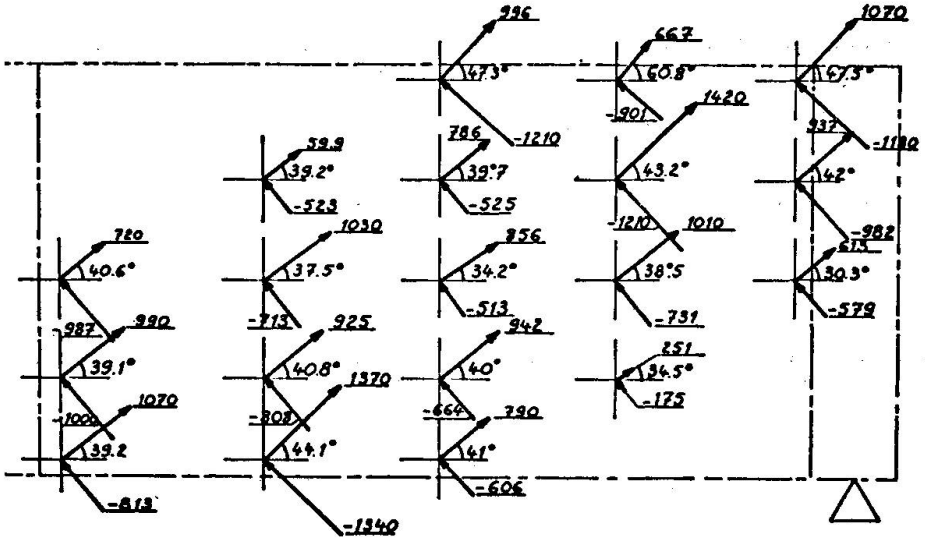

. CHARGE 20 T.

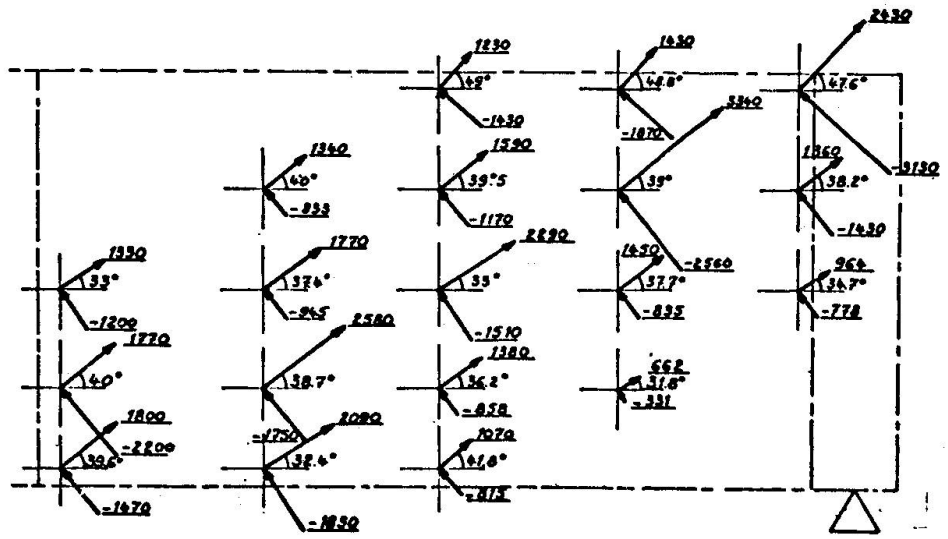

CHARGE 30 T.

- Fig. 8 - CHAMP DE DEFORMATION DE MEMBRANE DANS L'AME (en μ. def.)
(Panneau B)

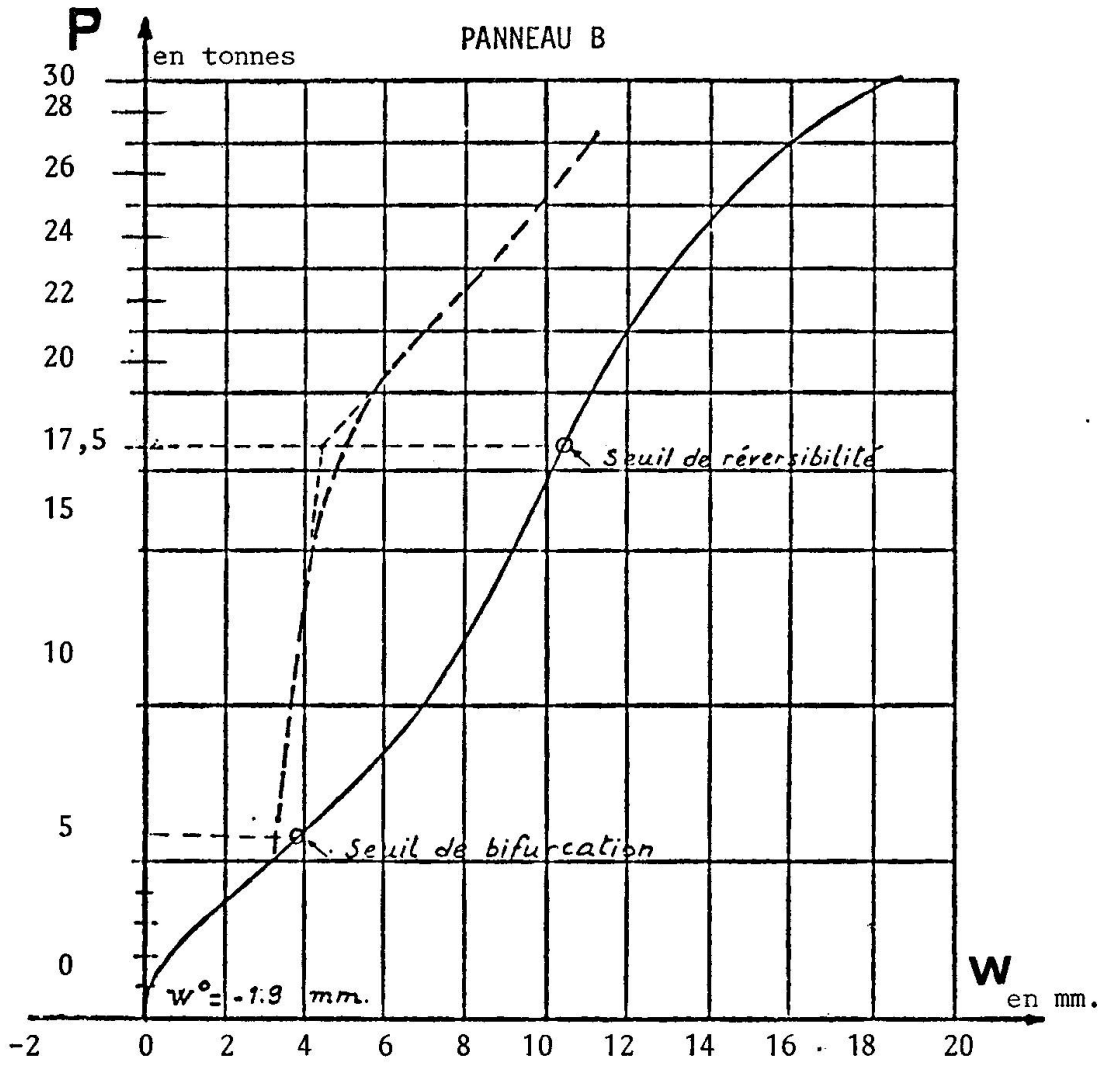

Fig. 9 - DEPLACEMENT D'UN POINT DE L'AME HORS DU PLAN MOYEN DU PANNEAU B (en mm.)

VI - ETUDE DU PANNEAU C

Le panneau C est soumis :

. à un effort tranchant de $\frac{5.5}{8} P_2$

. et à un moment fléchissant variant de (1.4 à 2.5) $\frac{5.5}{8} P_2$

Il présente :

. un coefficient d'élancement $\frac{b}{h} = \frac{700}{3}$

. et un coefficient d'aspect $\frac{a}{b} = \frac{1100}{700} = 1.57$

Les essais ont mis en évidence :

. Un seuil de bifurcation pour $P_2 \simeq$ 10 tonnes

. Un seuil de reversibilité pour $P_2 \simeq$ 20 tonnes

. Un seuil d'écoulement pour $P_2 \simeq$ 33 tonnes

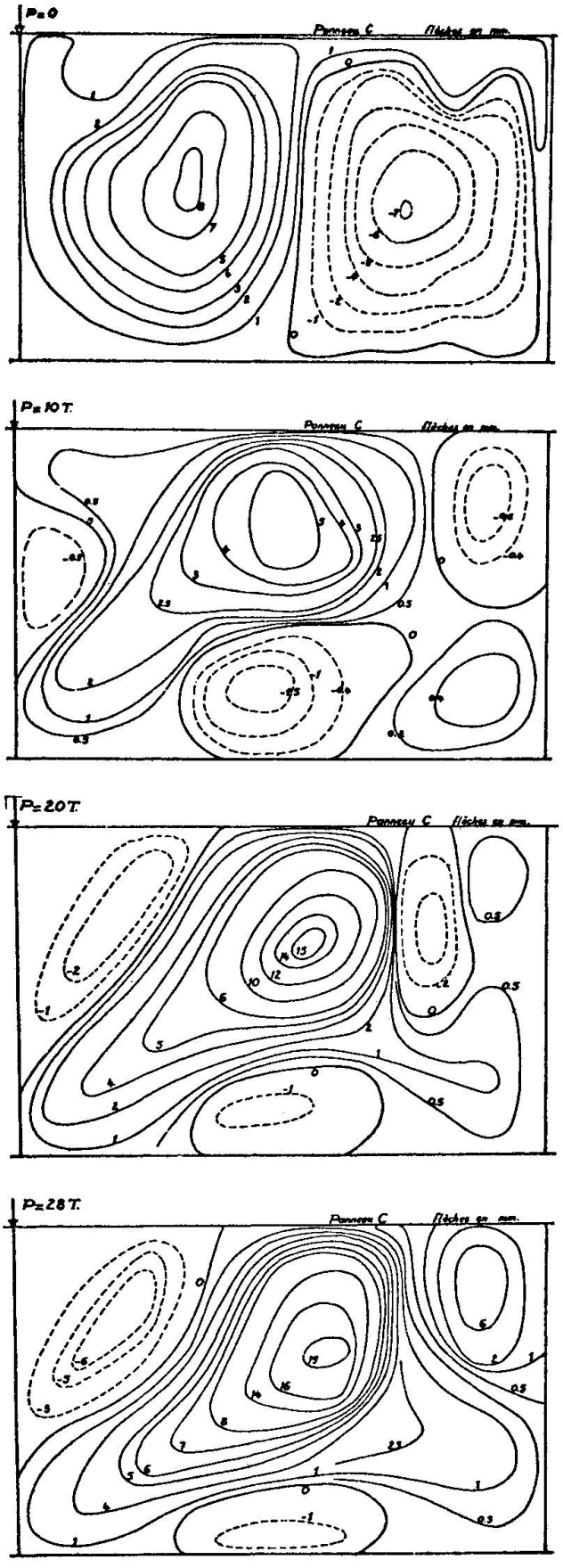

- Fig. 10 - DEFORMEE DE L'AME HORS DU PLAN MOYEN DU PANNEAU C
(en mm.)

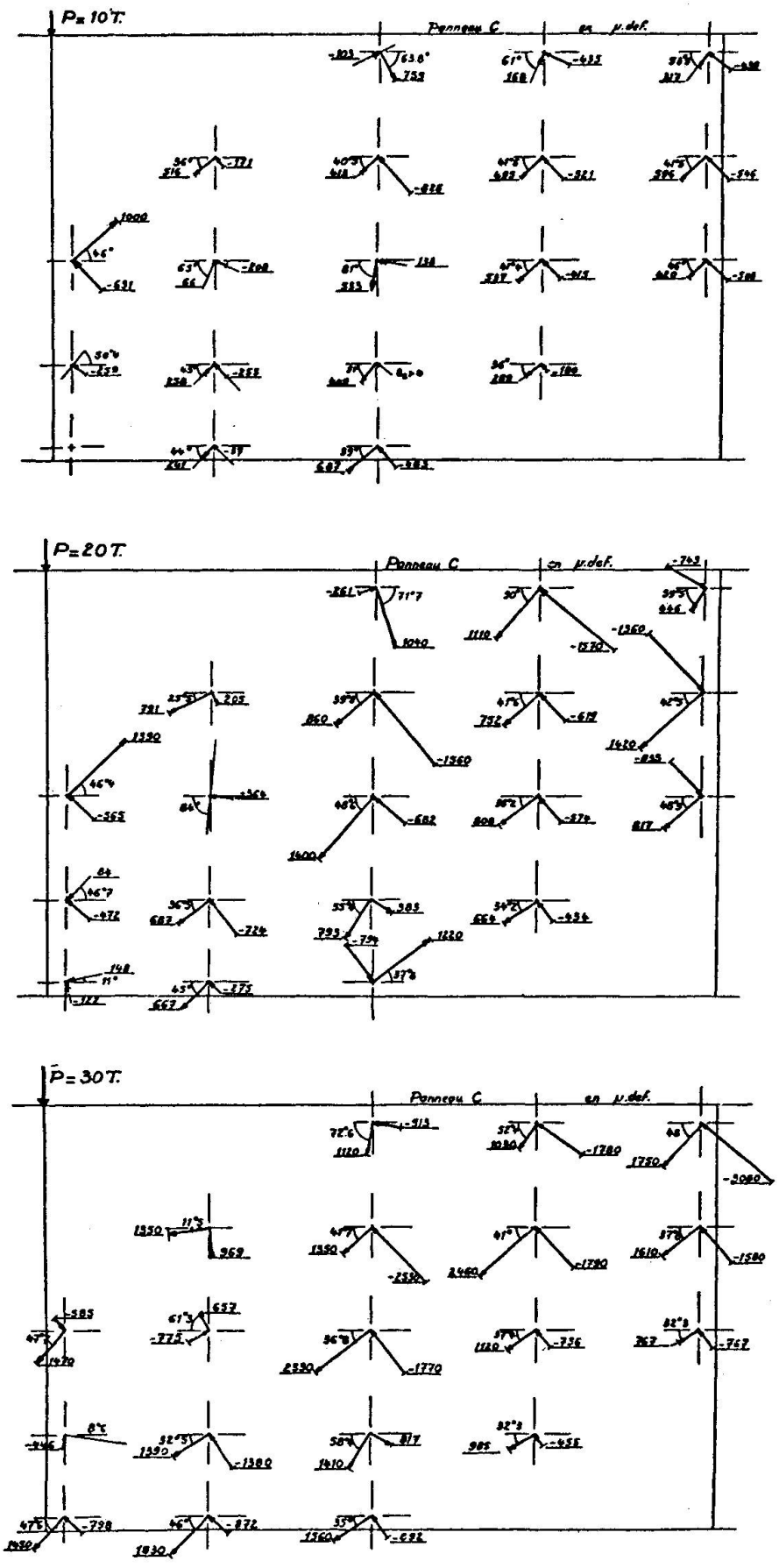

- Fig. 11 - CHAMP DE DEFORMATION DANS LA SURFACE MOYENNE DE L'AME DU PANNEAU C (en μ. déformations)

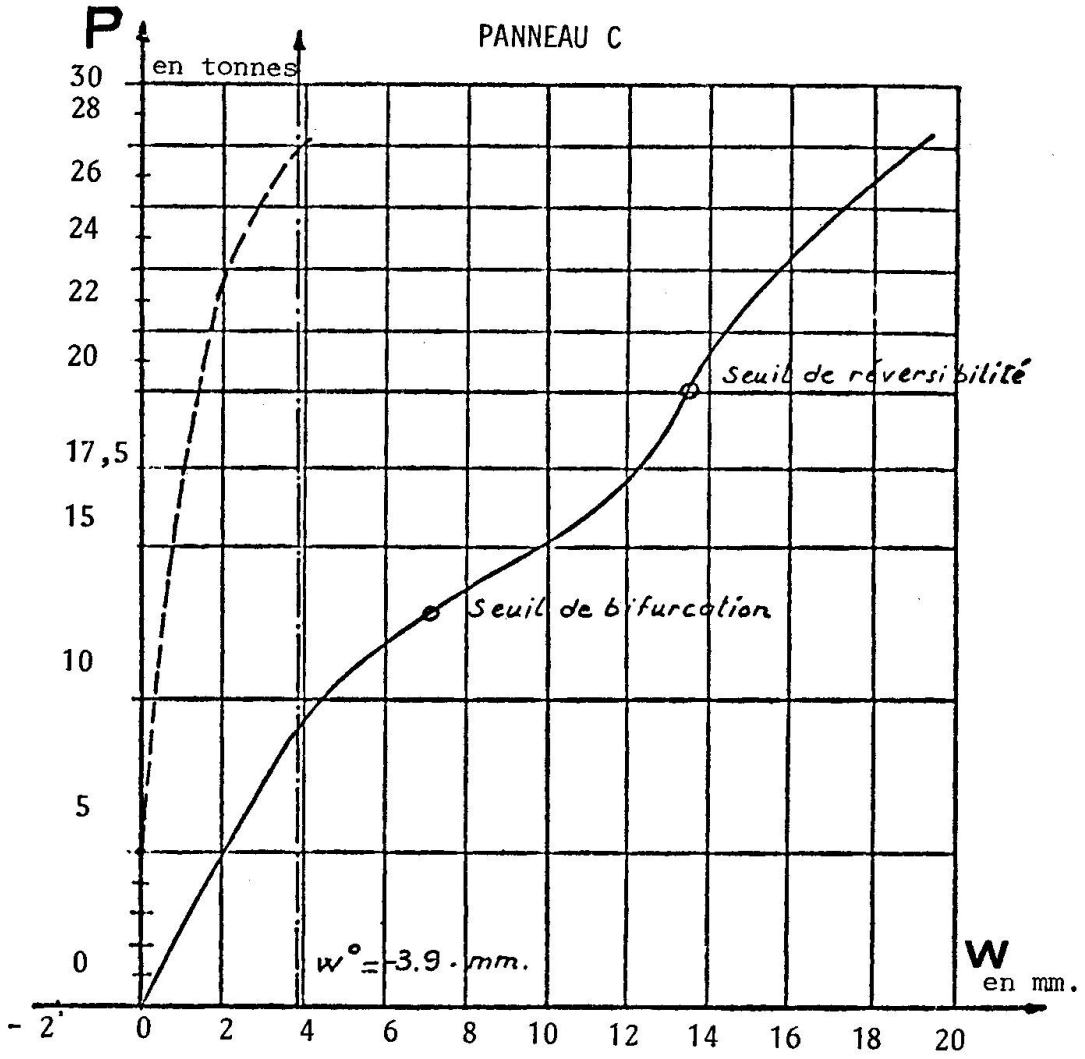

- Fig. 12 - DEPLACEMENT D'UN POINT DE L'AME HORS DU PLAN MOYEN DU PANNEAU C (en mm.)

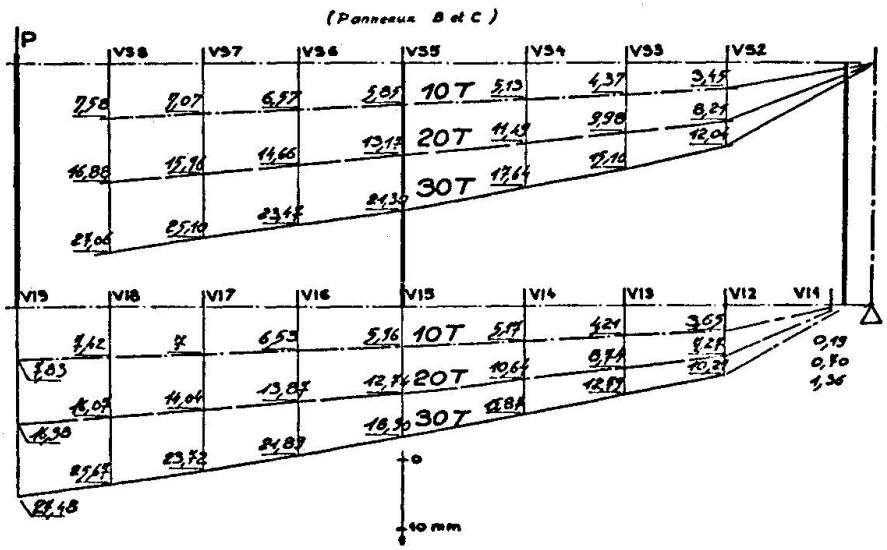

- Fig. 13 - DEFORMEE DES MEMBRURES SUPERIEURE ET INFERIEURE DES PANNEAUX C ET D (en mm.)

VII - CONCLUSION

A travers ces résultats, nous avons voulu montrer, pour les trois panneaux essayés, que :

1 - Ce que nous appelons seuil critique ou de bifurcation et que nous avions coutume de considérer comme un état d'instablité, ne marque aucun caractère particulier dans le comportement de la plaque si ce n'est un changement de signe de la courbure dans la variation de la déformée de l'âme hors du plan moyen du panneau en fonction de la charge. Ce seuil doit plutôt être considéré comme la naissance d'un champ de contraintes de membrane qui accroît la raideur apparente de la plaque dans la déformation hors de sa surface moyenne et qui est par conséquent très favorable à sa stabilité.

2 - Le seuil de reversibilité, déterminant le domaine du comportement élastique du panneau, pour les élancements considérés, se situe bien au-dessus du seuil critique et se distingue très nettement de l'état limite calculé par la méthode de Messieurs BASLER et THURLIMANN. Cette différence vient sans doute des approximations faites d'une part sur la constitution du modèle mathématique et d'autre part sur le défaut de prise en compte des contraintes propres ou rémanentes.

3 - Le seuil d'écoulement du panneau, pour lequel un assez large volume de la structure est dans le domaine plastique, répond mieux aux prévisions des méthodes de calcul basées sur la simulation schématique du mécanisme de ruine du panneau.

4 - Le champ de contraintes ou plus exactement de déformation, se développant dans la surface moyenne de l'âme, présente :

- en chaque point des panneaux B et C, une coordonnée principale tensorielle d'accourcissement (compression) sensiblement du même ordre de grandeur et parfois égale à la coordonnée principale tensorielle d'allongement (traction) et ce dans tout le domaine dit "post-critique".

- en chaque point du panneau A, une nette prédominance des composantes d'allongement (traction) sur les composantes d'accourcissement (compression) dans le secteur où l'inclinaison des composantes d'allongement principal a atteint sa pente limite (1/2.3) favorisées par les dimensions du panneau (Coefficient d'aspect $\frac{2.1}{0.7}$)

RESUME

Ce mémoire présente les résultats d'essais, à l'effort tranchant, effectués sur trois panneaux de poutre présentant des coefficients d'aspect différents et un même élancement.

Ces résultats apportent une information complète sur l'état de déformation de ces panneaux au seuil critique ou de bifurcation, au seuil de reversibilité et au seuil d'écoulement.

ZUSAMMENFASSUNG

Diese Abhandlung stellt Ergebnisse von Querkraftversuchen an Trägern dar, die mit drei verschiedenen Feldverhältnissen, aber mit derselben Schlankheit durchgeführt wurden. Die Ergebnisse bringen eine vollständige Uebersicht über den Formänderungszustand dieser Felder an der kritischen oder Verzweigungsgrenze, sowie an der Umkehrgrenze und an der Fliessgrenze.

SUMMARY

This study presents the results of transverse shear tests made on three beam panels with different panel aspect ratios and having the same slenderness.

These results give a complete information about the state of strain of the panels in the critical or equilibrium bifurcation limit, in reversibility limit as well as in the yield limit.

Leere Seite
Blank page
Page vide

II

An Ultimate Load Method for the Design of Plate Girders

Méthode de dimensionnement à la ruine des poutres à âme pleine

Ein Traglastverfahren zur Bemessung von Blechträgern

K.C. ROCKEY
M.Sc., C.Eng., Ph.D., F.I.C.E.
Professor of Civil and Structural Engineering
University College, Cardiff, England

1. INTRODUCTION

The economic design of plate girders frequently involves the use of thin web plates reinforced by longitudinal and vertical stiffeners. Since more often than not these stiffened webs will buckle before the girders collapse, the use of ultimate load methods of design are essential if full advantage is to be taken of the post buckling load carrying capacity of the web plates. The present paper presents an ultimate load design method for plate girders which has been developed from an extensive study into the ultimate load behaviour of plate girders (1 - 5).

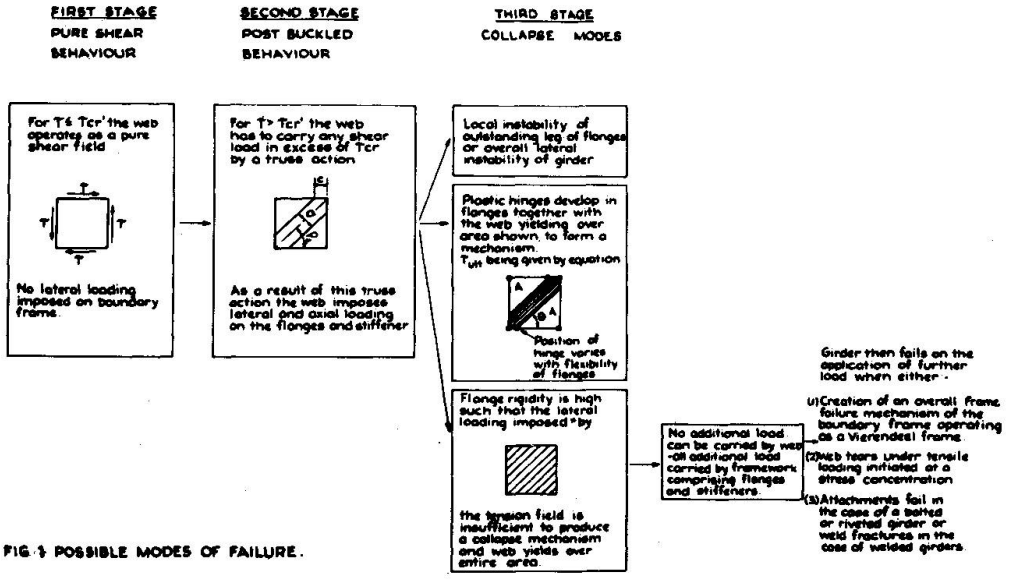

FIG. 1 POSSIBLE MODES OF FAILURE.

An extensive study of the behaviour of shear webs carried out by Skaloud and the writer (1 - 3) has shown that a shear web may fail in a number of different ways, see figure 1. From figure 1 it will be noted that if the webplate has no initial imperfections then prior to buckling it does not impose any lateral

loading upon the boundary members. However, once the web has buckled it is no longer capable of carrying any further compressive loading across the diagonal ab and as a result the web has to carry all additional shear loads by a diagonal tensile membrane action, this action being referred to as a 'truss type action'. This membrane action imposes a lateral load upon the flanges and it is possible for this membrane action to cause the flanges, and therefore the girder, to fail due to the development of plastic hinges in the flanges. Whether or not this type of failure will occur depends upon the stiffness of the flanges and upon the magnitude of the membrane loading which varies with the elastic buckling stress of the web; with an increase in the buckling stress there is a decrease in the membrane action. If the flanges are sufficiently stiff then the boundary members comprising of the flanges and the stiffeners permits the web to develop a full membrane action until it yields. Once this stage has been developed, the web cannot carry any further shear load and any further loads imposed upon the girder have to be carried by the flanges and stiffeners acting as a Vierendeel frame.

The first significant step in the development of plastic methods of design for plate girder webs, loaded in shear, occurred when Basler and his associates at Lehigh University (6 - 9) presented their design method some ten years or so ago. They assumed that the webplate would fail due to the development of an inclined plastic band anchored against the vertical stiffeners, see figure 3. In developing this mechanism, Basler et al assumed that the flanges of most girders were too flexible to withstand the membrane

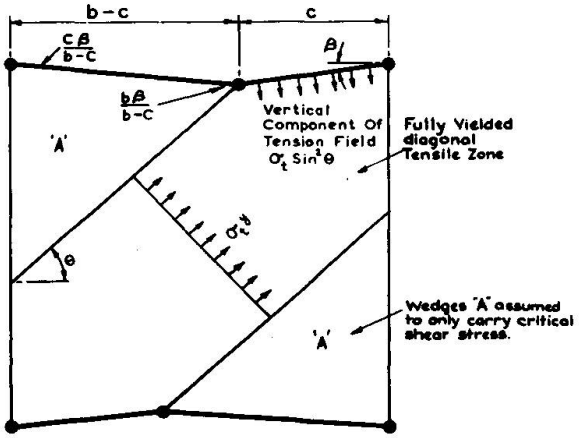

FIG. 2 COLLAPSE MECHANISM PROPOSED BY ROCKEY & SKALOUD (3)

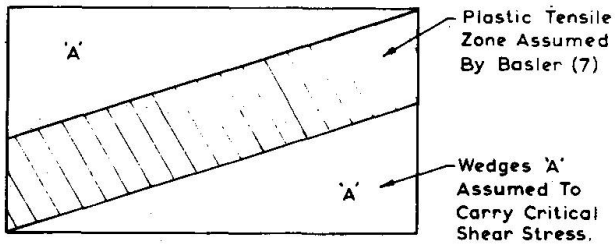

FIG. 3. COLLAPSE MODE ASSUMED IN BASLER THEORY.

action imposed by the buckled web. However, it has been shown in references (1 - 3) that their "collapse model" can both significantly underestimate and overestimate the strength of plate girders.

More recent research at Lehigh by Ostapenko et al (10 - 12) has developed the Basler model and shown how it can be applied to the design of plate girder webs reinforced by both transverse and longitudinal stiffeners. One very important contribution being the development of formulae for flange and stiffener design. Unfortunately, the model assumed still does not allow for the influence of transverse flange rigidity upon the behaviour of buckled webs.

The present paper indicates how the ultimate load method of design for transversely stiffened shear webs as proposed by Skaloud and the writer (3, 4) can be adapted to deal with the loading cases of combined shear and bending and also to deal with the design of plate girder webs reinforced by both transverse and longitudinal stiffeners.

2.1. ULTIMATE LOAD DESIGN OF WEBS LOADED IN SHEAR

In reference (1 - 3), Skaloud and the writer have shown that when a shear web plate buckles prior to yielding, it fails with the development of a diagonal tension band which is fully yielded together with the development of plastic hinges in the flange members to form a mechanism, see figures 1 and 2. It was established experimentally in reference (1) that the width of the diagonal band and therefore the position of the plastic hinges varies with the I/b^3t ratio where I is the flexural rigidity of the compression flange about an axis through its centroid and perpendicular to the web plate, b is the spacing of the transverse stiffeners and t is the thickness of the web.

Subsequently in reference 4 a theoretical solution based on the collapse model shown in figure 2 was developed and it was established that this method of analysis was capable of predicting with very good accuracy the failure load of transversely stiffened plate girders loaded in shear. In section 2.2, this solution will be briefly presented, whilst in section 2.3 and 2.4 it will be extended to deal with the design of plate girder webs reinforced by both longitudinal and transverse stiffeners and also with the design of hybrid girders.

2.2. DESIGN OF SHEAR WEBS

The behaviour of a plate girder web loaded in shear can be divided into three stages.

Stages I and II

In Stage I, which only applies to a perfectly flat plate, the applied shear stress is less than the critical shear buckling stress and therefore the web panel carries the applied load by a pure shear action.

The second mode of action results from the fact that in a buckled web the compressive stresses cannot increase and any additional load has to be carried by a tensile truss action.

With normal welded plate girders which have webs with significant permanent deformations, no buckling phenomena will be observed and the loadings which are associated with Stage II occur as soon as load is applied to the girder.

Failure occurs when the diagonal tension band, see figure 1 and 2 yields and the boundary members develop sufficient plastic hinges to result in a failure characterised by one of the three possible forms of failure listed under Stage III.

Stage III

(a) If the lateral membrane loading on the flange is sufficient to develop plastic hinges in the flanges, then failure will be due to the development of a mechanism consisting of a yielded diagonal strip together with plastic hinges in the tension and compression flanges; see figures 1 and 2.

(b) If, however, the membrane loading corresponding to a yielded web is not sufficient to develop plastic hinges in the flanges then failure will occur when either

(1) the web material fractures, such as occurs in an aluminium web

(2) the framework comprising the flanges and the stiffeners, acting as a Vierendeel frame develops a 'frame' mechanism

(3) the compression flange buckles laterally or torsionally

2.2a. THEORETICAL BASIS

Stage I

For an initially plane web, for loading below the buckling stress τ_{cr}, the stress state is assumed to be one of pure shear. Obviously the value of τ_{cr} will vary with the flexural and torsional rigidity of both the flanges and the stiffeners. However, since most conventional welded steel girders have flanges of low torsional rigidity it is reasonable to assume that the shear web is simply supported on all edges. If, however, a tubular flange is employed it would be necessary to use the corresponding buckling stress (13).

As stated earlier, following buckling, the web is unable to withstand any further compression loading and any additional loading has to be carried by a tension field action. The present solution does not attempt to deal with the very complicated stress field which occurs in the elastic post buckled range, it is solely concerned with the final collapse mode. This is essential, if a comparatively simple design procedure is to be developed since observation of the collapse behaviour of girders indicates that the stress and deflection distributions vary quite rapidly at loads close to the ultimate.

The experimental evidence resulting from the earlier study by Skaloud and the writer (1 - 3) is that at collapse the web develops a tension band as shown in figure 2 in which the angle of the tension band is equal to the inclination of the geometrical diagonal and that the tension band is symmetric with respect to the geometric diagonal. The width of this diagonal tension load is assumed to be such that the intercept of its boundary with the flange coincides with position of the plastic hinges in the flanges. The above assumptions will clearly result in slightly lower bound solutions for values of $\alpha > 1$, in the case of girders with very stiff flanges, since in such cases the inclination of the tension field will be closer to 45° than the inclination of the diagonal. This point will be discussed again later in the paper.

Thus we see that there are two stress regions, see figure 4.

(1) two triangular wedges in which the critical shear stress is assumed to act

(2) a yielded diagonal strip.

The tension stress σ_t is assumed to act uniformly over the diagonal band, yielding occurring when σ_t reaches a value σ_t^y.

The stress condition, see figure 5, in the diagonal web strip is given by

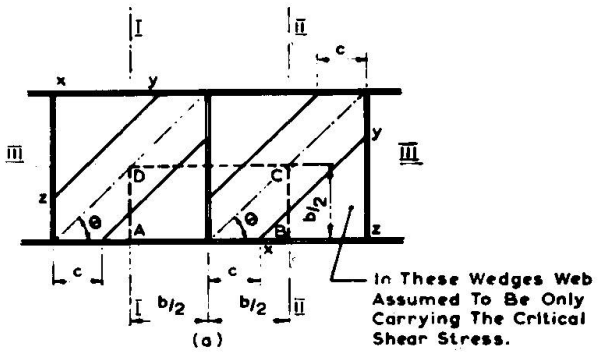

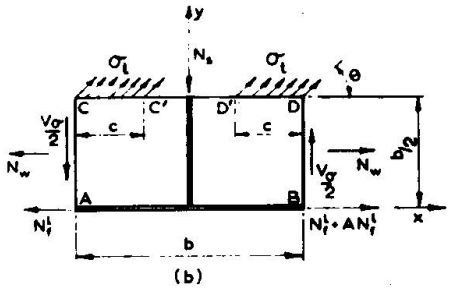

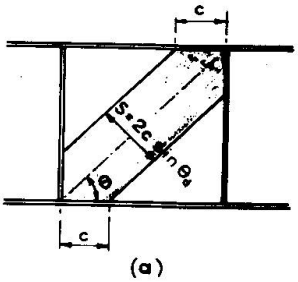

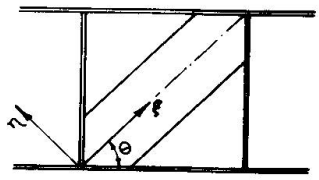

FIG 5

$$\sigma_\zeta = \tau_{cr} \text{ Sin } 2\theta + \sigma_t^{\,y}$$

$$\sigma_\eta = \tau_{cr} \text{ Sin } 2\theta \qquad (1)$$

$$\tau = \tau_{cr} \text{ Cos } 2\theta$$

Using the Huber Von Mises plasticity condition, the material yields when $\sigma_{mc} = \sigma_{yw}$ where

$$\sigma_{mc} = \sqrt{\sigma_\zeta^{\,2} + \sigma_\eta^{\,2} - \sigma_\zeta\sigma_\eta + 3\tau^2} \qquad (2)$$

Substituting equations (1) into (2) and rearranging yields

$$\sigma_t^{\,y} = -\frac{3}{2}\tau_{cr} \text{ Sin } 2\theta + \sqrt{\sigma^2_{yw} + \tau_{cr}^{\,2}\left[\left(\frac{3}{2} \text{ Sin } 2\theta\right)^2 - 3\right]} \qquad (3)$$

The vertical component V_σ of the diagonal stress $\sigma_t^{\,y}$ is given by equation (4)

$$V_\sigma = 2ct \text{ Sin}^2\theta \left(-\frac{3}{2}\tau_{cr} \text{ Sin } 2\theta + \sqrt{\sigma^2_{yw} + \tau^2_{cr}\left(\frac{3}{2}\text{Sin } 2\theta\right)^2 - 3}\right) \qquad (4)$$

The total shear force V_{ult} is equal to the sum of V_σ and the shear force V_{cr} necessary to cause the plate to buckle.

$$V_{ult} = V_{cr} + V_\sigma = \tau_{cr}\, dt + 2ct \text{ Sin}^2\theta \left(-\frac{3}{2}\tau_{cr} \text{ Sin } 2\theta + \sqrt{\sigma^2_{yw} + \tau^2_{cr}\left(\frac{3}{2} \text{ Sin } 2\theta\right)^2 - 3}\right) \qquad (5)$$

Since $\tau_{yw} = \sigma_{yw}/\sqrt{3}$, equation (5) may be rewritten as equation (6).

$$\frac{\tau_{ult}}{\tau_{yw}} = \frac{\tau_{cr}}{\tau_{yw}} + 2\sqrt{3}\,\frac{c\alpha}{b}\,\mathrm{Sin}^2\theta\left(-\frac{\sqrt{3}}{2}\,\mathrm{Sin}\,2\theta\,\left(\frac{\tau_{cr}}{\tau_{yw}}\right) + \sqrt{1 + \left(\frac{\tau_{cr}}{\tau_{yw}}\right)^2\left(\frac{3}{4}\,\mathrm{Sin}^2(2\theta) - 1\right)}\right) \qquad (6)$$

The position of the plastic hinge in the flanges may be theoretically determined using the collapse mechanism shown in figure 2. This mechanism assumes that the hinge coincides with the edge of the diagonal strip and that the loading consists of the vertical component of the diagonal tensile membrane stress σ_t^y. The solution of this simple mechanism reduces to the solution of the cubic equation given in equation (7).

$$\left(\frac{c}{b}\right)^3 - \left(\frac{c}{b}\right)^2 + \frac{4\,z_f\sigma_{yf}}{b^2 t\,\mathrm{Sin}^2\theta\,(\sigma_t^y)} = 0 \qquad (7)$$

where z_f denotes the plastic modulus for flange assembly. It is proposed that when the web buckling stress is less than half the shear yield stress, a depth of web plate $z = 30(1 - \frac{2\tau_{cr}}{\tau_{yw}})$ be assumed to act with the flange assembly.

It is of interest to consider how equation (6) satisfies a number of the limiting conditions.

(1) Very Thin Webs and Rigid Flanges

For very thin webs $\tau_{cr} \to 0$, in which case

$$\frac{\tau_{ult}}{\tau_{yw}} = 2\sqrt{3}\alpha\frac{c}{b}\,\mathrm{Sin}^2\theta$$

Since for rigid flanges, $\frac{c}{b} = 0.5$, then for square web panels in which $\theta = \frac{\pi}{4}$ one obtains the value for τ_{ult} of

$$\frac{\sqrt{3}}{2}\,\tau_{yw} \quad \text{or} \quad \frac{\sigma_{yw}}{2}$$

which agrees with the value obtained from Wagner's Theory (14) for a complete tension field.

(2) Very Thick Webs

When webs are very thick, then $\tau_{cr} \to \tau_{yw}$ and the terms inside the main brackets reduces to zero so that equation (6) reduces to $\tau_{ult} = \tau_{yw}$; which again is as to be expected.

(3) Very Flexible Flanges

Finally, if $\frac{c}{b} \to 0$, as would be the case if the flanges had zero stiffness, and could not withstand any lateral loading, then

$$\tau_{ult} = \tau_{cr}$$

Thus we have seen that equation (6) satisfies the extreme boundary conditions exactly.

When $\sqrt{3}\tau_{cr}$ exceeds the limit of propor tional stress of the material then the effective modulus E_r is less than the modulus of Elasticity E. This reduces the critical shear stress; and to allow for this Basler and his colleagues have recommended that τ_{cr} be replaced by τ_{cre} when $\tau_{cr} > \frac{0.8\sigma_y}{\sqrt{3}}$, τ_{cre} being obtained from equation 8.

$$\frac{\tau_{cre}}{\tau_{yw}} = 1 - \frac{0.16\tau_{yw}}{\tau_{cr}} \qquad (8)$$

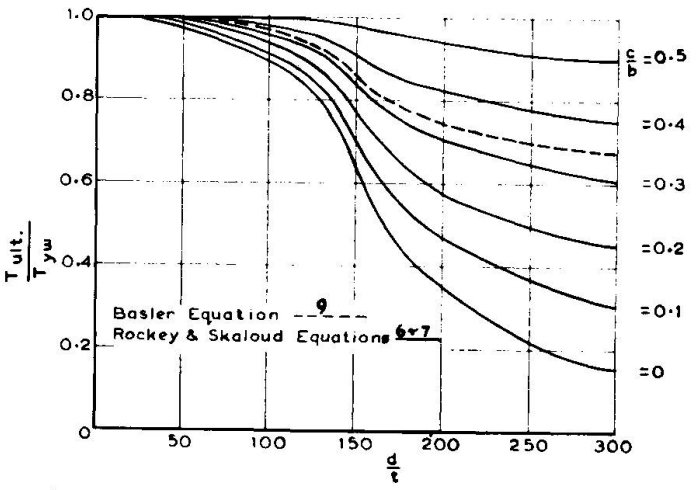

FIG. 6

Using equation (8) in conjunction with equation (6) the relationship between the ratio τ_{ult}/τ_{yw} and the depth to thickness ratio for different values of c/b have been plotted in figure 6 for the case of α equal to 1. The values of τ_{ult}/τ_{yw} as derived from Basler's ultimate load expression, see equation 9, have also been plotted using the same relationship between τ_{cre}, τ_{cr} and τ_{yw}, and it is clearly seen that for very flexible flanges Basler's equation overestimates the strength of the girder and for relatively stiff flanges it underestimates the strength, this being particularly true for larger values of α.

$$W_{ult} = dt\left[\tau_{cr} + \frac{\sqrt{3}\tau_{yw}}{2\sqrt{1+d^2}}\left[1 - \frac{\tau_{cr}}{\tau_{yw}}\right]\right] \qquad (9)$$

The present design procedure, see equations (7) and (8), has been checked (4, 5) against existing experimental data and as will be noted from Figure 7 very good correlation has been obtained.

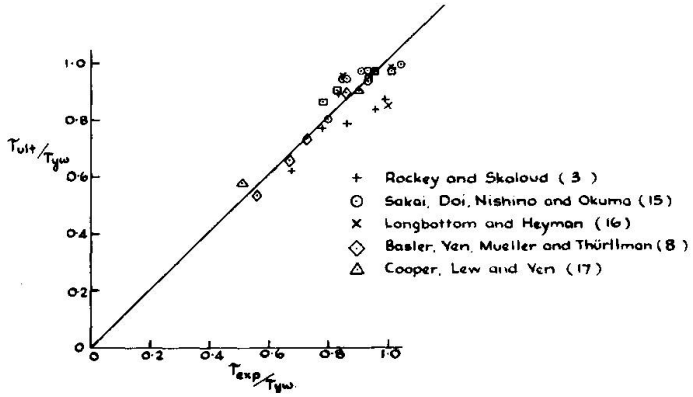

FIG: 7 COMPARISON OF PREDICTED ULTIMATE SHEAR STRESS (τ_{ult}) AND EXPERIMENTAL ULTIMATE SHEAR STRESS (τ_{exp}) FOR WEBS LOADED IN SHEAR.

2.2. Transversely stiffened web plates loaded in shear and bending

Web plates are normally subjected to a combination of shear and bending and in the present section an ultimate load method of design is proposed for this case of loading.

Three important additional factors have to be considered when determining the failure load of a web plate loaded in shear

and bending, these are

(1) the reduction in the buckling stress of the web due to the presence of a bending stress or a direct stress

(2) the influence of the inplane bending stresses upon the value of the diagonal tensile membrane stress σ_t^y which is developed in the diagonal strip

(3) the reduction in the magnitude of the plastic modulus z_f of the flanges due to the presence of the axial compressive and tensile stresses.

For the case of a webplate subjected to combined shear and bending the reduction in the buckling stress τ_{cr} due to the presence of a bending stress σ can be calculated with reasonable accuracy from equation (10).

$$\left(\frac{\sigma_{mb}}{\sigma_{crb}}\right)^2 + \left(\frac{\tau_m}{\tau_{cr}}\right)^2 = 1 \qquad (10)$$

where σ_{crb} = critical bending stress when the plate is subjected to pure bending

τ_{cr} = critical bending stress when the plate is subjected to pure shear

σ_m, τ_m = critical bending and shear stresses when acting together

For the case of all edges being simply supported σ_{cr} and τ_{cr} can be determined from equations (11) and (12)

$$\sigma_{crb} = 23.9 \left(\frac{\pi^2 E}{12(1-\mu^2)}\right)\left(\frac{t}{d}\right)^2 \qquad (11)$$

$$\tau_{cr} = \left(5.35 + \frac{4d^2}{b^2}\right)\left(\frac{\pi^2 E}{12(1-\mu^2)}\right)\left(\frac{t}{d}\right)^2 \quad \text{when } b \geqslant d \qquad (12a)$$

$$\tau_{cr} = \left(5.35\,\frac{d^2}{b^2} + 4\right)\frac{\pi^2 E}{12(1-\mu^2)}\left(\frac{t}{d}\right)^2 \quad \text{when } b \leqslant d \qquad (12b)$$

The plastic modulus z_f will be reduced by the presence of the axial force and for flanges having a simple rectangular cross section the following relationship may be employed to determine the reduced modulus z_{fr}

$$z_{fr} = z_f \left[1 - \left(\frac{\sigma}{\sigma_{yf}}\right)^2\right] \qquad (13)$$

where σ is the axial stress in the flange and σ_{yf} is the yield stress for the flange material.

As stated earlier when a plate girder web buckles in shear it loses its capacity to carry any additional compressive load, likewise when a panel loaded in direct compression buckles the central area of the panel is unable to carry any further direct stress, and any add-

itional direct load has to be carried by the web material adjacent to the flanges and stiffeners.

Since the stress distribution in a yielded panel subjected to shear and bending is very complex it is assumed in the proposed design procedure that after the plate buckles, the flanges alone carry the additional bending moments. Furthermore, it is assumed that the web carries the additional shear loads by the development of a diagonal membrane stress σ_t^y.

When a webplate is loaded by direct bending stresses as well as by shear stresses, the value of the diagonal stress σ_t^y at which yielding occurs is changed from that given in equation (3) to the value obtained from equation (14).

$$\sigma_t^y = \frac{1}{2}\left[-(3\tau_m \sin 2\theta + \sigma_m \sin^2\theta - 2\sigma_m \cos^2\theta) + \sqrt{(+3\tau_m \sin 2\theta + \sigma_m \sin^2\theta - 2\sigma_m \cos^2\theta)^2 - 4\left[\sigma_m^2 + 3\tau_m^2 - \sigma_{yw}^2\right]}\right] \quad (14)$$

Figures 8 and 9 show how the value of σ_t^y varies with the presence of a direct stress. It will be noted that the presence of

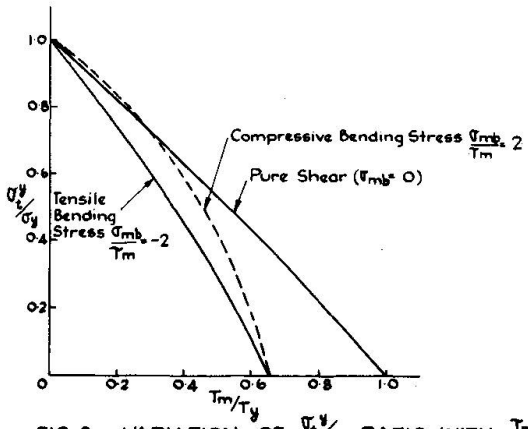

FIG. 8 VARIATION OF σ_t^y/σ_y RATIO WITH τ_m/τ_y RATIO

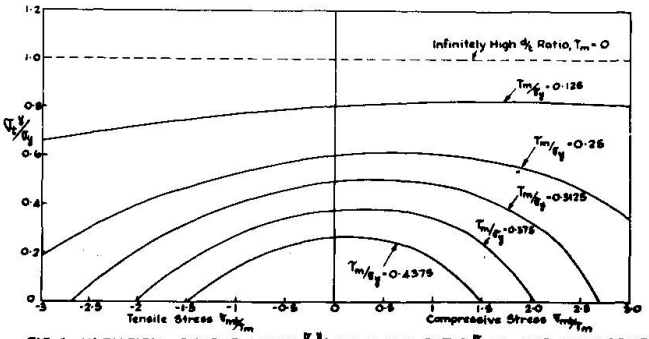

FIG. 9 VARIATION OF THE RATIO σ_t^y/σ_y WITH THE RATIO σ_m/σ_m FOR DIFFERENT VALUES OF THE BUCKLING STRESS τ_m.

a tensile bending stress reduces the capacity of σ_t^y more significantly than does the compressive bending stress. Because of these factors one would expect to observe a spreading of the diagonal band either side of the neutral axis and that the diagonal band in the tension area, because of its reduced σ_t^y value being wider than the band in the compression zone.

It should be appreciated that the bending stresses, σ in the tension zone continue to grow after the plate buckles and therefore the value of σ_t^y in the tension zone will continue to be affected, and that this area will yield first.

The experimental tests conducted by Rockey and Skaloud have shown that the distance 'c' giving the position of the 'central' plastic hinges in the tension flanges is larger than the distance 'c' which occurs in the compression flange. This is to be expected because of the reduced σ_t^y value and the presence of the tension forces in the tension flange which will have the tendency to keep the flanges straight.

In the present design procedure the values of τ_m and σ_m which are to be used in equation (14) are the stresses at which the plate buckles under the combined loading, τ_m being the average shear stress across the web and σ_m is the compressive bending stress at the web/flange junction.

A general expression for the ultimate load can be obtained by combining equations (7), (13) and (14). In section 2.2 the position of the central hinge was obtained by solving equation (7)

$$\left(\frac{c}{b}\right)^3 - \left(\frac{c}{b}\right)^2 + \frac{4z_f\sigma_{yf}}{b^2t\sin^2\theta\ (\sigma_t^{\,y})} = 0 \qquad (7)$$

When a bending stress acts with the shear stress, the value of z_f which has to be used in equation (7) is the reduced value z_{fr} as given by equation (13) and $\sigma_t^{\,y}$ is the modified value of $\sigma_t^{\,b}$ given by equation (14). Equation (7) thus becomes

$$\left(\frac{c}{b}\right)^3 - \left(\frac{c}{b}\right)^2 + \frac{4\sigma_{yf}}{b^2t\sin^2\theta}\ \frac{z_f\left[1 - \left(\frac{\sigma}{\sigma_{yf}}\right)^2\right]}{\sigma_t^{\,y}} = 0 \qquad (15)$$

It will be noted from figures 8 and 9 that $\sigma_t^{\,y}$ varies with the value AM which is the ratio of the applied bending stress to the applied shear stress before buckling occurs. The value of the flange bending stress σ in equation (15) can, for values of σ up to σ_{yf}, be obtained from equation (16).

$$\sigma = \frac{M_y}{I_z} = \frac{(WF)(d + 2t_f)}{2I_z} = W_{ult}(q) \qquad (16)$$

Where I_z = Moment of inertia of a section comprising the flanges only, F is a factor depending upon the type of loading, which for the case of a centrally loaded simply supported girder = $\frac{1}{2}$ where l is the distance of the section to the nearest support. Now for a centrally loaded, simply supported girder,

$$W_{ult} = 2dt\left[\tau_{cr} + \frac{2C}{d}\sin^2\theta\sigma_t^{\,y}\right] \qquad (17)$$

Substituting (15) and (16) into (14) yields

$$\left(\frac{c}{b}\right)^3 - \left(\frac{c}{b}\right)^2 + \frac{4}{b^2t\sin^2\theta}\ \frac{z_f\left[\sigma_{yf}^2 - q^2d^2t^2\left[\tau_{cr} + 2\frac{c}{d}\sin^2\theta\sigma_t^{\,y}\right]2\right]}{\sigma_t^{\,y}\ \sigma_{yf}} \qquad (18)$$

which reduces to an equation of the form

$$\left(\frac{c}{b}\right)^3 - (A)\left(\frac{c}{b}\right)^2 + B\left(\frac{c}{b}\right) + D = 0 \qquad (19)$$

The solution of this equation leads to the solution of $\frac{c}{b}$ and hence the position of the hinge c which when substituted into equation (17) will give the ultimate load W_{ult}.

The above solution does not require the use of any assumed interaction relationship between the shear load ratio (v/v_u) and the moment ratio (M/M_u), since this relationship is incorporated in the solution.

Figure 10 gives typical interaction curves between the ratio v/v_u and M/M_u, which have been obtained using equation for two

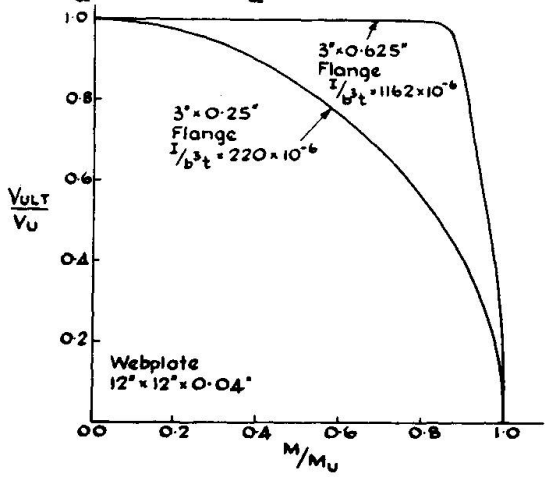

FIG.10 INTERACTION DIAGRAMS - DEMONSTRATING INFLUENCE OF FLANGE RIGIDITY UPON SHAPE OF DIAGRAM

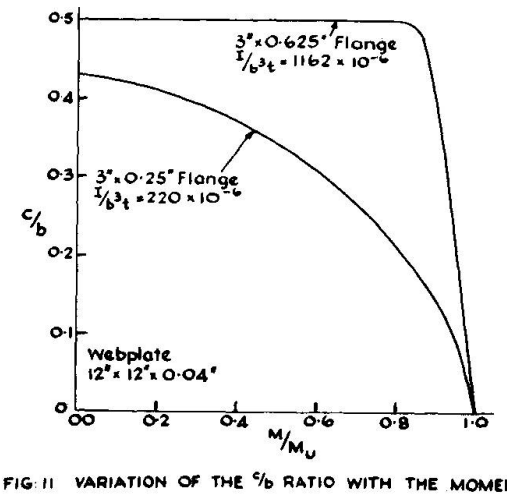

FIG. 11 VARIATION OF THE c/b RATIO WITH THE MOMENT RATIO M/M_u

girders from which it will be noted that the shape of the interaction curves is greatly influenced by the flange rigidity parameter and the slenderness of the web (d/t). For girders with very stiff flanges the loss in shear strength with applied bending stresses is not significant, but with the case of girders with relatively flexible flanges, the influence of the bending stresses upon the z_f value becomes critical and there is a steady loss in shear load carrying capacity. The manner in which the position of the central hinges varies the M/M_u ratio is clearly shown in figure 11. It will be noted that with 'flexible' flanges, as the applied bending stress increases the effective shear stress as buckling decreases and the position of the central hinge moves towards the stiffeners. The reduction of the width of the diagonal tension band together with the reduction in the critical shear stress, which is the stress acting in the triangular areas either side of the diagonal band, means that the shear load capacity decrease steadily with the (M/M_u) ratio.

2.3. Web plates reinforced by both transverse and longitudinal stiffeners and subjected to shear

2.3.1. Pure shear

Figure 12 shows the typical collapse pattern which can be assumed to occur in a longitudinally reinforced web plate subjected to shear.

Consider Panel 1, this panel will impose lateral loading on the flange and it can be assumed that a yield zone will develop as indicated with hinges forming in the flanges as shown, the position of the internal hinge (C_1) in the flange varying with the rigidity of the flange and the buckling stress in the panel. However, since

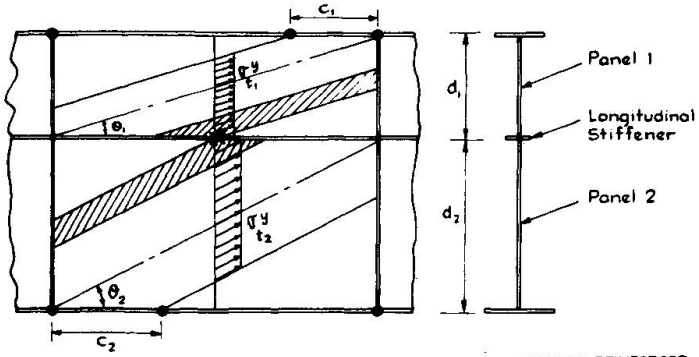

FIG.12 PROPOSED COLLAPSE MECHANISM FOR A LONGITUDINALLY REINFORCED WEB SUBJECTED TO SHEAR

the adjacent panel will act as a very stiff flange at the position of the longitudinal stiffener, the position of the hinge can be assumed at 0.5b. Thus for a panel such as 1, the shear load V_1 will be given by equation (18). In equation (18), the subscripts 1 signify Panel 1.

$$V_1 = \left[\tau_{cr_1} d_1 t + t \sin^2\theta_1 \sigma_{t_1}^{y} \ (C + 0.5b)\right] \tag{20}$$

For Panel 2, a similar procedure can be followed, the load V_2 for this panel can be calculated from equation (19).

$$V_2 = \left[\tau_{cr_2} d_2 t + (0.5b + C_2) \sin^2\theta_2 \sigma_{t_2}^{y}\right] \tag{21}$$

where C_2 is the position of the hinge in the tension flange,

$$V = \left[\tau_{cr_1} d_1 t + \tau_{cr_2} d_2 t + \left[C_1 + 0.5b\right] \sigma_{t_1}^{y} \sin^2\theta_1 + (C_2 + 0.5b)\, \sigma_{t_2}^{y} \sin^2\theta_2\right] \tag{22}$$

When two or more longitudinal stiffeners are employed the shear load carried by the internal panels can be calculated from equations (6) and (7) assuming c/b = 0.5 in these cases.

In such cases if the inclination of the diagonal θ is used then a lower bound solution would be expected, since for such internal panels it would be reasonable to expect that the inclination of the

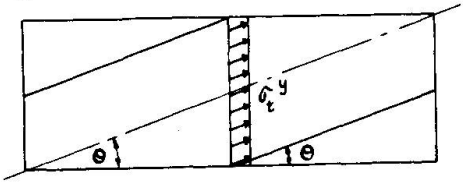

Stress Distribution assumed in Present Theory

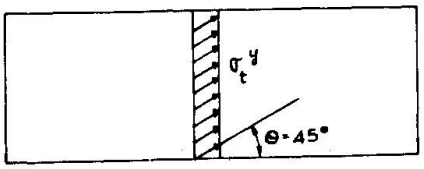

With very rigid flanges, such as occures in an internal bay of a longitudinally stiffened girder, a normal tension field will develop and $\phi \doteq 45°$

FIG.13 PROPOSED COLLAPSE MECHANISM FOR A LONGITUDINALLY REINFORCED WEB SUBJECTED TO SHEAR.

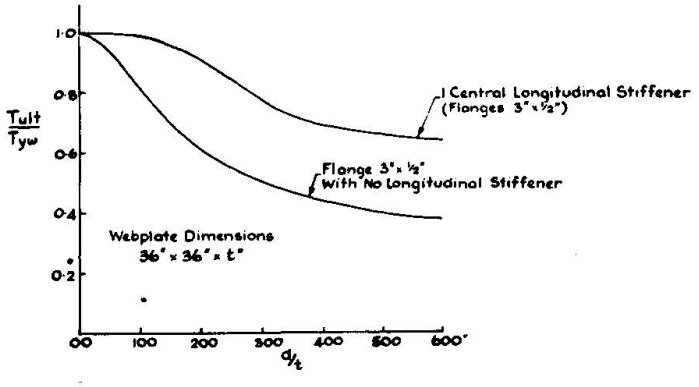

FIG.14 INFLUENCE OF A LONGITUDINAL STIFFENER ON THE SHEAR ULTIMATE STRENGTH OF A WEB

tensile membrane field would approach 45^{o}, as indicated in figure 13. However, further research studies are required before this further

Figure 14 shows the significant gain in ultimate shear load which can be achieved by employing a longitudinal stiffener at mid depth.

2.4. Webplates reinforced by both transverse and longitudinal stiffeners and subjected to shear and bending

Figure 15 shows a typical panel subjected to a combined linearly varying axial direct stress and a shear stress τ. The linearly varying axial stress distribution can be replaced by an axial stress together with a pure bending stress as shown. For example, in Panel 1, there will be a direct compressive stress of σ_{mc1} and a pure bending stress at the flange/web junction of σ_{mb1}.

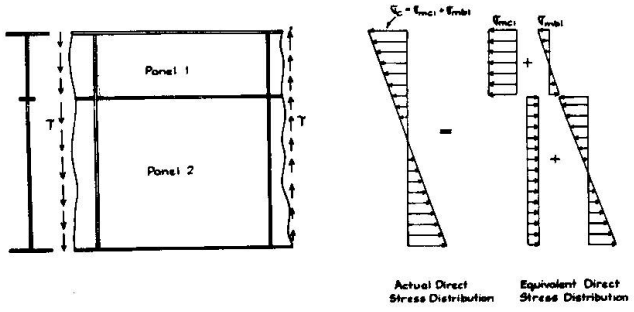

FIG.15 STRESS DISTRIBUTION IN PANELS OF A PLATE GIRDER SUBJECTED TO SHEAR AND BENDING

The critical stresses σ_{mc}, σ_{mb} and τ_m at which will cause buckling under their combined action occurs can be predicted with reasonable accuracy by equation (23).

$$\left(\frac{\sigma_{mc}}{\sigma_{crc}}\right) + \left(\frac{\sigma_{mb}}{\sigma_{crb}}\right)^2 + \left(\frac{\tau_m}{\tau_{cr}}\right)^2 = 1 \qquad (23)$$

where :

σ_{crc} = the critical uniform direct axial stress to cause buckling see equations (24) and (25)

σ_{crb} = the compressive edge stress causing buckling in the panel when loaded in pure bending, see equations (11) and (26)

τ_{cr} = the uniform shear stress to cause buckling, see equations (12a), (12b) and (27)

$$\sigma_{crc} = 4\left[\frac{\pi^2 E}{12(1-\mu^2)}\right]\left[\frac{t}{d}\right]^2$$ when all edges are simply supported (24)

$$\sigma_{crc} = 5.41\left[\frac{\pi^2 E}{12(1-\mu^2)}\right]\left[\frac{t}{d}\right]^2$$ when one longitudinal edge is clamped, the others simply supported (25)

$$\sigma_{crb} = 41.7\left[\frac{\pi^2 E}{12(1-\mu^2)}\right]\left[\frac{t}{d}\right]^2$$ when the compressive longitudinal edge is clamped, the other simply supported (26)

$$\tau_{cr} = \left[7.07 + \frac{3.91}{(b/d)^{\frac{3}{2}}}\right]\left[\frac{\pi^2 E}{12(1-\mu^2)}\right]\left[\frac{t}{d}\right]^2$$ when one longitudinal edge is clamped, the others being simply supported (27)

Once the critical stresses, σ_{mc1}, σ_{mb} and τ_m for the individual panels have been determined, the stress distribution at buckling will be known and the collapse load for each of the panels determined using the basic equations (7) and (14). In a longitudinally stiffened web plate this will involve an iterative procedure since the

axial stresses in the flanges will vary with the shear load. Thus the use of either a desk calculating machine or a small computer is highly desirable.

CONCLUSION

The paper establishes an ultimate load method of design for plate girders having transversely and longitudinally reinforced webplates. In particular, it is shown that the flexural stiffness of the flange members has a significant influence upon the post buckled behaviour of webplates and the design method allows for the interaction which occurs between the buckled webplate and the flanges.

ACKNOWLEDGEMENT

This research project has been sponsored in part by the Construction Industry Research and Information Association, in part by the British Constructional Steelwork Association and by the University College, Cardiff.

SYMBOLS

t	thickness of web plate
t_f	thickness of flange plate
d	clear depth of webplate between flanges
b	clear width of webplate between stiffeners
$\alpha = \frac{b}{d}$	aspect ratio of panel
I	flexural rigidity of flange members about an axis passing through their centroid and perpendicular to the web plate
c	position of plastic hinge, see Figure 2
V_B	ultimate shear load provided by Basler collapse mechanism
V_{exp}	experimental ultimate shear load
V_{ult}	theoretical ultimate shear load
W	applied load
W_{ult}	theoretical ultimate shear load
W_B	collapse load according to Basler mechanism
W_{exp}	experimental ultimate load
M	applied bending moment
M_u	applied bending moment to cause collapse when acting alone
τ	applied shear stress
τ_{cr}	critical shear stress $= K \frac{\pi^2 E}{12(1-\mu^2)} \left(\frac{t}{d}\right)^2$ where K is a non dimensional parameter
τ_{cre}	reduced critical shear stress - see equation (8)
τ_{yw}	shear yield stress of web material
τ_{ult}	ultimate shear stress

σ_{yw}	tensile yield stress of web material
σ_{mc}	maximum comparison stress in Huber Von Mises plasticity condition
σ_{yf}	tensile yield stress of flange material
z_f	plastic modulus of flange
E	Young's Modulus of Elasticity
μ	Poisson's ratio
θ	inclination of diagonal of panel with respect to flanges
σ_{crb}	compressive critical bending stress for a panel loaded in pure bending
σ_{crc}	critical direct stress for a panel loaded in pure compression
σ_{mb}, σ_{mc}, τ_m	compressive bending stress, direct compressive stress and shear stress which when acting in a combined system cause buckling

All other terms are defined as they appear in the text

BIBLIOGRAPHY

(1) Rockey, K.C., "Factors influencing ultimate behaviour of plate girders". Conference on Steel Bridges. June 24th-30th, 1968. British Constructional Steelwork Association, Institution of Civil Engineers, London.

(2) Rockey, K.C. & Skaloud, M., "Influence of flange stiffness upon the load carrying capacity of webs in shear". Final report. 8th Congress New York. Sept. 1968. 11 pages.

(3) Rockey, K.C. & Skaloud, M., "Influence of the flexural rigidity of flanges upon the load carrying capacity and failure mechanism of web in shear". P. 295 - 313. Acta Technica, C.S.A.V. No. 3, 1969.

(4) Rockey, K.C. & Skaloud, M., "The ultimate load behaviour of plate girders loaded in shear", University College, Cardiff, Department of Civil & Structural Engineering Report 1969.

(5) Rockey, K.C. & Skaloud, M., "A survey of the post buckled behaviour of web loaded in shear". University College, Cardiff, Departmental Report.

(6) Basler, K. "Strength of plate girders". Ph.D. Thesis. Lehigh University, 1959.

(7) Basler, K. "Strength of plate girders in shear". A.S.C.E. Proc. No. 2967. ST. 7, p. 151, Oct. 1969. Pt. I.

(8) Thurlimann, B., "Static strength of plate girders". Extract des Memoires de la Societe Royale des Sciences de Liege. Vol. VIII. 1963. p. 137 - 175.

(9) Basler, K., Jen, B.T., Mueller, J.A. & Thurlimann, B., "Web buckling tests on welded plate girders". Welding Research Council Bulletin. No. 64. Sept. 1960.

(10) Chern, C. & Ostapenko, A., "Ultimate strength of plate girders under shear". Fritz Engineering Laboratory Report August, 1969. Report No. 328.7.

(11) Dimitri, J.R. & Ostapenko, A., "Pilot tests on the ultimate static strength of unsymmetrical plate girders". Fritz Engineering Report No. 328.5. Lehigh University, U.S.A. 1968.

(12) Schueller, W. & Ostapenko, A., "Static tests on unsymmetrical plate girders main test series". Fritz Engineering Lab. Report No. 328.6, Lehigh University, U.S.A. 1968.

(13) Cook, I.T. & Rockey, K.C., "Shear buckling of rectangular plates with mixed boundary conditions". The Aeronautical Quarterly, Vol. XIV. March, 1963.

(14) Wagner, H., "Flat sheet metal girders with very thin metal webs". Parts I, II and III. N.A.C.A. T.M. 604, 605 and 606, 1931.

(15) Sakai, F., Doi, K., Nishino, F. & Okumwa, T., "Failure tests of plate girders using large sized models". Structural Engineering Laboratory Report. Department of Civil Engineering, University of Tokyo (1966). In Japanese.

(16) Longbottom, E. & Heyman, J., "Experimental verification of the strengths of plate girders designed in accordance with the revised British Standard 153: Tests on Full Size and on Model Plate Girders". Inst. of Civil Engineers, 1956.

(17) Cooper, P.B., Lew, H.S. & Yen, B.T., "Welded constructional alloy steel plate girders". Journal Structural Division. A.S.C.E. Vol. 90. No. ST1. pl. 36. 1964.

Ultimate Static Strength and Fatigue Behavior of Longitudinally Stiffened Plate Girders in Bending

Résistance à la ruine statique et comportement à la fatigue des poutres à âme pleine fléchies, munies de raidisseurs longitudinaux

Statische Tragfähigkeit und Ermüdungsverhalten längsversteifter, biegebeanspruchter Vollwandträger

YUKIO MAEDA
Dr.-Eng.
Professor of Civil Engineering
Osaka University, Osaka, Japan

I. INTRODUCTION

This paper is intended to present a study on ultimate static strength and fatigue behavior of thin-walled deep plate girders. The present study is based on experiments conducted at Osaka University, Japan, on longitudinally stiffened large -size welded steel plate girders, aiming at their test panel in pure bending.

Firstly, static bending tests are carried out to examine the influence of initial web deflection, slenderness ratio of web, rigidity of longitudinal stiffener and hybrid combination of materials upon the behavior of test panel in pure bending of the plate girders. Secondly, fatigue tests are made to examine patterns of initiation of fatigue cracks in the panels in pure bending of the plate girders. subjected to repeated loads, and the influence of aspect ratio of the test panels, slenderness ratio of web and longitudinal stiffeners upon lateral deflections of the web in relation with the initiation of fatigue cracks.

In this paper, the test results will be mainly described with discussions.

II. STATIC BENDING TESTS

1. Design of Test Girders

Design details of eight girders for the tests are given in Fig. 1 and Table 1.

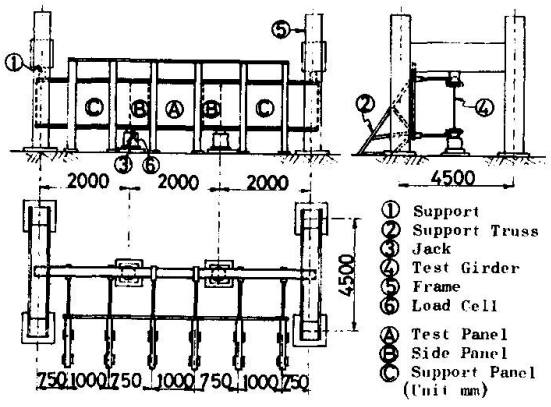

Fig. 1. Test Set-Up.

Table 1. Dimensions of Test Panel of Static Test Girders

Girder No.	Size of Flange Comp.	Size of Flange Ten.	Size of Flange	Size of Longi. Stiff.	t	b	$\frac{b}{t}$	$\frac{a}{b}$	$\frac{A_w}{A_f}$	$\frac{c}{d}$	$\frac{c_s}{d_s}$	$\frac{\gamma}{\gamma^*}$
	(mm)	(mm)	(mm)	(mm)	(mm)	(mm)						
B-1	200x13	200x13	—	—	4.50	1125	250	0.75	1.95	7.69	—	—
B-2	200x13	200x13	—	—	4.59	1349	294	0.75	2.38	7.69	—	—
B-3	200x13	200x13	—	60x5	4.72	901	191	0.75	1.56	7.69	12	3.65
B-4	200x13	200x13	—	65x5	4.56	1126	247	0.75	1.95	7.69	13	4.44
B-5	200x13	200x13	—	70x5	4.58	1351	295	0.75	2.38	7.69	14	4.72
B-6	200x10	200x10	50x50x6	60x5	4.65	902	194	0.75	1.56	6.00	12	3.84
B-7	200x10	200x10	50x50x6	65x5	4.51	1123	249	0.75	1.98	6.00	13	4.61
B-8	200x10	200x10	50x50x6	70x5	4.58	1351	295	0.75	2.41	6.00	14	4.72

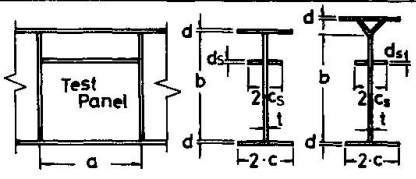

The large-size test girders are provided with a span length of 6.0 m and a web thickness of 4.5 mm, and consist of a test panel at the middle part, two supporting panels and two side panels, so that the girders can fail at the test panel subjected to pure bending. The girders are designed into three kinds of slenderness ratio b/t such as about 200 (Test Girders B-3 and -6), about 250 (Test Girders B-1, -4 and -7) and about 300 (Test Girders B-2, -5 and -8). The test girders B-6, -7 and -8 are provided with a Y - shape compression flange instead of a T - shape flange. All of

the test girders except B-1 and B-2 are stiffened by single double-sided longitudinal stiffener.

Thickness of the flange plates is designed to avoid a local buckling in plastic range of flange material. An actual rigidity γ of the longitudinal stiffener is selected to be 3 to 5 times γ^*, which expresses a theoretical rigidity required for an ideal stiffener by the linear theory of web buckling. These design rigidities were determined with the results of the author's preliminary tests [1] at Osaka University. Furthermore, the preliminary tests have required that a connection of compression flange with transverse stiffeners and the one of longitudinal stiffener with transverse ones should be welded, to increase the ultimate strength. The girders were fabricated carefully by welding to make initial web deflections less than the web thickness, but a heating had to be applied to the weld part of flanges and stiffeners along the boundary of test panel, to satisfy the requirement for initial deflections of the girders except B-3 and B-6.

Steel material used for flange plates and angles is a corrosion resistant quenched and tempered alloy steel SMA58 (designated at JIS which is short for the Japanese Industrial Standards, with tensile strength 58~73 kg/mm^2) . Steels used for webs and stiffeners are corrosion resistant high strength steel SMA50 (designated at JIS with tensile strength 50~62 kg/mm^2) and SS41 (designated at JIS with tensile strength 41~52 kg/mm^2, ordinary carbon steel), respectively. Coupon tension tests showed the following average yield stresses in kg/mm^2, as 52.60 and 51.50 for 13 mm thick and 10 mm thick flange plates, respectively and 52.65 for flange angles and 50.80 for web plates.

2. Test Apparatus and Measurements

The test girders are simply supported at the upper ends below a shoe attached to two support frames fixed to a test floor, and loaded upward equally at a distance of 2.0 m from the both ends by means of two oil jacks of 200 tons capacity, so that the girder can be subjected to a constant pure bending moment between two loading points. The applied loads are recorded by two load cells of 200 tons capacity.

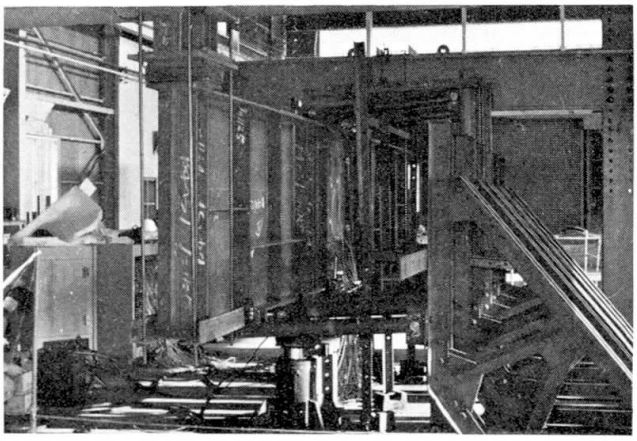

Fig. 2. Truss Frames against Lateral Buckling.

The flanges are restrained laterally by the use of six supporting truss frames rigidly connected to the test floor, as seen in Fig. 2. Lever arms of steel pipe with a diameter of 70 mm are pin-connected to the girder flanges at one end and to the truss frames at the other end, so as to allow free vertical and rotational movements, but restrict lateral movements of the flange .

Lateral deflections of web at the teat panel before and during the test, are recorded by means of such a device made specially for the present tests, as shown in Fig.3. Two steel square pipes of 50 x 50 in mm are fixed horizontally to two transverse stiffeners at the loading points. An aluminum angle bar to which dial gages are attached, will move along the square pipes which will act as a rail, and will be fixed by magnet stands when readings are made. Recordings of the web deflection are made by dial gages at points of 7 x 5 for the test girders B-1, -3, -4, -6 and 8 x 5 for B-2, -5, -8.

Each girder is instumented with electrical resistance strain gages to measure strains on the transverse and longitudinal stiffeners as well as the flange and web plates, and readings are recorded by a digital automatic strain indicator. Vertical deflections of each girder and lateral and rotational movements of the flange at the test panel are recorded by dial gages.

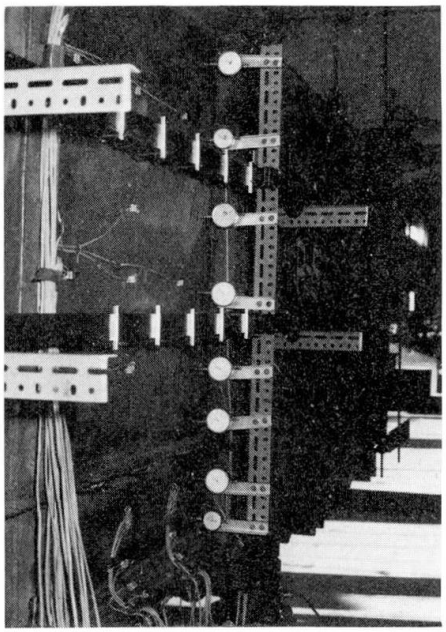

Fig. 3. Measurement of Web Deflections.

3. Test Results and Discussions

(1) Overall behavior of girders

It is noted that the girders which have a hybrid feature, showed a more rapid progress of deformation approaching to failure near the ultimate load than the one observed for the non-hybrid girders at the author's preliminary tests[1]. This observation could be explained by the facts that the compression flange had acted as one of the frame members to restrain strains in a web up to the first yield of web material at its upper edge, and then, with a progress of yielding of the flange material, the web strains in plastic region began to flow rapidly released from restraint by the flange, and that, on the other hand, ductility of the material used for the flange is smaller.

(2) Failure modes and ultimate strength

Ultimate loads P_u for each girder are given in terms of the total failure load in Table 2 with theoretical loads of web buckling P_{cr} calculated from the linear theory, theoretical loads of compression flange yielding P_y and theoretical full-plastic loads P_p calculated from the simple plastic theory. Table 2 indicates that each value of P_u is larger than the corresponding value of P_{cr} for all of the girders, and that all of the values of P_u except for B-1 girder are larger than the corresponding ones of P_y, and furthermore the value of P_y for B-3 and B-7 girders is larger than even the one of P_p.

Table 2. Theoretical Critical Loads and Observed Ultimate Load (in Ton)

Test Girder	P_{cr}	P_y	P_p	P_u
B-1	29.0	198.0	226.8	175.0
B-2	26.0	248.8	289.1	210.0
B-3	143.0	151.0	170.2	175.0
B-4	136.1	198.0	226.8	210.0
B-5	119.6	248.8	289.1	265.0
B-6	152.3	158.2	171.9	185.0
B-7	144.4	205.3	227.9	230.0
B-8	126.8	256.3	289.7	280.0

Stresses which the web plate cannot resist owing to its deformations, have been generally redistributed to the compression flange, although the stress redistribution at B-3 and B-6 girders of $b/t = 200$ was not remarkably observed. Therefore, it seems that the collapse of plate girders can be governed by a failure of flange in compression.

Recorded ultimate collapse moments and observed failure modes of the compression flange for each girder are shown in Table 3. For examples, the failure modes of the girders B-2, -5, -7 and -8 are demonstrated in (a), (b), (c) and (d) of Fig.4, respectively. The critical slenderness ratio of web against vertical buckling of the compression flange, when calculated with the equation given by Basler[2], is larger than that given for the web of each test girder. Also, Toprac's equation[3] shows for all of the test girders that critical stresses for the vertical buckling are smaller than those for the lateral buckling and the torsional buckling. Therefore, it follows that the vertical buckling may not occur theoretically for any of the test girders, but B-2 girder collapsed due to the vertical buckling of compression flange with 70 mm inward penetration into the web after yielding of the flange over its whole thickness. Because an increase of lateral deflec-

Table 3. Modes of Failure of Compression Flange

Test Girder	Ultimate Moment (t-m)	Mode of Failure
B-1	175	Torsional buckling
B-2	210	Vertical buckling
B-3	175	Torsional buckling with local buckling
B-4	210	Lateral buckling with local buckling
B-5	265	Lateral-torsional buckling with local buckling
B-6	185	Lateral buckling with local buckling
B-7	230	Lateral buckling with local buckling
B-8	280	Lateral buckling with local buckling

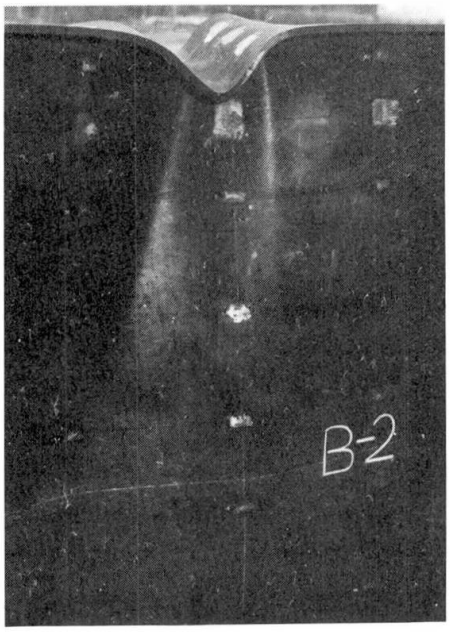

Fig. 4 (a)

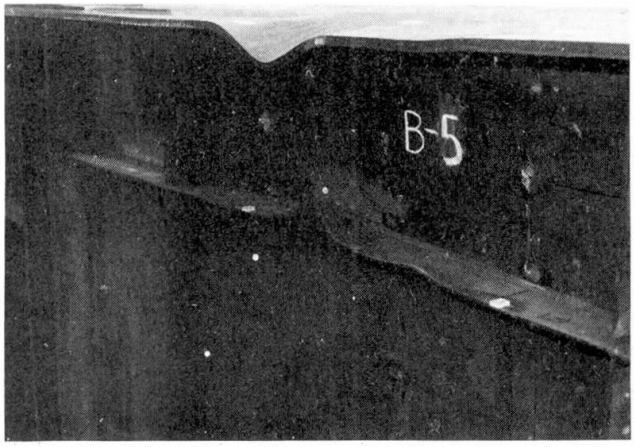

Fig. 4 (b)

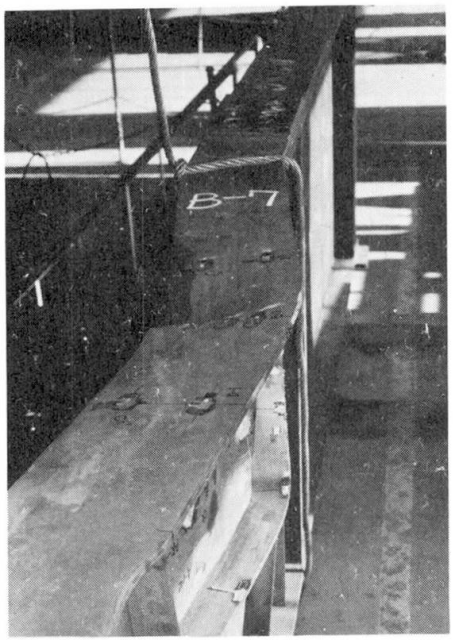

Fig. 4 (c)

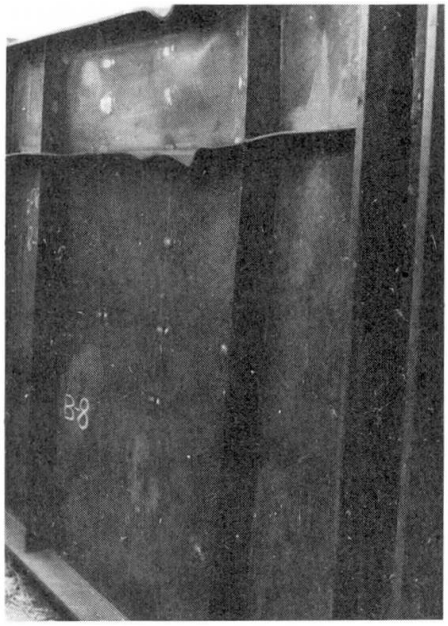

Fig. 4 (d)

Fig. 4. Examples of Failure Modes of Test Girders.

tions of the web which is not provided with a longitudinal stiffener, decreased greatly its vertical stiffness against the flange penetration.

Among B-2, -5 and -8 girders which have the same slenderness ratio of web 300, B-5 and B-8 did not show the vertical buckling, because the former is provided with the longitudinal stiffeners and the latter has a more stiff Y - shape flange. The test values of flange buckling for the test girders B-4, -5, -6, -7 and -8 which collapsed due to the lateral buckling, agreed fairly well with the calculated values by Basler's equation[2]. On the other hand, the test values of flange stress at the time of torsional flange buckling in the girders B-1 and B-3 verify well the

equation given by Basler [2] and Haaijer [4].

It is evident that a shape of compression flange influences greatly upon the pattern of flange buckling and the ultimate strength of girders. The sectional area of compression flanges is designed to be 260 cm^2 through all of the girders, but the shape is selected to be either T - shape or Y - shape. While vertical flexural rigidity and torsional rigidity of the Y- shaped flange are 15 times and 4 times the corresponding rigidity of the T - shaped flange, lateral flexural rigidity of the Y - shaped flange is 0.86 times that of the T - shaped one. In fact, B-6, -7 and -8 girders collapsed due to the lateral buckling of their Y -shaped flange. Furthermore, the girders with a Y -shaped flange showed a larger ultimate load than the girders with a T - shaped flange, compared under the slenderness ratio of web.

(3) Strain distributions in compression flange

The compression flange showed a uniform distribution of strains over its width up to 40~60 % of the ultimate load, and afterwards exhibited in general a non-uniform distribution of strains due to lateral bending of the girder.

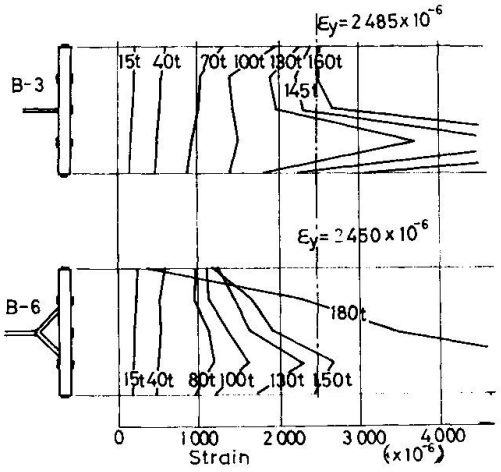

Fig. 5. Strain Distributions in Compression Flange

Fig. 5 shows the strain distribution in the compression flange of the girder B-3 which collapsed after the full yielding over its entire section and of the girder B-6 which corresponds to B-3 in the web slenderness ratio.

(4) Strain distributions on cross section of girder

Observation of strain distributions due to vertical bending reveals that, in the girders without longitudinal stiffener, redistribution of the web stresses to the compression flange develops accompanied by a large amount of movement of the neutral axis to the tension side, since lateral deflections of compressed part of the web increase from the initial stage of loading. Lateral deflections of the web of the girders provided with longitudinal stiffeners are restrained, so that especially the girders B-3 and B-6 of b/t = 200 may demonstrate little the stress redistribution and their almost entire section acts effectively even at the final stage of loading, with only a little movement of the neutral axis. In the girders with b/t of 250 and 300, however, the web stresses are redistributed to the compression flange and the longitudinal stiffeners due to a decrease of resistance of the web against compression, because lateral deflections in a sub-panel in compression increase locally. Fig. 6 illustrates the observations for B-1 and B-7 girders.

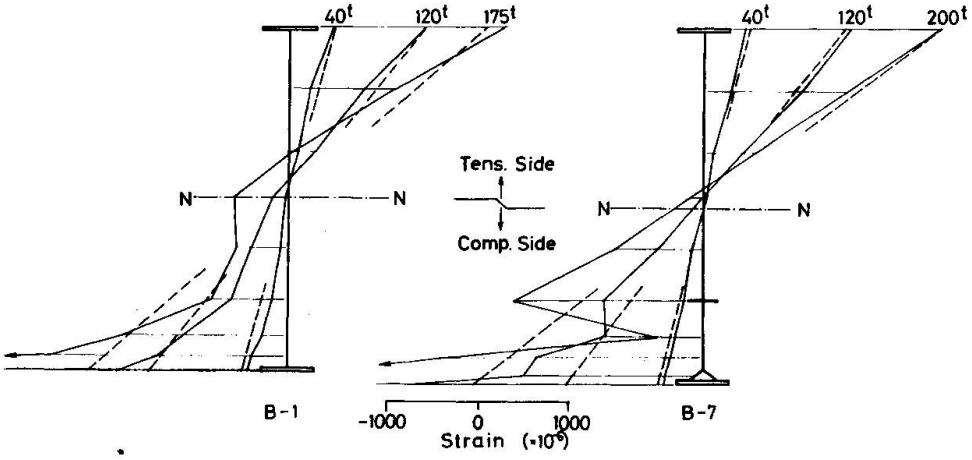

Fig. 6. Strain Distributions due to Bending

(5) Lateral deflection of web

Measurements showed that the maximum value of initial web deflections was 0.3~0.7 t for the girders of b/t = 200 and 300, and 1.3 t for the girder B-2 to 1.6 for B-8 of b/t = 300, and that those values

were less than the limit b/ 150 specified by AWS Specifications[5]. A decrease of strength due to these initial deflections was not clearly observed in the ultimate collapse load.

During loading, lateral deflections of the web of the girders not provided with longitudinal stiffeners, increased rapidly in the compressed part with an increase of load, to reach 3∼4 t near the ultimate load. The lateral deflections of the web of the girders with longitudinal stiffeners increased gradually, but near the ultimate load increased abruptly, to reach to the maximum value of 0.5∼1.0 t for the girders b/t = 200 and 1.0∼2.0 t for b/t = 250 and 300.

In general, the configuration of web deflections is the one of increased initial deflections, but the deflection curve of the girders without longitudinal stiffeners changed from an initial one with double curvatures to a final one with single curvature. Fig. 7 illustrates some measurements for the girders B-1, -4 and -7.

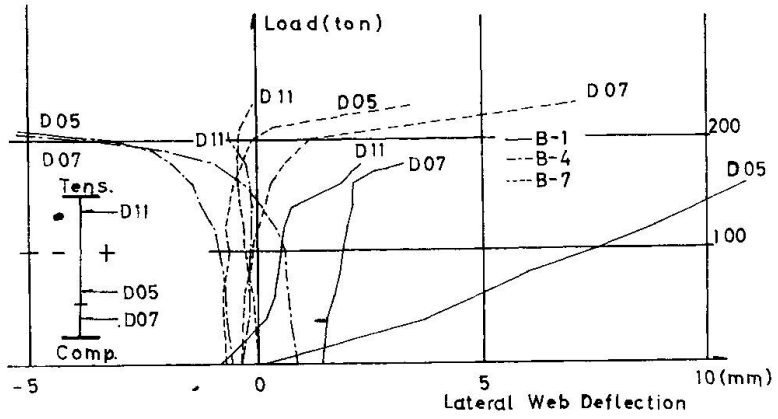

Fig. 7. Load versus Lateral Web Deflection

(6) Strains in longitudinal and transverse stiffeners

In the author's preliminary tests[1] on large-size plate girders, an increase of strain of a longitudinal stiffener was hardly observed with increasing loads, because the longitudinal stiffeners not welded to transverse ones, were not restrained from their rotation with increasing deflections of the web. At the present tests, however, the both stiffeners are welded together, so that the longitudinal stiffener behaved like a member of rigid frame for the sub-panel of the web, and its compressive strains increased with increasing loads, to exceed the yield strain of material near the ultimate load and then, to buckle with a similar mode with the flange.

On the other hand, transverse stiffeners showed a slight increase of strains with increasing loads, and finally reached to only about 500 x 10^{-6} .

(7) Effective width of web plate

The flexural strains on a section at the center line of the test panel are shown for various loads in Fig. 6. The strains showed a nonlinear distribution due to an initial deflection of the web with an increase of load, and when loaded in the post buckled range of the web, a loss of effective width of the web resulted in moving of the neutral axis, a reduction of the effective sectional modulus and a corresponding increase of compressive strains.

Basler [2] gave 30 t for the effective width of web at the ultimate load for the girders without longitudinal stiffeners, but the present tests showed about 60 t for B-1 and about 48 t for B-2 as the effective width in the compressed side of the web. Table 4 gives the values of effective width, which are calculated by equating the resisting moment due to the compressive stress distribution about the neutral axis to the moment of idealized stress distribution, taking into consideration a loss of the section at the compressed part of web or at each sub-panel in compression at the ultimate state. Since it could be observed that a full section of the girders B-3 and B-6 of b/t = 200 acted almost full effectively

Girder No.	$\frac{b}{t}$	$\frac{b_1}{t}$	$\frac{b_2}{t}$	$\frac{b_3}{t}$	$\frac{b_e}{t}$	$\frac{b_n}{t}$	$\frac{b_e}{b_n}$
B-1	250	59.1	—	—	0.236	0.633	0.373
B-2	294	47.6	—	—	0.162	0.619	0.262
B-4	247	18.9	21.1	65.1	0.426	0.560	0.761
B-5	295	22.6	16.1	45.8	0.286	0.548	0.522
B-7	249	18.6	15.0	47.0	0.324	0.541	0.599
B-8	295	31.1	17.6	42.0	0.307	0.563	0.545

$b_e = b_1 + b_2 + b_3$

Table 4. Effective Width of Web

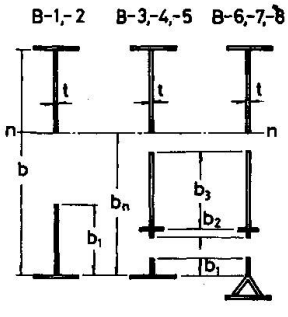

without its loss, the values for those girders are excluded from Table 4. The Table indicates that the overall effective width is about 0.5∼0.8 of the width in compression.

(8) Ultimate strength

The ultimate collapse load of plate girders will be governed by such parameters related to the pattern of buckling of their compression flange, as aspect ratio, web slenderness ratio, strength and rigidity of longitudinal stiffeners, sectional area ratio of web to flange, lateral and torsional rigidities of the compression flange, etc.

The ratio of test values of the ultimate moment to theoretical values of the full-plastic moment calculated from the simple plastic theory, is 0.77 for B-1, and 0.73 for B-2, but 1.03, 0.93 and 0.92 for B-3, -4 and -5, respectively and 1.08, 1.01 and 0.97 for B-6, -7 and -8, respectively. The girders provided with longitudinal stiffeners may resist against the ultimate moment almost close to the full - plastic moment.

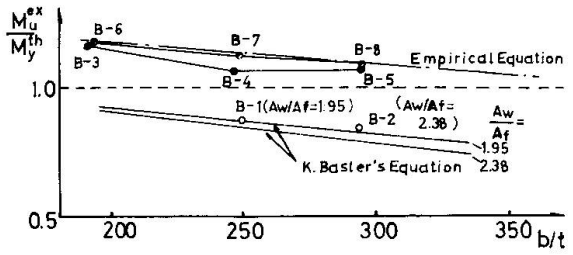

Fig. 8. Ultimate Moment versus Slenderness Ratio

Fig. 8 shows the relation between test values of ultimate moment M_u^{ex} divided by theoretical yield moment M_y^{th} in the compression flange and slenderness ratio of the web. The ultimate load which the girders with longitudinal stiffeners can carry, is about 1.2 times for b/t = 250 and 1.3 times for b/t =300 as large as that for the girders with no longitudinal stiffener. It is seen that the ultimate loads calculated by the following equation which was proposed by Basler[2]

$$\sigma_u = \sigma_y \left\{ 1 - 0.0005\, A_w/A_f' \left(b/t - 5.7 \sqrt{E/\sigma_y} \right) \right\}$$

are in good agreement with those obtained in the tests for the girders which are built-up with a hybrid combination of material.

It is furthermore recognized that the ultimate moments M_u^{ex} for the girders with longitudinal stiffeners are larger than the theoretical moments M_y^{th} correspondingly, and that M_u^{ex} for the girders with Y - shaped flange are larger than those for the girders with T - shaped flange. M_u^{ex} for the girders B-6, -7 and -8 will be expressed as an upper limit by the following experimental equation:

$$M_u^{ex}/M_y^{th} = - 0.000796\ b/t + 1.322,$$

which results in $M_u^{ex}/M_y^{th} = 1.0$ for b/t = 405.

III. FATIGUE TESTS

1. Design of Test Girders

Design details of six large-size welded test girders are illustrated in Fig.9 and dimensions of test panels are given in Table 5. Span length of the girders is 7.0 m, their web thickness is 3.2 mm, their web height is 80 cm or 96 cm, aspect ratio of the test panels is 0.75 or 1.0, and slenderness ratio of the web is 250 or 300. Half of the test girders are provided with single one-sided longitudinal stiffener in the test panels and the others are not provided with it. It should be noticed that the longitudinal stiffener is welded to transverse stiffeners, but the transverse stiffeners in the test panels are not welded to a flange in tension,

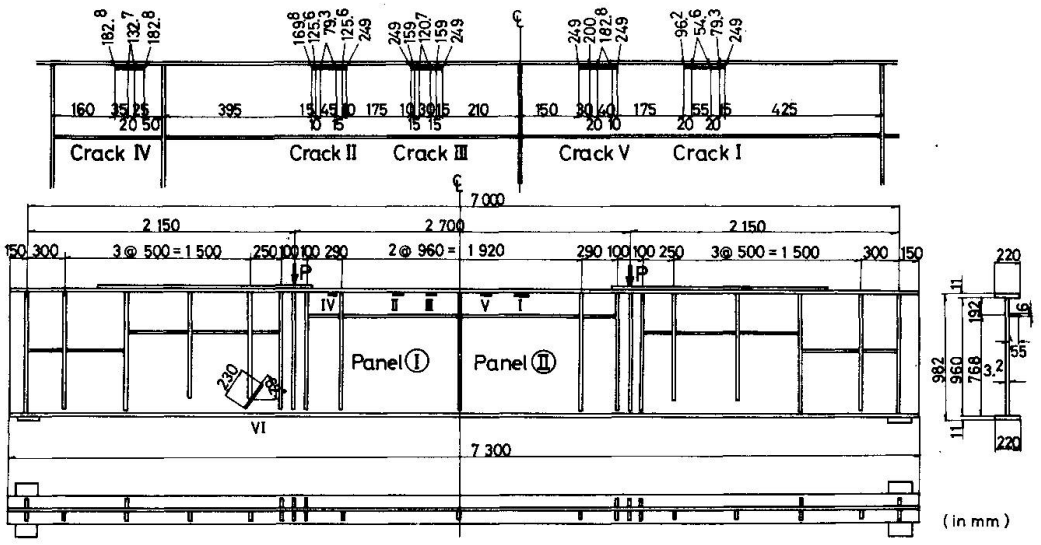

Fig. 9. Overall View and Fatigue Cracks of Girder F-5.

Table 5. Dimensions of Test Panels of Fatigue Test Girders

Girder No.	F-1	F-2	F-3	F-4	F-5	F-6
Size of Flanges (mm)	220x11	220x11	220x11	220x11	220x11	220x11
Depth of Web, (b) (mm)	800	800	960	960	960	960
Thickness of Web, (t) (mm)	3.2	3.2	3.2	3.2	3.2	3.2
Slenderness Ratio, (b/t)	250	250	300	300	300	300
Spacing of Transverse Stiffeners, (a) (mm)	800	800	720	720	960	960
Aspect Ratio, (a/b)	1.0	1.0	0.75	0.75	1.0	1.0
Number of Longi. Stiff.	1	0	1	0	1	0
δ/δ^* for Longi. Stiff.	4.28	—	5.30	—	3.83	—

but cut at 2 cm above the flange, to avoid a decrease of fatigue strength of the flange due to its welding to transverse stiffeners. The test girders are simply supported, and two concentrated equal loads P are applied to the girders downward at the distance of 2.15 m from each support. Therefore, the two test panels are subjected to a constant bending moment.

Steel material used for the flanges is a corrosion resistant high strength steel for welded structures SMA50 designated at JIS, and steel for the web and the stiffeners is respectively a high strength steel for ordinary structures SM50 and a carbon steel for welded structures SM41, designated at JIS.

2. Test Apparatus and Measurements

Repeated loads are applied with 285 cycles per minute by jacks of a Losenhausen-type universal fatigue testing machine, up to the number of cycles of $2\sim3 \times 10^6$, as seen in Fig. 10. The upper limit of one applied load is selected 20~22 tons, up to which strains in the tension flange can keep a linear relationship with the load. The lower limit is selected 6~8 tons so that the strains in the tension flange can be nearly equal to the dead load stress, which will occur at an actual bridge for which the test girders will be intended. Table 6 gives applied loads and stresses for each girder.

The girder is provided with truss-type frames against lateral buckling. At each number of loading such as 1×10^4, 3×10^5, 7×10^5, 1×10^6, 2×10^6, the loads are lowered down to zero and measurements are carried out. For the test panels, stresses in flanges and web are recorded by strain indicators, and lateral deflections of the web are measured by dial gages. Also, vertical deflections at the span center and at $\frac{1}{4}$ span are measured by dial gages. An initiation of cracks due to fatigue is observed every number of loading of 3.5×10^4.

3. Test Results and Discussions

(1) Fatigue cracks

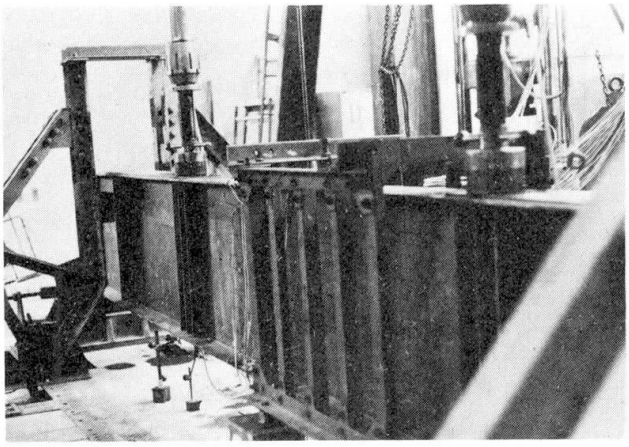

Fig. 10. Overall View of Test Set-Up.

Table 6. Applied Loads and Lower Flange Stresses

Girder No.	Applied Loads P (ton)		Applied Stresses σ (kg/cm^2)		
	P_{max}	P_{min}	σ_{max}	σ_{min}	$\sigma_{max}-\sigma_{min}$
F-1	21	8	2001	762	1239
F-2	20	8	1895	758	1137
F-3	22	6	1694	462	1232
F-4	20	6	1534	460	1074
F-5	21	6	1616	462	1154
F-6	20	6	1534	460	1074

Fig. 11. Location of Cracks Type BM-1 in Girder F-5.

Table 7. Initiation of Fatigue Cracks

Girder No.	Sequence of Cracks In Test Panels	Sequence of Cracks Outside Test Panels	Type of Cracks	Number of Cycles (x10^4)	Crack Length (mm)
F-1		I	BS-1	82.1	95
		II	BS-1	84.1	20
F-2	I		BM-1	40.5	125
		II	—	60.5	85
	III		BM-1	85.5	75
	IV		BM-1	104.0	75
		V	BS-1	162.8	140
F-3		I	BS-1	144.0	20
		II	—	150.0	130
F-4		I*	BM-1	56.6	30
		II*	BM-1	154.9	40
F-5	I		BM-1	54.6	55
	II		BM-1	79.3	45
	III		BM-1	120.7	30
		IV*	BM-1	132.7	20
	V		BM-1	182.8	40
		VI	BS-1	203.4	10
F-6	I		BM-1	12.7	95
	II		BM-1	25.7	105
	III		BM-1	40.2	70
		IV	BS-1	123.3	40

Toprac[6] divided the types of fatigue crack observed at his study on full-size hybrid girders under pure moment into three types, according to the location of cracks: Type BM-1, cracks found in the compression part of the web along the toe of fillet welds to connect web to flange; Type BM-2, cracks found in the web at the end of transverse stiffeners; and Type BM-3, cracks initiated in a tension flange.

Gurney[7] found at his study on fatigue strength of high tensile steel beams with transverse stiffeners under combined bending and shear, that Type BS-1 cracks among five types of fatigue cracks will be initiated prevailingly as the first crack. Type BS-1 cracks are found near the end of transverse stiffeners either in the heat affected zone of the web along the toe of the fillet welds or in the welds themselves, and propagate in the direction perpendicular to the tensile principal stress.

The initiation of cracks is summarized as shown in Table 7 , where number of cycles and crack length at the time of crack finding are shown, and classifications are given according to the designation of Toprac and Gurney. In the table — mark means a crack not designated by the both, and * mark expresses a crack outside the test panels, but in the region of pure bending moment.

Figs. 9 and 11 shows initiations and propagations of cracks for the girder F-5. Fig. 12 illustrates a crack Type BM-1 found in the girder F-6. The test results indicate the following features:

1) Among the types of crack designated by Toprack and Gurney, only BM-1 and

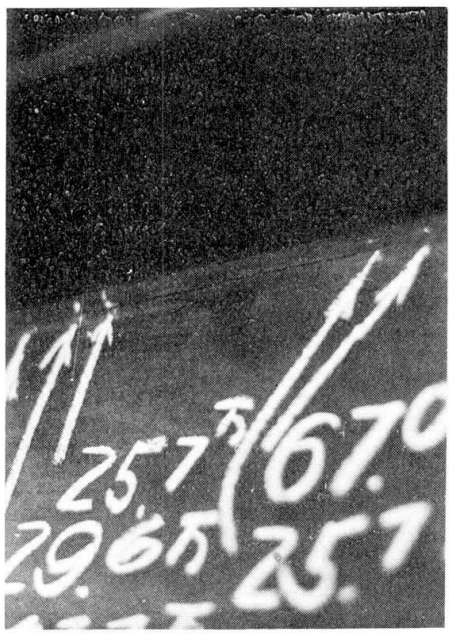

Fig. 12. Crack Type BM-1 in Girder F-6.

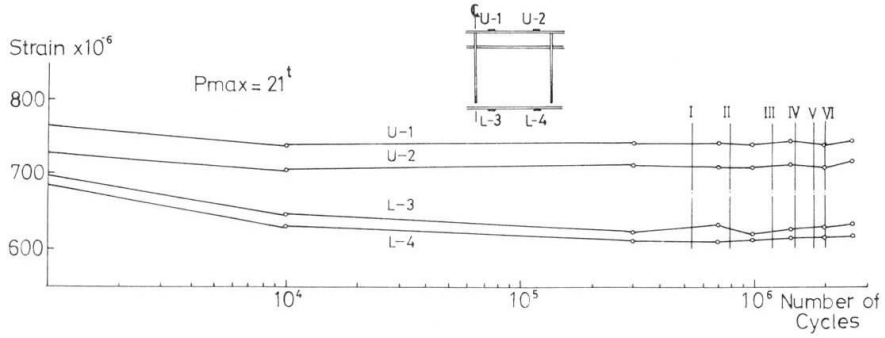

Fig. 13. Variation of Strains in Flanges of Girder F-5.

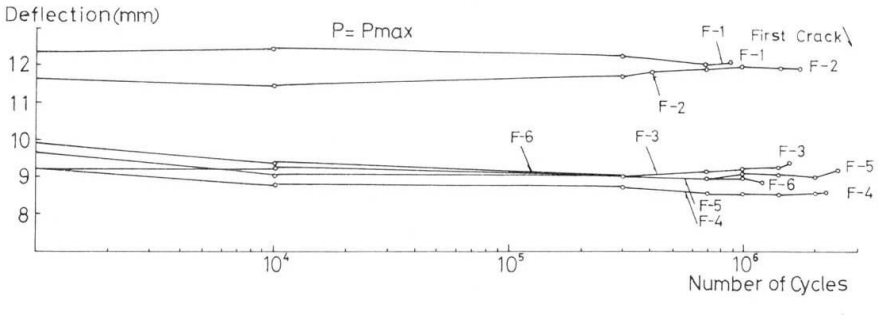

Fig. 14. Variation of Center Deflections for Girders.

BS-1 were found. Two cracks which did not belong to any type, were observed.

2) All of the cracks observed in the test panels are Type BM-1, which can be said to be a crack proper to thin-walled deep plate girders.

3) The cracks initiated outside the test panels are Type BM-1 or Type BS-1.

4) A decrease of flexural rigidity of the girder due to an initiation of Type BM-1 cracks in the test panels, do not have any distinct influences upon variations of strain in the flange and of deflection at the span center, as seen in Figs. 13 and 14, respectively.

(2) Lateral deflections of web and their influence on initiation of cracks Type BM-1

Since $b/t = 250$ and 300 are rather large and $t = 3.2$ mm is relatively so small, the maximum values of observed initial deflections of the web which are $0.62\ t \sim 1.9\ t$, are larger than those for the static test girders. The vertical distribution of initial web deflections at a section in the test panels consist of a double or triple curvature.

Configurations and amounts of the lateral deflections during loading are governed greatly by the state of initial deflections. With repetitions of loads, in general, the configuration of initial deflection moves upward and the deflections in the compression part of the web increase, while those in the tension part of the web decrease, with an increase of number of cycles. The web with a distribution of initial deflections in a single or double curvature showed larger lateral deflections, and in the case of triple curvature it showed smaller ones. It has been generally observed just before the initiation of cracks Type BM-1 that the lateral deflection increased almost linearly with the repetition of loads.

Although large lateral deflections were observed in the tension part of web, these did not result in the initiation of crack Type BM-1, and after all the lateral deflections of part of web very near the compression flange have had a greater influence upon the initiation of Type BM-1, as seen in Fig. 15. This fact

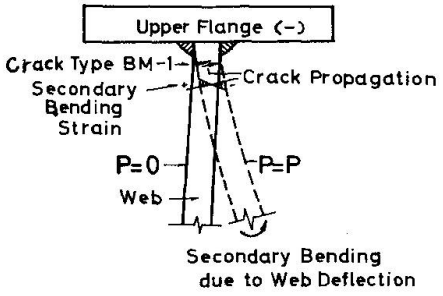

Fig. 15. Initiation of Crack Type BM-1 due to Secondary Bending of Web.

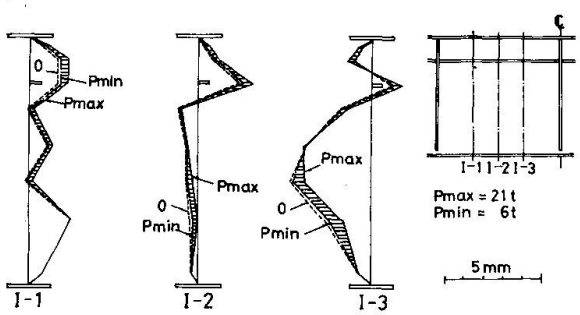

Fig. 17. Lateral Deflections of Web of Girder F-5.

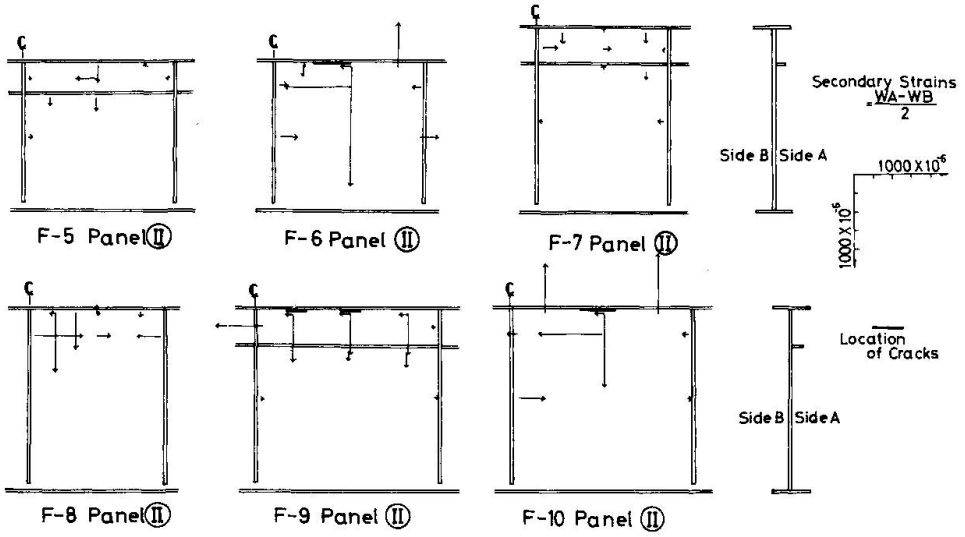

Fig. 16. Secondary Bending Strains due to Web Deflections.

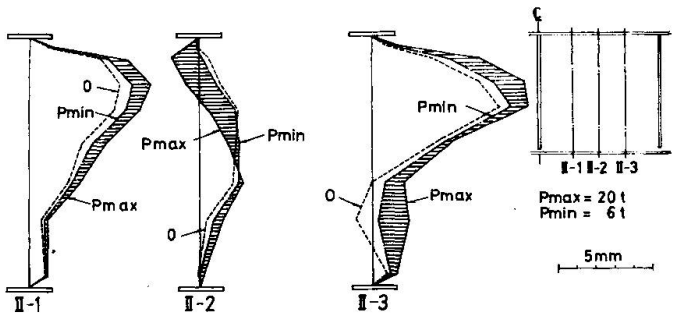

Fig. 18. Lateral Deflections of Web of Girder F-6.

was also shown by the report of Yen and Mueller [8] that there would be a certain interaction between secondary stresses at web boundaries due to the lateral deflection and the number of cycles of loads at the time of crack initiation.

At the present study, the interaction is not recognized clearly because of rather small numbers of measurement points for web strains near possible locations of the crack initiation, but Fig. 16 shows that the secondary bending strains due to web deflections influence greatly on the crack initiation. Fig. 17 and Fig. 18 show the lateral deflection of web at zero number of cycles of loads for the girders F-5 and F-6, respectively. Fig. 19 indicates variation of web deflections at zero and 150 x 10^4 numbers of cycles of loads for the girder F-3.

(3) Effects of slenderness ratio, aspect ratio and longitudinal stiffeners

1) Effect of slenderness ratio of web b/t.

As mentioned before, all of the cracks found in the region of pure bending including the test panels, are of Type BM-1. The relation of crack numbers with

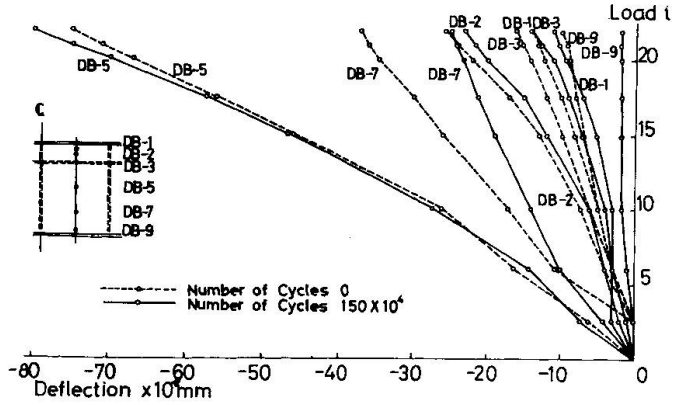

Fig. 19. Variation of Web Deflections for Girder F-3.

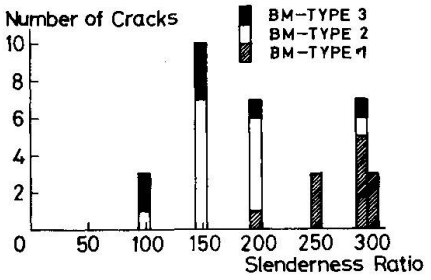

Fig. 20. Number of Cracks versus Slenderness Ratios.

Table 8. Effects of b/t, a/b and Longitudinal Stiffener

Test Girder	F-A	F-B	F-1	F-2	F-3	F-4	F-5	F-6
b/t	250				300			
a/b	0.5	0.5	1.0	1.0	0.75	0.75	1.0	1.0
Longi. Stiffener	1	1	1	0	1	0	1	0
No. of Cracks	0	0	0	3	0	2	5	3
No. of Cycles at Discovery of 1st Crack ($x10^4$)	-	-	-	40.5	-	56.6	54.6	12.7

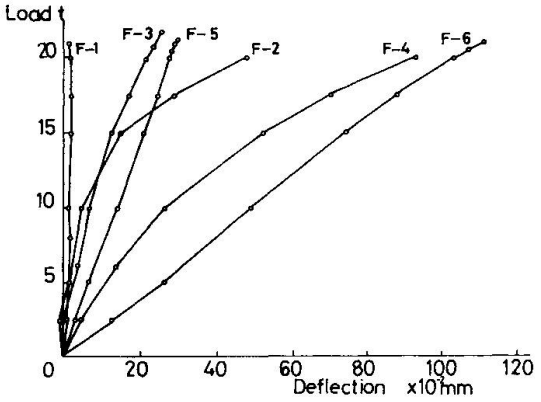

Fig. 21. Web Deflections versus Loads.

slenderness ratio for each type of cracks is illustrated in Fig. 20, from the test results obtained at the author's past and present studies and Toprac's studies[9),10)], in which the test data are limited to those of the girders with no longitudinal stiffener and with aspect ratio a/b of 1.0, because they are intended to know the effects of only slenderness ratio. It will be evident from Fig. 20 that the cracks Type BM-1 ocuurs for girders with the slenderness ratio larger than about 200.

2) Effects of aspect ratio a/b and longitudinal stiffener.

By comparing web deflections of Girders F-1,-3 and -5, with those of Girders F-2, -4 and -6, respectively, it will be noticed that a longitudinal stiffener in the test panel is very effective on restraining the web deflections near the compression flange, which have a close relation with the initiation of cracks. Similarly, by comparing web deflections of Girders F-3 and F-4 with those of Girders F-5 and F-6, respectively, it can be said that a smaller aspect ratio restrains the web deflections. Fig. 21 illustrates variation of web deflections at the point of 0.1 b from the upper edge of web in the test panel for the girders.

The effect of aspect ratio and longitudinal stiffener will be seen clearly in restraining from the secondary bending strains of web as indicated in Fig. 16, and in reducing the flexural compressive strains in the flange. Girders F-5, however, shows rather large web deflections and secondary bending strains, because the rigidity of its longitudinal stiffeners seem to be relatively smaller. It is shown in Table 8 including the author's previous study results on Girder F-A and F-B, that the aspect ratio and longitudinal stiffeners are related closely with the number of cracks Type BM-1. With the same reason as mentioned above, the number of cracks at F-5 is rather larger. In Girders F-2, -4 and -6, the cracks were found on the both side of web, but those in F-5 did not propagate to the back side

through the web, because of stiffening by the longitudinal stiffeners.

IV. CONCLUSIONS

When the test panels stiffened by transverse and / or longitudinal stiffeners of thin-walled deep plate girders, are subjected to static pure bending or dynamic repeated pure bending, the behavior of web and its influence on the ultimate strength or on the initiation of fatigue cracks have been examined at the present experimental study. The test results will be concluded as follows:

(1) The test girders which have some hybrid features, showed a similar static behavior to non-hybrid girders, except a rather fast progress of collapse toward their ultimate strength.

(2) The linear buckling could not be observed due to initial deflections of web, but, with 0.3 t~1.6 t in the maximum, they do not seem to have influenced greatly upon the overall ultimate collapse load. In the fatigue tests, however, they influence greatly on the initiation of fatigue cracks Type BM-1 due to the lateral deflections of web in cyclic loadings. The cracks Type BM-1 will be initiated for a plate girder larger than 200 in its web slenderness ratio.

(3) The single, double-sided or one-sided longitudinal stiffener welded to transverse stiffeners influence greatly on a decrease of lateral deflections of web, patterns of stress distribution over a cross section and an increase of ultimate strength, while it will be subjected to a compressive force. The fatigue tests revealed that it would be possible to prevent the cracks Type BM-1 by providing with longitudinal stiffener, together with a smaller aspect ratio. Rigidities of the longitudinal stiffener were selected to be 3.65~4.72 for the static tests and 3.83~5.30 for the fatigue tests in terms of relative flexural rigidity γ / γ^*, and a larger ultimate strength, possibly a full-plastic strength could be achieved and an improved fatigue behavior toward prevention of cracks Type BM-1, with a greater rigidity of the longitudinal stiffeners, will be expected.

(4) For the girders stiffened by a longitudinal stiffener, the reduction of effective width at the ultimate load was observed remarkably in case of b/t = 250 and 300, followed by redistribution of web stresses to the compression flange and to the longitudinal stiffeners, where the effective width reduced to 29~43 % of the total depth of web.

(5) For the longitudinally stiffened girders, Y - shaped compression flanges are more effective than T - shaped flanges in terms of ultimate load, and the former's failure will be governed by lateral buckling and the latter's failure by lateral and/ or torsional buckling. The given width versus thickness ratio of the compression flange did not prevent it from local buckling in plastic range of the stress in the compression flange.

The further experimental studies on large - size hybrid plate girders stiffened by longitudinally stiffeners are being carried out at Osaka University, to obtain more informations for the design of thin-walled deep plate girders.

References

1) Y. Maeda and Y. Kubo, "Experimental Study on Ultimate Strength of Longitudinally Stiffened Plate Girders in Bending", 23rd Annual Conference of Japan Society of Civil Engineers, Oct. 1968 (in Japanese).

2) K. Basler and B. Thürlimann, "Strength of Plate Girders in Bending", Proc. ASCE, ST 6, 1961.

3) H. S. Lew and A. A. Toprac, "Static Strength of Hybrid Plate Girders", S. F. R. L. Tech. Rept. P550 - 11, The University of Texas, Jan. 1968.

4) G. Haaijer and B. Thürlimann, "On Inelastic Buckling in Steel", Proc. ASCE, EM 2, 1958.

5) American Welding Society, "Article 407. Dimensional Tolerances", Specifications for Welded Highway and Railway Bridges, 1966.

6) A. A. Toprac, "Fatigue Strength of Full-Size Hybrid Girders", Proc. AISC National Eng. Conference, 1963.

7) T. R. Gurney, "Investigation into the Fatigue Strength of Welded Beams", Part III, British Welding J., Sept. 1962.

8) B. T. Yen and J. A. Mueller, "Fatigue Tests of Large-Size Welded Plate Girders", Welding Research Council, Bulletin 118, Nov. 1966.

9) H. S. Lew and A. A. Toprac, "Fatigue Tests of Welded Hybrid Plate Girders under Constant Moment", Research Rept. No. 77-2F, Center for Highway Research, The Univ. of Texas, Austin, Jan. 1967.

10) Y. Kurobane, D. J. Fielding and A. A. Toprac, "Additional Fatigue Tests of Hybrid Plate Girders under Pure Bending Moment", Res. Rept. No. 96-1F, Center for Highway Research, The Univ. of Texas, Austin, May, 1967.

II

Effect of Initial Distortions on the Carrying Capacity of Welded I-Girders

L'influence des déformations initiales sur la résistance à la ruine des poutres en I soudées

Der Einfluss anfänglicher Verformungen auf die Traglast geschweisster I-Träger

S.V. OSSIPOV
Moscow, UdSSR

The welded I-girders are in common use in all the areas of structural steel construction. The theoretical assumptions of the current technique for both analysis and design of such girders suppose any idealized cross section with absolutely regular geometrical contours.

In practice, however, there are always existing some distortions in the theoretical geometry of a girder and their causes are very different.

In the first place such a cause may lie in welding stresses of the metal as a result of high local heating due to welding and plastic compressive deformations arising in the weld sone.

In the fight against unfavourable effects of deformations due to welding there are provided both constructive and industrial measures. One of industrial measures is the straightening of an article after welding, i.e. its plastic straining by thermal or mechanical action. The straightening process has also to be used for structures with local distortions due to imperfections in relled plates or shock in the course of transportation and erection.

The straightening process itself, either mechanical or thermal, leads inevitably to the initiation of residual stresses and changes in mechanical properties of the metal.

The amount of straightening depends in large part on the specified tolerance on the steel members.

Local distortions in the web of girders are the least studied type of total and local residual deformatione.

The importance of problem to throw light on the actual behaviour of a girder with initial web distortions is governed by the practical

need to define the tolerances on the fabrication of plate girders to avoid a great deal of work in straightening rolled plates and articles at the shop.

The allowable value of initial web buckling is principally defined by its effect extent on the carrying capacity with respect the local stability of a girder, i.e. with respect to such limit state in which a structure loses its capability to resist external effects or receives residual deformations which do not permit any possibility of further service.

To assess the effect of initial distortions in the web of welded I - girders and define the values of corrections for critical stresses of ideally plane plates, it is used an analysis procedure proposed by Dr. B.M. Broude (1) and based on the linear bending theory of plates and non-linear bending theory of low-curvature shells.

There are two modes of buckling to be distinguished, namely : the first mode which is possible only in case of ideal geometrical, physical and static conditions and the second mode, in such systems where under some conditions such load redistribution is possible that its resultant will be well above the critical load resultant.

The second-mode buckling occurs in all cases in which there are existing initial deviations from the exact geometrical shape or some eccentricities in the application of forces.

From the second-mode critical state definition itself as a reached maximum load condition it follows that a post-critical stage does not take place, i.e. the critical load is a limit quantity. Loss of web carrying capacity is the upper boundary of a limit state considered as a service stopping condition.

The behaviour of a thin-walled plate I-girder under load may be reproduced as that of a truss with flexible diagonals between posts-stiffeners.

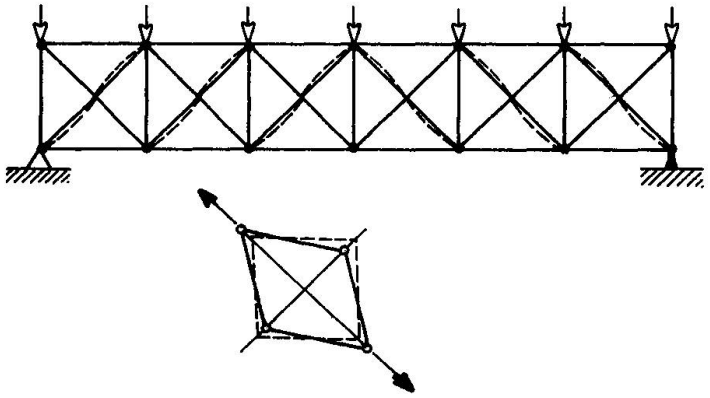

The diagonals in compression are buckled under load and only diagonals in tension are working.

Under these conditions the significance of chords and stiffeners is particularly increased.

The limit state with respect to strength in the thin-walled I-girders occurs when the stress in the most stressed diagonals in tension becomes equal to the yield point.

Given initial distortions, the thin web of a girder, incapable of bending resistance, will again function only in tension. In addition to that the web bands in tension shall at first become straight (to compensate initial buckling).

As the plate thickness increases, the diagonals in compression will resist the straightening of diagonals in tension. In this case the additional tensile stresses (membrane stresses) will start to develop in the diagonals in tension. The plate will function in the same manner as a low-curvature shell and some initial buckling will cause no additional deformations of a girder.
As the thickness of a increases, a difference between the values of critical loads with respect to web local stability and those of ultimate carrying capacity with respect to strength of web diagonals in tension will decrease.

The initial distortions may be divided into two modes which are as follows :

(a) The plate is bent over a cylindrical surface and subjected to compression along the generatrix; in this case the buckling mode remains the same as in the ideal plane plate.

(b) The plate has an initial distortion with either full or partial invariability of a contour; in addition to that a growth of deflections takes place from the very beginning of loading up to the critical state development.

Just the second mode of initial distortions is of the most interest when considering the behaviour of plate I-girders.

The restraining conditions of plate edges in the plane of its contour are of great importance for estimating the critical load. If the edges of a rectangular plate may be freely deformed under loading conditions, the initial distortion reduces always the critical load as compared to the case of a plane plate.

If the loaded edges of a plate can move only in the translation motion form when remaining rectilinear, the critical load may be either increased or decreased in terms of the design plate depth-to-thickness ratio and initial deflection rise.

To study the first case the linear bending theory of plates may be used. In the second case the middle plane extensibility shall be considered. To accomplish this the mathematical means of the non-linear bending theory of low-curvature shells shall be applied. This is particularly essential for the relatively thin plates or in case of large initial deflection rises.

If a critical plate stress σ_o is not over the proportional limit and the ratio of an initial deflection rise f_o to a plate thickness :

$$\left(\frac{f_o}{\tau} \leq 0,3\right)$$

is not over 0,3, the linear bending theory of plates shall be used. In the case where these conditions are exceeded the non-linear bending theory of low-curvature shells shall be applied.

This criterion is also applicable to other states of stress (pure bending, load on the upper edge of a web).

The ratio $\frac{\sigma}{\sigma_o}$ where σ is the maximum normal stress and σ_o is the critical stress, is used as a figure of a state of stress.

As the initial deflection rise increases, the $\frac{\sigma}{\sigma_o}$ value for a given plate depth-to-thickness ratio at first decreases and next increases.

The ratio $\frac{\sigma}{\sigma_o}$ in thin plates may exceed the unity.

Since the crane girder operation conditions do not permit to consider the web edge to which a load is applied as nondeformable, the initial web distortion effect shall be defined by the methods of the linear bending theory of plates.

The girders carrying the nodal or static load may be permitted to have considerably greater web deformations as compared to those of crane girders and here the effect of initial distortions shall be considered in accordance with the second case conditions by using the non-linear bending theory of low-curvature shells.

The studies carried out in conformity with the above mentioned statements permit to formulate the following recommendations :

(a) The initial distortion effect on the stability of a web may be taken into account by the use of a special coefficient w which is introduced into the plate stability equation together with the simultaneous action of a moment as well as lateral and compressive forces :

$$\sqrt{\left(\frac{\sigma}{\sigma_o} + \frac{\rho}{\rho_o}\right)^2 + \left(\frac{\tau}{\tau_o}\right)^2 + \frac{1}{6} \cdot \frac{\tau}{\tau_o} \cdot \frac{\sigma}{\sigma_o}} \leq m_o w$$

where

σ, τ, ρ – normal, tangential and local compressive stress, respectively;

σ_o, τ_o, ρ_o – critical normal, tangential and local compressive stress, respectively;

m_o – rated coefficient of work conditions;

w – coefficient of critical stress reduction for account of initial distortions of a plate.

(b) The average w = 0,9 is permitted to be accepted for crane girders and similar structures, the top chord of which is subjected to a direct effect of movable load.

(c) w = 1 is permitted to be accepted for girders where the load is applied only at the location points of transverse stiffeners.

The above mentioned principles of theoretical definition of the initial web distortion effect were used as a basis of an analysis technique for designing a steel-reinforced concrete superstructure with welded plate girders of I-section (3).

A girder portion between transverse stiffeners was treated as a flexible rectangular plate having an initial distortion and rigid external contour.

For the maximum approximation of a design scheme to the actual structure it was imperative to introduce trigonometrical as well as hyperbolic - and - trigonometrical infinite series into the stress function along with biharmonic polynomial terms.

In accordance with the requirements of variational methods a made of both initial and additional distortions was prescribed in the form of trigonometrical functions of two variables.

The analysis of behaviour of a girder at the two stages was carried out according to a single procedure, but with appropriate variations in the geometrical properties of a section, actual forces and initial distortion amount. The distortion amount for the second stage was determined as a sum of initial and additional distortions at the first stage (prior to the introduction of a slab into work in conjunction with girders).

At the first stage of loading in a girder (prior to the introduction of the reinforced concrete slab into work) a web portion is under eccentric compression conditions, while at the second stage the web is subjected to eccentric tension when loading the gipder.

The analysis has shown that the local stability in the studie panel at the first stage of girder work may be provided only with due regard for fixing the web in the chords. An initial web distortion is a cause of development of additional stresses in a structure and particularly in the cross sections of a girder.

If the average stresses for a panel in the chords are known, it is possible to estimate the reducing correction coefficients for the design values of both cross section area and moment of inertia of a girder for a given initial distortion of its web and given load. As the initial distortion increases, these coefficients decrease.

The initial distortion effect is more essential to the axial deformability of girders.

The available technique provides for a possibility to take into account the deformed web effect on the state of stress and deformations in a girder with vertical stiffeners. For analysis goals one must know the actual forces, size of a structure and initial distortion outline in the panel.

The carried out studies have shown that the Standard allowed initial distortions of the web of welded bridge girders are not dangerous for the carrying capacity of a structure.

An experimental study of the initial web buckling effect on the carrying capacity with respect to both local stability and strength in the welded bridge I-girders made of low alloy steel "15XCHD" and provided with transverse stiffeners was carried out at the All-Union Research Institute of Transport Construction (2).

The experimental girders having overall sizes corresponding to actual values were loaded by successive steps, at first by 10- ton steps and next a step intensity was decreased to 3 to 5 tons up to the maximum load.

It is important to note, however, that in this case the experimental load was applied through the stiffeners and this was not in full accord with conventional work conditions of girders.

A comparison of obtained experimental critical load values for girders with different deflection rises has shown that these loads for girders with larger distortions were no lower, but even higher than those for girders with lesser distortions. These data allowed to draw a conclusion that the existence of initial web distortions up to 0,024 times the web depth did not reduce a critical load with respect to local stability.

An examination of variations in web buckling rise values at the centre of tested girder portions in terms of load increments has shown that some existence of initial distortions does not increase the web buckling intensity and even somewhat decreases it.

It was also found that initial distortions do not worsen the state of stress in both web chords of a girder.

On the basis of these studies and also generalization of statistical data on deflection rise values in initial web distortions of fabricated girders, the current Standards for fabrication of bridge superstructure plate girders accept the allowable buckling rise as equal to 0,006 times the web depth, i.e. twice the tolerance accepted in the earlier Standards.

The experimental studies of the behaviour under load in case of welded I-section crane girders with initial web distortions have shown a somewhat other picture (4).

Unlike the bridge plate girders where live load forces are transferred to the girders through a rigid reinforced concrete slab of roadway or ballast bed and a unit pressure transferred to the girder is relatively small, the crane girders are subjected to the direct effect of a concentrated movable dynamic load which is transferred through crane rails. Any eventual eccentricities of crane load application, caused by imperfections in the position of rails and lateral effects of crane wheels, have also a significant influence upon the state of stress in girders.

In addition to that there are arised bending-and-torsional deformations which result in both yielding and loss of carrying capacity of a girder.

The experimental studies of crane girders have shown that the existence of initial distortions above a certain value increases deformations, predestines a point of failure and, hence, reduces the service ability of girders. The decisive buckling has initiated just at the panels with a deformed web.

The theoretical analyses performed by the method put forward by Dr. B.M. Broude (1) have defined the allowable deflection rise value of initial distortions in a welded I-section crane girder as equal to 0,003 times the web depth. This tolerance was accepted in the current Structural Standards.

Present-day in our country no comprehensive data are available on all the aspects of behaviour of a girder with initial distortions under complicated loading conditions.

The experimental studies of girders under dynamic load action will give rather important corrections to our conceptions of the behaviour of girders with initial distortions.

Such studies of the 11.0 m - span welded I-girder 1.5m high with vertical stiffeners are being carried out at present.

The experimental girder is subjected to the pulsating load with the constant amplitude of vibrations.

Resistance wire-strain gauges are placed at the points of the most probable initiation of fatigue cracks due to "breathing" of the web, at the bottom portions of panels near stiffeners.

It is proposed to subject the girder to the effect of pulsating load with 2-million cycles.

The experimental data on the normal stress maximum-to-minimum ratios $(\frac{\sigma \text{ max}}{\sigma \text{ min}})$ will permit to evaluate the effect of initial web distortion on the carrying capacity of a girder with respect to its endurance.

To summarize the above mentioned statements the conclusions to be drawn are as follows :

(a) A rated value of the allowable deflection rise of initial web distortions in crane girders is confirmed by both theoretical and experimental studies;

(b) It would be sound practice to check this characteristic for the girders of bridge superstructures by means of testing under non-nodal (non only above the stiffeners) load application conditions;

(c) Experimental studies of the behaviour of girders under dynamic loads will permit to evaluate the effect of initial web

distortions on the carrying capacity of a girder with respect to its endurance and substantially complement our conception of the behaviour of girders with initial distortions under diverse conditions of both loading and state of stress.

SUMMARY

The methods of the linear bending theory of plates and non-linear bending theory of low-curvature shells, accepted as the basis of analysis, permitted to prove the rated values of allowable deflection rises of initial distortions in welded I-girders. Experimental studies under static load have confirmed these data for crane girders and defined those more exactly for plate girders of bridge superstructures.

Nowadays, an experimental study of the behaviour of I-girders with initial distortions is being carried out under dynamic load conditions.

II

The Ultimate Bending Moment for Plate Girders

Moment de flexion limite des poutres à âme pleine

Biegetragfähigkeit von Blechträgern

PETER B. COOPER
Department of Civil Engineering
Kansas State University
Manhattan, Kansas, USA

INTRODUCTION

The purpose of this report is to review some aspects of previously developed methods for estimating the ultimate bending moment for plate girders, to examine the applicability of these methods in predicting the bending strength of test girders and to suggest some areas where additional research would be appropriate. Limited in scope to homogeneous, symmetrical girders which are statically loaded in pure bending, the report considers longitudinally stiffened as well as transversely stiffened girders.

REVIEW OF BASLER AND THURLIMANN'S THEORY

The basic concepts used in evaluating the bending strength of plate girders were presented by Basler and Thurlimann in 1961 [1]. It was first established from ultimate load tests on plate girders subjected to pure bending that, when the applied moment exceeds the moment associated with web buckling, a redistribution of stress from the compressed portion of the web to the compression flange occurs. As a consequence of this stress redistribution, the bending strength of a girder is limited by the strength of the compression flange acting with a portion of the web as a column. Three compression flange column buckling modes were considered: torsional (local) buckling, lateral buckling and vertical buckling. As a further consequence of the stress redistribution, the ultimate bending moment must be reduced from the value calculated on the basis of a linear stress distribution.

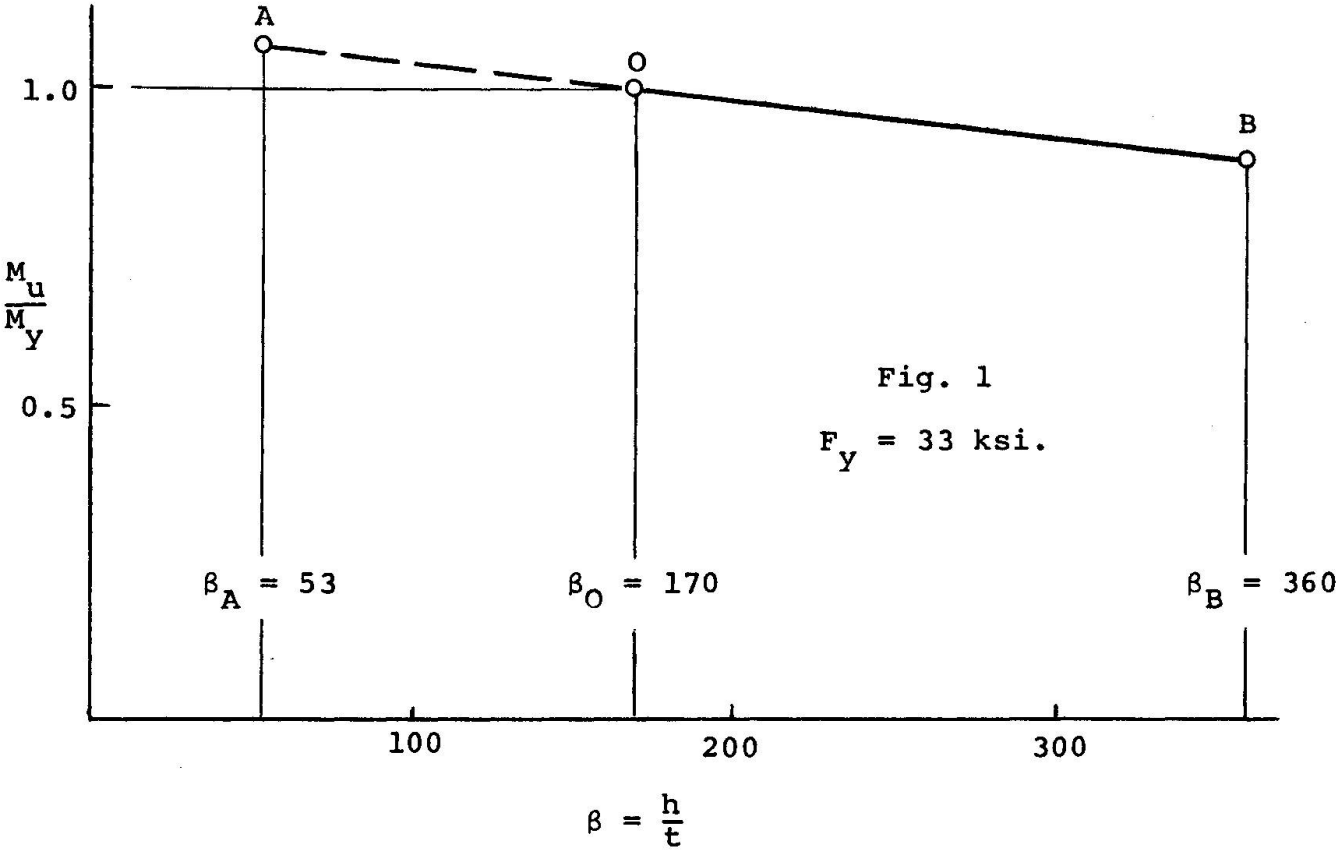

Fig. 1

F_y = 33 ksi.

The essential features of Basler and Thurlimann's development of an equation for the ultimate bending moment, which accounts for stress redistribution, can be described with the assistance of Fig. 1, where the ordinate is the ratio of the ultimate moment to the moment required to initiate flange yielding, M_u/M_y, and the abscissa is the web slenderness ratio, $\beta = h/t$. β_A is the highest slenderness ratio for which the full plastic moment M_p can be attained, and was taken to be 53 for F_y = 33 ksi. β_o is the slenderness ratio at which web buckling would occur when the applied moment reaches M_y. Assuming partial flange restraint, $\beta_o = 5.7/\sqrt{F_y/E}$, which gives β_o = 170 for F_y = 33 ksi. At the maximum slenderness ratio permitted by a vertical buckling analysis, β_B (β_B = 360 for F_y = 33 ksi.), it was assumed that the effective section to resist bending consists of the portion on the tension side of the neutral axis plus the compression flange acting with an effective width of the web equal to 30t. Values of M_u/M_y at β_A and β_B depend on the ratio of the area of the web to the area of one flange, A_w/A_f. Since a curve passing through points A, 0 and B is essentially a straight line, the following equation for the ultimate bending moment was adopted:

$$\frac{M_u}{M_y} = 1 - 0.0005 \frac{A_w}{A_f}\left(\beta - \frac{5.7}{\sqrt{F_y/E}}\right). \quad (1)$$

The influence of local or lateral buckling of the compression flange on the ultimate bending moment was incorporated in Eq. 1 by including the lower value of M_{cr}/M_y obtained from separate local and lateral buckling analyses,

$$\frac{M_u}{M_y} = \frac{M_{cr}}{M_y}\left\{1 - 0.0005 \frac{A_w}{A_f}\left[\beta - \frac{5.7}{\sqrt{\frac{M_{cr}}{M_y} \cdot \frac{F_y}{E}}}\right]\right\} \quad (2)$$

The numerical values of β_A, β_o and β_B used in the development of Eq. 1 could each be modified based on more recent research findings. Research in plastic design has demonstrated that, in the absence of axial force, M_p can be attained in members with β - values substantially higher than β_A. The AISC specification[2], for example, permits the use of members having $\beta \leq 412/\sqrt{F_y}$ ($\beta \leq 72$ for $F_y = 33$ ksi.) in plastically designed structures. At least one investigator[3] has suggested that the flanges provide full fixity to the web of a welded plate girder. If full fixity is assumed, a slight increase in β_o to $6.0/\sqrt{F_y/E}$ (180 for $F_y = 33$ ksi.) would result. Experimental results cited later in this report indicate that plate girders with web slenderness ratios considerably in excess of β_B can be used without suffering premature vertical buckling of the compression flange.

In spite of these possible modifications to the values of β_A, β_o and β_B used in developing the equation for ultimate bending moment, it has been shown that Eq. 2, when used in conjunction with appropriate local and lateral buckling equations, provides a good prediction of the observed bending strength of full size test girders.[1] Furthermore, it will be shown in the following sections that there is good reason to believe that Eq. 2 could be adopted for girders with web slenderness ratios outside the range originally proposed by Basler and Thurlimann.

GIRDERS WITH LOW WEB SLENDERNESS RATIOS

Basler and Thurlimann recommended that Eq. 2 be applied only when $\beta > \beta_o$; thus for girders with $\beta < \beta_o$, $M_u = M_{cr}$. For $F_y = 36$ ksi., this corresponds

to $\beta \leq 162$. However, in a recently completed series of tests on eight A36 steel girders with web slenderness ratios between 61 and 123, all girders reached M_p before failure.[4] These results suggest that it would be reasonable, and probably conservative, to apply Eq. 2 in the range $\beta_A < \beta < \beta_o$, so that for girders with stocky webs, the calculated ultimate moment could exceed M_y. Before this extension of Eq. 5 could be permitted, it would be necessary to develop more severe local and lateral buckling requirements. The development of such requirements would be a worthwhile objective for new analytical and experimental research.

GIRDERS WITH HIGH WEB SLENDERNESS RATIOS

Based on the previously mentioned vertical buckling analysis, β_B was originally intended to be the upper limit of the allowable web slenderness ratio for plate girders without longitudinal stiffeners. Accordingly, β_B also served as the upper limit of the range of applicability of Eq. 2. The results of three tests are available to investigate the possibility of using Eq. 2 to predict the bending strength of girders having $\beta > \beta_B$. The three specimens were fabricated from A36 steel or the equivalent, and had web slenderness ratios ranging from 388 to 751. The test results are summarized below.

Ref.	Test	β	$\frac{M_{cr}}{M_y}$	% Red.	$\frac{M_u^{ex}}{M_u^{th}}$
5	G4-T2	388	1.00	8.0	1.03
6	LBI	444	0.99	10.7	1.00
7	TTGO	751	0.98	24.4	1.01

For two of the tests, M_{cr} is slightly less than M_y according to the lateral buckling equation[1], but in all tests, the compression flange width-thickness ratio was low enough to preclude premature local buckling. The reduction in M_{cr}/M_y, given by the second term in the brackets of Eq. 2, ranged from 8.0% to 24.4%. Each of the specimens reached the ultimate moment as a result of general yielding of the compression flange, and in tests

G4-T2 and TGO, the tests were continued beyond the ultimate load until vertical buckling of the compression flange into the web occurred. Since the experimentally observed ultimate moments M_u^{ex} were very close to the predicted values M_u^{th} based on Eq. 2, these tests indicate that Eq. 2 provides a good estimate of the bending strength of plate girders with web slenderness ratios higher than β_B.

LONGITUDINALLY STIFFENED GIRDERS

Ultimate load tests on longitudinally stiffened plate girders have indicated that longitudinal stiffeners can contribute to the bending strength by controlling lateral web deflections in the compressed portion of the web, thereby eliminating the need for the reduction in the ultimate moment represented by the second term in the brackets of Eq. 2.[8] That is, properly positioned and proportioned longitudinal stiffeners can, by controlling lateral web deflections, prevent the stress redistribution discussed previously. The increase in bending strength due to the use of longitudinal stiffeners will therefore increase with the web slenderness ratio, and will only be significant for girders with very high web slenderness ratios.

It has been suggested that longitudinal stiffeners should be located at the optimum position to increase the web buckling load.[8] For a single stiffener, a distance between the compression flange and the stiffener equal to one-fifth of the web depth has been commonly adopted. Three longitudinal stiffener proportioning requirements have been proposed for girders having a stiffener at the one-fifth depth position:

(a) a maximum stiffener width-thickness ratio to prevent premature local buckling (for stiffeners having a rectangular cross section);

(b) a minimum stiffener moment of inertia to force a nodal line in the deflected web up to the theoretical web buckling load; and

(c) a minimum slenderness ratio to ensure adequate longitudinal stiffener column strength up to the ultimate moment.

For computing the stiffener moment of inertia and radius of gyration for requirements (b) and (c), a section consisting of the stiffener acting with an effective width at the web equal to 20t has been suggested. Since a longitudinal stiffener, in controlling lateral web deflections, will subject the transverse stiffeners to concentrated forces, a requirement for the minimum transverse stiffener section modulus has also been formulated.

When all of the longitudinal and transverse stiffener proportioning requirements have been satisfied, the ultimate bending moment will be

$$\frac{M_u}{M_y} = \frac{M_{cr}}{M_y} \tag{3}$$

If the stiffener requirements are not satisfied, a longitudinal stiffener may still increase M_u/M_y above the value given by Eq. 2. However, no method has been developed to evaluate the magnitude of this increase; therefore, it is conservatively suggested that the influence of a longitudinal stiffener be ignored if the stiffener proportioning requirements are not satisfied.

The results of four tests, summarized below, are available to check the usefulness of Eq. 3 in estimating the bending strength of longitudinally stiffened plate girders.

Ref.	Test	β	$\frac{M_{cr}}{M_y}$	% Red.	$\frac{M_u^{ex}}{M_u^{th}}$
9	D	299	0.76	17.2[a]	1.00
9	3	300	0.89	16.4[a]	1.02
8	LB6	407	0.99	13.7[a]	0.96
7	TG4-1	751	0.98	24.4[a]	0.96

[a] reduction not applied in calculating M_u^{th}

Constructed of structural carbon steel, each of the test specimens had a single longitudinal stiffener at the one-fifth depth position. All of the previously described stiffener requirements were satisfied in each test. Lateral buckling controlled M_{cr}/M_y, and in each case the actual length between bracing points was used in the calculations. The percent reductions shown in the table were not used in computing the predicted ultimate moments, but are listed to indicate the increase in bending strength achieved through the use of a longitudinal stiffener. The agreement between test results and predicted ultimate moments based on Eq. 3 is close enough to provide some confidence in the theory.

It would be logical to expect that, as the web slenderness ratio is increased, a point will eventually be reached where two or more longitudinal stiffeners are needed in the compression region to adequately control web deflections and prevent stress redistribution to the compression flange. Very little research on the bending strength of girders with multiple longitudinal stiffeners has been conducted to date, although some ultimate load tests have been carried out on girders having two longitudinal stiffeners.[7,9] The initial objectives of research on this topic should include the determination of the web slenderness ratio above which two longitudinal stiffeners are required to prevent stress redistribution and the development of positioning and proportioning requirements for the stiffeners.

LIST OF SYMBOLS

h clear depth of web plate

t web thickness

A_w area of web

A_f area of one flange

E modulus of elasticity

F_y yield stress

M_{cr} moment at which compression flange buckling occurs

M_p plastic moment

M_u ultimate moment

M_y yield moment

M_u^{ex} experimentally measured ultimate moment

M_u^{th} theoretical ultimate moment

β web slenderness ratio ($\beta = h/t$)

REFERENCES

1. Basler, K. and Thurlimann, B., "Strength of Plate Girders in Bending", Journal of the Structural Division, ASCE, Vol. 87, No. ST6, Aug., 1961.

2. American Institute of Steel Construction, Specification for the Design, Fabrication and Erection of Structural Steel for Buildings, New York, 1969.

3. Chern, C., "Ultimate Strength of Transversely and Longitudinally Stiffened Plate Girders", Fritz Engineering Laboratory Report No. 328.11, Lehigh University, Aug., 1969.

4. Della Croce, A., "The Strength of Continuous Girders with Unstiffened Webs", Report No. 2, AISI Project No. 157, The University of Texas at Austin, Jan., 1970.

5. Basler, K., Yen, B. T., Mueller, J. A. and Thurlimann, B., "Web Buckling Tests on Welded Plate Girders", Bulletin 64, Welding Research Council, Sept., 1960.

6. D'Apice, M. A., Fielding, D. J. and Cooper, P. B., "Static Tests on Longitudinally Stiffened Plate Girders", Bulletin 117, Welding Research Council, Oct., 1966.

7. Owen, D. R. J., Rockey, K. C. and Skaloud, M., "Behavior of Longitudinally Reinforced Plate Girders", Final Report, 8th Congress, International Association for Bridge and Structural Engineering, Sept., 1968.

8. Cooper, P. B., "Strength of Longitudinally Stiffened Plate Girders", Journal of the Structural Division, ASCE, Vol. 93, No. ST2, April, 1967.

9. Longbottom, E. and Heyman, J., "Experimental Verification of the Strengths of Plate Girders Designed in Accordance with the Revised British Standard 153: Tests on Full Size and Model Plate Girders", Proceedings, Institution of Civil Engineers, Vol. 5, Part III, 1956.

SUMMARY

Basler and Thurlimann's bending strength theory for unstiffened and transversely stiffened plate girders is reviewed and discussed. Based on the available test results, the application of the theory to girders with web slenderness ratios considerably higher than the originally proposed upper limit is suggested. A bending strength theory for longitudinally stiffened plate girders is also reviewed and compared with test results. Finally, several research topics related to plate girder bending strength are suggested.

RESUME

L'auteur discute la théorie de Basler-Thürlimann concernant la résistance à la ruine des poutres à âme pleine fléchies, non raidies ou raidies transversalement. Les résultats expérimentaux disponibles permettent de proposer une extension de la théorie à des poutres dont les âmes sont considérablement plus élancées que la limite supérieure indiquée à l'origine. De plus, on présente une théorie pour la résistance à la ruine des poutres à âme pleine fléchies, munies de raidisseurs longitudinaux, et on la compare aux résultats expérimentaux. Enfin, divers sujets apparentés sont suggérés en vue de recherches additionnelles.

ZUSAMMENFASSUNG

Die Theorie von Basler-Thürlimann über die Tragfähigkeit von auf Biegung beanspruchten, unversteiften oder querversteiften Blechträgern wird zusammengefasst und besprochen. Auf Grund der vorhandenen Versuchsergebnisse wird eine Anwendung der Theorie auf Träger mit wesentlich über der ursprünglichen Schlankheitsgrenze liegenden Stegschlankheiten vorgeschlagen. Ferner wird eine Theorie der Tragfähigkeit von längsversteiften, auf Biegung beanspruchten Blechträgern dargestellt und mit Versuchsergebnissen verglichen. Schliesslich werden weitere Forschungsthemen auf dem gleichen Gebiet vorgeschlagen.

Leere Seite
Blank page
Page vide

II

Ultimate Strength of Longitudinally Stiffened Plate Girders under Combined Loads

Résistance à la ruine des poutres à âme pleine cisaillées et fléchies, munies de raidisseurs longitudinaux

Traglast längsversteifter Blechträger unter Biegung und Querkraft

A. OSTAPENKO
Professor of Civil Engrg.
Lehigh University
Bethlehem, Pa., USA

C. CHERN
Assistant Prof. of Civil Engrg.
North Dakota State University
Fargo, N.D., USA

1. INTRODUCTION

Recognition of the fact that the web of plate girders possesses considerable post-buckling capacity led to research on their ultimate strength. Plate girders with transverse stiffeners (1) as well as girders with transverse and longitudinal stiffeners (5) were investigated. However, essentially all of this research dealt with symmetrical girders, that is, the centroidal axis was at the mid-depth. Since many plate girders are unsymmetrical, the authors developed a new ultimate strength method first for transversely stiffened girders (2,3,4,8). Then the method was extended to longitudinally stiffened girders (7). Besides handling unsymmetrical girders, this new theory gave not only the shear or bending strength, but also a continuous determination of the girder strength under any combination of shear and moment (7). Presented here is a brief description of the method and a comparison with some test results.

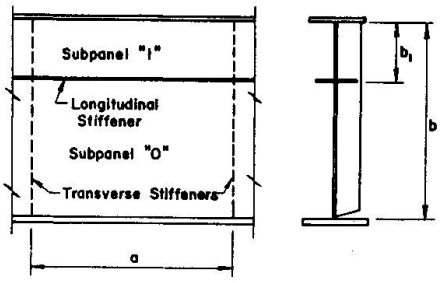

Figure 1

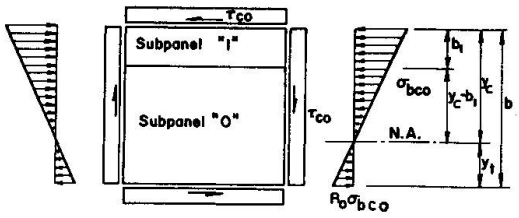

Figure 2

A plate girder panel subdivided by the longitudinal stiffener into two subpanels, subpanels "1" and "0", is shown in Fig. 1. The narrow subpanel "1" is subjected to shear and a linearly varying compression stress as shown in Fig. 2. The other subpanel (subpanel "0") is under shear and a normal stress varying linearly from compression to tension.

Deformation of a plate subpanel under shear is linear up to the point of buckling (γ_c). The shear in excess of the buckling value will be carried by the tension field action of the web (2). The shear strain at the

instant of reaching the ultimate load can be approximated by assuming that it corresponds to tensile yielding along the panel diagonal.

$$\gamma_u = \frac{\sigma_{yw}}{E} \left(\alpha + \frac{1}{\alpha}\right) \tag{1}$$

After this, the shear strain is assumed to increase at a constant average shear stress. For simplicity, the transition from the buckling strain to the ultimate strain may be assumed to be linear.

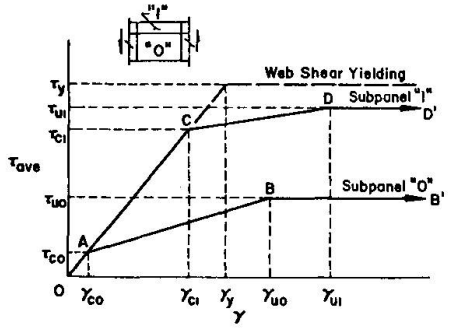

Figure 3

Consideration of the buckling and ultimate shear strains for each subpanel individually and the requirement of compatibility that the shear deformations in both subpanels be equal provide a means of defining the shear-deformation response of the whole web panel. The panel behaves like a beam until subpanel "0" reaches its buckling stress τ_{co}, indicated by point A in Fig. 3. From then on, subpanel "0" develops tension field action which produces a more rapid shear deformation as illustrated by line AB. Subpanel "1" remains flat and continues behaving linearly until it reaches its buckling stress at point C. Subpanel "0" has not yet attained its ultimate strength since the compatibility relationship of the subpanels indicates that $\gamma_{c1} < \gamma_{uo}$. After subpanel "1" buckles, the subpanels develop their ultimate strengths individually. The web shear forces at each stage of loading are obtained by multiplying the corresponding average shear stresses by the respective web subpanel areas.

When in addition to shear, bending stresses are acting on the subpanels as shown in Fig. 2, the web deformation pattern is analogous to that shown in Fig. 3, except that the critical buckling stresses τ_{co} and τ_{c1} are computed for a combined state of stress rather than for pure shear. It is assumed that the moment in excess of the moment which causes buckling of a subpanel web is carried only by the flanges, lontiduinal stiffener, and the unbuckled subpanel.

Stresses and forces that develop in the flanges and the longitudinal stiffener in the course of the deformation of the web panel may cause failure in one of them, thus precipitating failure of the whole panel. The following modes of failure may be possible: (a) shear failure of the web plate, (b) buckling or yielding of the compression flange, or (c) yielding of the tension flange. Failure of the longitudinal stiffener by lateral or torsional buckling may precede (a), (b) and (c), but it will usually only reduce rather than limit the panel capacity by changing the panel in effect from a longitudinally stiffened to a transversely stiffened one.

The applicable mode is determined by calculating the stresses in the flanges and the longitudinal stiffener at each significant loading level and checking them against the critical stresses. This way a continuous interaction curve is obtained.

A girder panel subjected to a particular combination of shear and moment is visualized to be a panel in a girder shown in Fig. 4a. The moment at the mid-panel is then defined in terms of the shear span ratio.

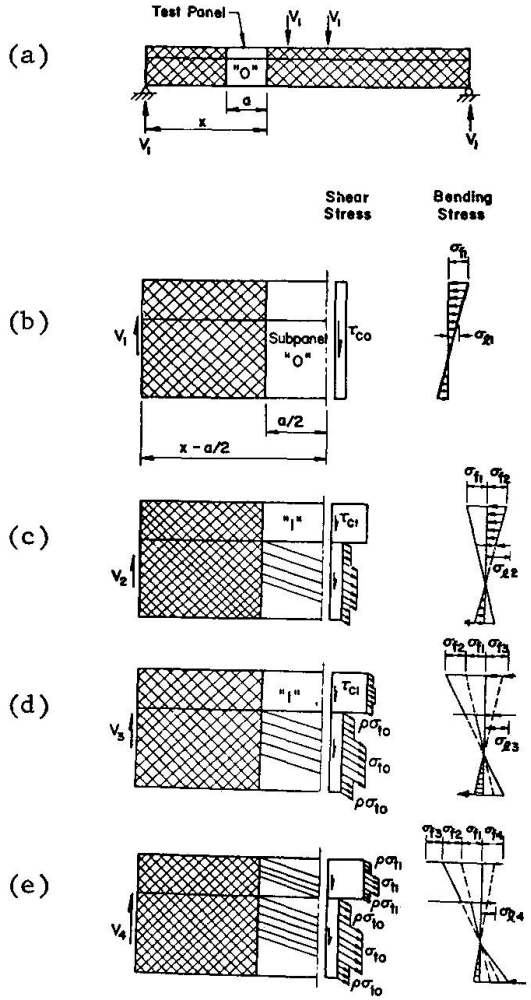

Figure 4

$$\mu = \frac{M}{bV} = \frac{x - a/2}{b} \tag{2a}$$

that is,
$$M = \mu\, bV \tag{2b}$$

2. REFERENCE STRESSES

Stresses in the flanges, stiffener, and the web subpanels are developed at various levels of loading by different mechanisms involving pre-buckling, post-buckling, and post-ultimate behavior of the individual panel components. The stresses at the transition from one mechanism to another are the reference stresses which provide a means of determining the mode of panel failure and the ultimate load.

Stresses at the Load Causing Buckling of Subpanel "0" - When subpanel "0" reaches the buckling stress τ_{co}, the total panel shearing force V_1 (Fig. 4b) is given by

$$V_1 = \tau_{co}\, A_w \tag{3}$$

where $A_w = bt$ = panel web area.

The stress at the web-to-longitudinal stiffener junction, $\sigma_{b_{co}}$, and at the bottom flange, $R_o\sigma_{b_{co}}$, can be obtained from the ordinary beam equations as a function of V_1 and thus of τ_{co} (see Fig. 2).

With this information, τ_{co} is computed from the following interaction equation of a plate subjected to a combination of shear and bending stresses (6).

$$\left(\frac{\tau_{co}}{\tau_{cro}}\right)^2 + \frac{1 + R_o}{2}\left(\frac{\sigma_{bco}}{\sigma_{cpo}}\right) + \frac{1 - R_o}{2}\left(\frac{\sigma_{bco}}{\sigma_{cpo}}\right)^2 = 1.0 \tag{4}$$

in which the buckling stresses for pure shear, τ_{cro}, and for pure bending, σ_{cpo}, are computed from

$$\tau_{cro} = k_{vo}\, \sigma_e \tag{5a}$$

$$\sigma_{cpo} = k_{bo}\, \sigma_e \tag{5b}$$

where $\sigma_e = [(\pi^2 E)/(12\,(1-\nu^2))]/\beta_o^2$.

The buckling coefficients k_{vo} and k_{bo} for a web plate assumed to be fixed at the horizontal edges and pinned at the vertical edges may be obtained from (4,7)

$$k_{vo} = \frac{5.34}{\alpha_o^2} + \frac{6.55}{\alpha_o} - 13.71 + 14.10\,\alpha_o \text{ , for } \alpha_o < 1.0 \tag{6a}$$

or

$$k_{vo} = 8.98 + \frac{6.18}{\alpha_o^2} - \frac{2.88}{\alpha_o^3}, \quad \text{for} \quad \alpha_o \geq 1.0 \tag{6b}$$

and

$$k_{bo} = 13.54 - 15.64\, R_o + 13.32\, R_o^2 + 3.38\, R_o^3 \tag{7}$$

where R_o is the ratio of the maximum tensile stress (or minimum compressive stress) to the maximum compressive stress for subpanel "0" under combined loads as shown in Fig. 2, and α_o and β_o are, respectively, the aspect ratio, $(a)/(b-b_1)$, and the slenderness ratio, $(b-b_1)/t$, of subpanel "0".

With τ_{co} thus computed, the buckling strength contributed by subpanel "0" alone is

$$V_{\tau o} = \tau_{co}\, A_{wo} \tag{8}$$

where $A_{wo} = (b-b_1)t$ is the web area of subpanel "0".

As shown in Fig. 4b, the stresses in the compression flange and in the longitudinal stiffener are, respectively,

$$\sigma_{f1} = \frac{V_1\, \mu b}{I}\, y_c \tag{9a}$$

and

$$\sigma_{\ell 1} = \frac{V_1\, \mu b}{I}\, (y_c - b_1) \tag{9b}$$

Stresses at the Load Causing Buckling of Subpanel "1" - Following the procedure described above for panel "0", the buckling shear of subpanel "1" is

$$V_{\tau 1} = \tau_{c1}\, A_{w1} \tag{10}$$

When $V_{\tau 1}$ is reached, the shear force carried by the whole panel web is

$$V_2 = V_{\tau o} + V_{\tau 1} + V_{\sigma o} \left(\frac{\gamma_{c1} - \gamma_{co}}{\gamma_{uo} - \gamma_{co}} \right) \tag{11}$$

where $V_{\sigma o}$ is the shear strength of subpanel "0" when the tension field action is fully developed (Eq. (14)), $\gamma_{co} = \tau_{co}/G$ and $\gamma_{c1} = \tau_{c1}/G$ are the strains of subpanels "0" and "1" corresponding to the web buckling stresses τ_{co} and τ_{c1} and γ_{uo} is the approximate shear strain when subpanel "0" reaches its ultimate load (it is obtained from Eq. (1) by substituting α_o for α).

The increments of stresses for the interval of the panel shear from V_1 to V_2 are, as shown in Fig. 4c

$$\sigma_{f2} = \frac{(V_2 - V_1)\, \mu b}{I}\, y_c \tag{12a}$$

and

$$\sigma_{\ell 2} = \frac{(V_2 - V_1)\, \mu b}{I}\, (y_c - b_1) + \frac{H_o'}{2A_{\ell s}} \tag{12b}$$

where

$$H'_o = V_{\sigma o}\left(\frac{\gamma_{c1} - \gamma_{co}}{\gamma_{uo} - \gamma_{co}}\right) \cot \varphi_{co} \tag{13}$$

is the horizontal component of the tension field force of subpanel "0" which must be carried by the longitudinal stiffener in addition to the stress contributed by the bending moment.

Stresses at the Load Developing the Post-Buckling Strength of Subpanel "0" - The stress distribution for this stage is shown in Fig. 4d. The strain condition is indicated in Fig. 3 by γ_{uo} and the tension field action of subpanel "1" has formed only partially.

The full tension field action contribution of subpanel "0" to the shear strength is given by

$$V_{\sigma o} = \frac{1}{2}\sigma_{to} A_{wo}\left[\sin 2\varphi_{co} - (1-\rho)\alpha_o + (1-\rho)\alpha_o \cos 2\varphi_{co}\right] \tag{14}$$

with σ_{to} from

$$\sigma_{to} = \sigma_{yw}\left(D_o + \sqrt{1 + B_o - C_o^2 + D_o^2}\right) \tag{15}$$

where

$$B_o = 3\sqrt{C_o^2 + (\tau_{co}/\sigma_{yw})^2} \tag{16a}$$

$$C_o = -0.25\, R_o\, (\sigma_{bco}/\sigma_{yw}) \tag{16b}$$

$$D_o = -0.5\left\{B_o \sin\left[\tan^{-1}(C_o\, \sigma_{yw}/\tau_{co}) + 2\varphi_{co}\right] + C_o\right\} \tag{16c}$$

φ_{co} is the optimum inclination of the tension field of subpanel "0" under combined loads*.

The shear carried by the whole panel web is thus

$$V_3 = V_{\tau o} + V_{\sigma o} + V_{\tau 1} + V_{\sigma 1}\left(\frac{\gamma_{uo} - \gamma_{c1}}{\gamma_{u1} - \gamma_{c1}}\right) \tag{17}$$

where $V_{\sigma 1}$ is the contribution of the fully developed tension field of subpanel "1" to the shear strength (Eq. (19)).

The additional stresses in the compression flange and longitudinal stiffener are indicated in Fig. 4d. They are, respectively,

$$\sigma_{f3} = \frac{(V_3 - V_2)\,\mu b}{I} y_c + \frac{H'_1}{2A_{fc}} \tag{18a}$$

and

$$\sigma_{\ell 3} = \frac{(V_3 - V_2)\,\mu b\,(y_c - b_1)}{I} + \frac{H'_1 + H''_o}{2A_{\ell s}} \tag{18b}$$

---

*φ_{co} is determined by optimizing $V_{\sigma o}$ (4).

where

$$H_o'' = V_{\sigma o} \left(\frac{\gamma_{uo} - \gamma_{c1}}{\gamma_{uo} - \gamma_{co}}\right) \cot \varphi_{co} \tag{18c}$$

and

$$H_1' = V_{\sigma 1} \left(\frac{\gamma_{uo} - \gamma_{c1}}{\gamma_{u1} - \gamma_{c1}}\right) \cot \varphi_{c} \tag{18d}$$

Stresses at the Load Developing the Post-Buckling Strength of Subpanel "1" - The tension field action contribution of subpanel "1", analogously to Eq. (14) is

$$V_{\sigma 1} = \frac{1}{2} \sigma_{t1} A_{w1} [\sin 2\varphi_{c1} - (1-\rho) \alpha_1 + (1-\rho) \alpha_1 \cos 2\varphi_{c1}] \tag{19}$$

with

$$\sigma_{t1} = \sigma_{yw} \left(D_1 + \sqrt{1 + B_1 - C_1^2 + D_1^2} \right) \tag{20}$$

where subscript "1" denotes subpanel "1". The only variable, which is different from those in Eq. (15) is

$$C_1 = 0.25 \left(\frac{y_c - b_1}{y_c}\right) \left(\frac{\sigma_{f1} + \sigma_{f2}}{\sigma_{yw}}\right) \tag{21}$$

The web strengths of both subpanels are now fully developed and the total shear is

$$V_4 = V_{\tau o} + V_{\sigma o} + V_{\tau 1} + V_{\sigma 1} \tag{22}$$

The resultant increases in the compression flange stress and the longitudinal stiffener stress are (Fig. 4e)

$$\sigma_{f4} = \frac{(V_4 - V_3)\ \mu b}{I}\ y_c + \frac{H_1''}{2A_{fc}} \tag{23a}$$

and

$$\sigma_{\ell 4} = \frac{(V_4 - V_3)\ \mu b}{I}\ (y_c - b_1) + \frac{H_1''}{2A_{\ell s}} \tag{23b}$$

where

$$H_1'' = V_{\sigma 1} \left(\frac{\gamma_{u1} - \gamma_{uo}}{\gamma_{u1} - \gamma_{c1}}\right) \cot \varphi_{c1} \tag{23c}$$

The first terms of Eqs. (23a) and (23b) are due to the bending produced by the increase in the shear force from V_3 to V_4 and the second terms are the reactions to the horizontal component of the tension field force in subpanel "1".

Stresses Due to Frame Action - The shear carrying capacity contributed by the flanges and the longitudinal stiffener is evaluated by considering a frame consisting of the flanges and the longitudinal stiffener of a typical panel as shown in Fig. 5a. It is assumed that the neighboring panels provide sufficient restraint so that the flanges and longitudinal stiffener will resist shear by the formation of plastic hinges at both ends.

The shearing force V_f, contributed by the resulting plastic mechanism, is

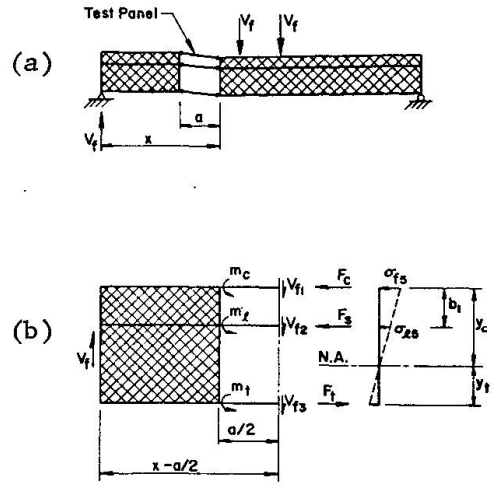

Figure 5

$$V_f = \frac{2}{a} (m_c + m_\ell + m_t) \tag{24}$$

The plastic moments m_c, m_ℓ and m_t are computed considering the axial forces and are assumed to be equal at both ends of a member.

The additional normal stresses in the flanges and stiffener are assumed to be proportional to the distance from the centroid of the girder cross section*. Moment equilibrium gives then

$$\sigma_{f5} = \frac{\mu V_f}{A_{fc} + A_{\ell s} \left(1 - \frac{b_1}{y_c}\right) \left(1 - \frac{b_1}{b}\right)} \tag{25a}$$

$$\sigma_{\ell 5} = \sigma_{f5} \left(1 - \frac{b_1}{y_c}\right) \tag{25b}$$

Critical Stresses of the Compression Flange and Longitudinal Stiffener - These critical stresses are obtained as the buckling stresses of the pin-ended columns formed by the compression flange and the longitudinal stiffener, σ_{cf} and $\sigma_{c\ell}$, respectively (1,3,5). The lateral and torsional buckling equations** given for the compression flange in Ref. 3 (Eqs. (13) and (14)) or Ref. 5 are used here also for the longitudinal stiffener with the following slenderness parameters ($\lambda = \sqrt{\sigma_y/\sigma_{cr}}$) for lateral and torsion buckling, respectively:

$$\lambda_\ell = a \sqrt{\frac{\epsilon_{ys} A_{\ell s} + 20t^2}{\pi^2 I_{\ell s}}} \tag{26a}$$

$$\lambda_t = \frac{c_s}{d_s} \sqrt{\frac{12 (1 - \nu^2) \epsilon_{ys}}{\pi^2 k_t}} \tag{26b}$$

where $k_t = 0.425$.

When the stiffener is one-sided, its critical stress $\sigma_{c\ell}$ should be obtained as that of an eccentrically loaded beam-column.

Summary of Reference Stresses - The total normal stresses introduced into the compression flange and the longitudinal stiffener are, respectively,

$$\sigma_{fs} = \sigma_{f1} + \sigma_{f2} + \sigma_{f3} + \sigma_{f4} + \sigma_{f5} \tag{27a}$$

and

$$\sigma_{\ell s} = \sigma_{\ell 1} + \sigma_{\ell 2} + \sigma_{\ell 3} + \sigma_{\ell 4} + \sigma_{\ell 5} \tag{27b}$$

*This assumption violates horizontal equilibrium, but the resultant inaccuracy is insignificant.

**Ordinary column and plate buckling equations may be used as well.

The capacities of the flange and stiffener are given by the critical stresses σ_{cf} and $\sigma_{c\ell}$, respectively.

3. ULTIMATE STRENGTH

Web or Compression Flange Failure - Depending on the relative magnitudes of the moment and shear, the capacity of a plate girder panel will usually be limited by the failure of the web plate or buckling of the compression flange. A continuous plot of the ultimate combinations of shear and moment is shown in Fig. 6.

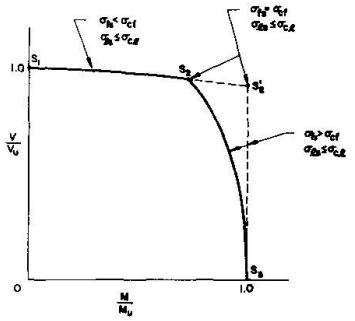

Figure 6

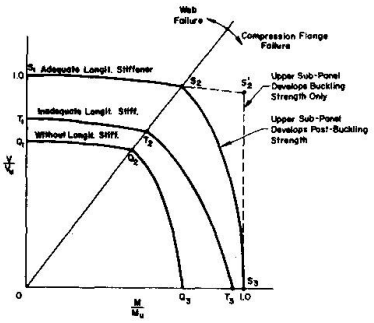

Figure 7

The failure of the web plate is typical for combinations of high shear and low moment as indicated by curve S_1-S_2 in Fig. 6. The total stresses in the flange and the longitudinal stiffener are below their critical values ($\sigma_{sf} < \sigma_{cf}$ and $\sigma_{s\ell} \leq \sigma_{c\ell}$). The subpanel webs buckle and develop their individual post-buckling strengths. With the concurrent formation of the frame action mechanism, the shear strength of the panel is then reached and is thus given by the sum of the shears from Eqs. (22) and (24)

$$V_{th} = V_4 + V_f = V_{\tau o} + V_{\sigma o} + V_{\tau 1} + V_{\sigma 1} + V_f \tag{28a}$$

The corresponding mid-panel moment is

$$M_{th} = V_{th}\, \mu b \tag{28b}$$

When the panel is subjected to a high moment, the subpanel webs will not be able to develop their full capacities before the stress in the compression flange reaches its buckling stress. The portion of the interaction curve in Fig. 6 for this case is S_2-S_3. The capacity of the panel will be given by the contribution of the web subpanels developed up to this point and a portion of the frame action. For simplicity it is assumed that the frame action shear develops in proportion to the growth of the web shear as the panel strain increases.

$$V_{th} = V_w \left(1 + \frac{V_f}{V_4}\right) \tag{29}$$

where V_w is equal to V_1, V_2, V_3, V_4 or some intermediate value corresponding to the following flange stress produced by the web forces, that is, excluding the frame action:

$$\sigma_{fw} = \frac{\sigma_{cf}}{1 + [\sigma_{f5}/(\sigma_{f1} + \sigma_{f2} + \sigma_{f3} \mp \sigma_{f4})]} \tag{30}$$

Very often the aspect ratio of subpanel "1" is greater than 3.0 and it is recommended to neglect its post-buckling strength (2,4). Then, the compression flange stress will be due to the moment only, and the interaction curve in Fig. 6 will be S_1-S_2' and S_2'-S_3. With the maximum moment capacity of the panel being

$$M_{th} = \sigma_{cf} \frac{I}{y_c} \tag{31a}$$

the shear force for S_2'-S_3 is

$$V_{th} = M_{th}/\mu b \tag{31b}$$

Tension Flange Yielding - The total stress in the tension flange due to various effects is indicated in Figs. 4b to 4e and 5b. It should not be greater than the yield stress of the flange.

Maximum Moment in Panel - Since under combined loads the moment at one end of the panel is greater than the mid-panel moment, this maximum panel moment may control the panel strength. The shear producing the maximum panel moment may not exceed

$$V_{th}' \leq \frac{M_u}{b\ (\mu + \frac{1}{2}\alpha)} \left(\frac{\sigma_{yc}}{\sigma_{cf}}\right) \tag{32}$$

A seemingly reasonable and sufficiently accurate approach, mostly on the safe side, is to keep the maximum panel moment below the moment which would produce yielding in the tension or compression flange according to the ordinary beam theory.

Panels with Inadequate Longitudinal Stiffener - When the longitudinal stiffener, subjected to the compressive force due to the panel moment and the horizontal components of the tension field forces, buckles before the panel develops its strength, the ultimate capacity of the panel will be reached in a different manner. The true failure mechanism in this case is too complicated to be analyzed at present. However, two limits of the ultimate strength are suggested here: (a) the panel develops its ultimate strength as if it had no longitudinal stiffener -- the interaction diagram is indicated by curve Q_1-Q_2-Q_3 in Fig. 7; or (b) the strength attained at the point when the longitudinal stiffener column fails -- this case is given by curve T_1-T_2-T_3 in Fig. 7. One or the other limit will give a higher value which is then to be taken as the ultimate load.

For limit (a), the ultimate strength is determined by setting b_1 and all properties of the longitudinal stiffener equal to zero, thus, leaving only the web and the flanges for computations.

For limit (b), the shear strength is given by

$$V_{th} = V_{\tau o} + V_{\sigma o}' + V_{\tau 1} + V_{\sigma 1}' + V_f \tag{33}$$

where $V_{\sigma o}'$ and $V_{\sigma 1}'$ are the incomplete tension field shears.

$$V'_{\sigma o} = \frac{2\,A_{\ell s}\left[\sigma_{c\ell} - \sigma_{\ell 5} - \frac{(V_{\tau o} + V_{\tau 1} + V'_{\sigma 1})\,\mu b}{I}(y_c - b_1)\right] - V'_{\sigma 1}\cot\varphi_{c1}}{2\,\frac{A_{\ell s}\,\mu b}{I}(y_c - b_1) + \cot\varphi_{co}} \qquad (34)$$

When the aspect ratio of subpanel "1" is greater than 3.0, as is the case for majority of plate girders, $V'_{\sigma 1}$ should be set equal to zero.

4. COMPARISON WITH TEST RESULTS

The ratio of the experimental to theoretical load is shown for twenty test results in Fig. 8. Fourteen tests on symmetrical girders are from Refs. 5 and 10 as indicated by the numbers on the dimension line in the figure. The

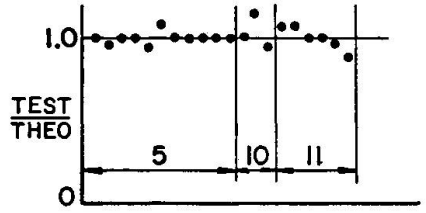

Figure 8

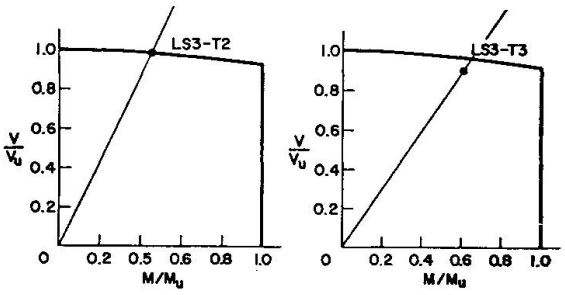

Figure 9

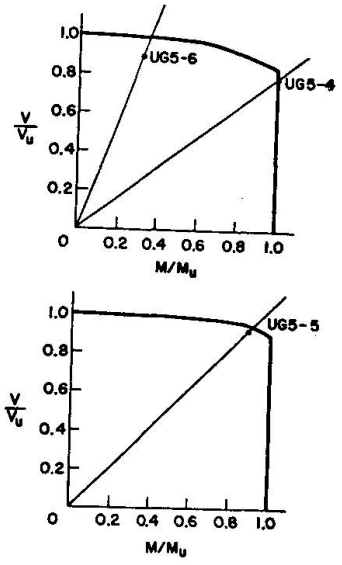

Figure 10

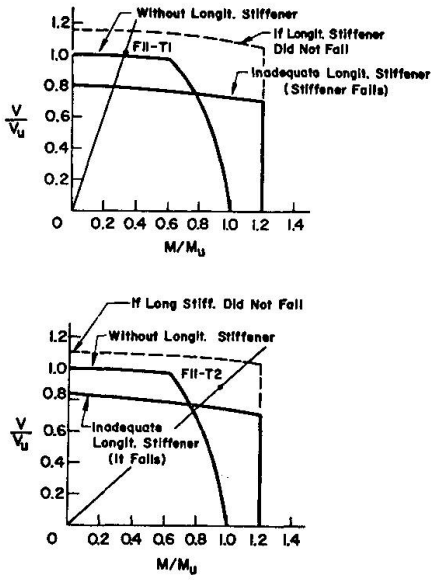

Figure 11

remaining six tests are on unsymmetrical girders from Ref. 11. The average deviation is 4%. The maximum deviation of 14% is for a panel with an inadequate longitudinal stiffener (Test F11-T2 in Fig. 11).

Interaction diagrams for two symmetrical test panels from Ref. 5 are given in Fig. 9. Three unsymmetrical panels from Ref. 11 are shown in Fig. 10. Panels UG5-6 and UG5-4 (the top sketch) were identical but were subjected to different combinations of shear and moment.

Tests on two panels with inadequate longitudinal stiffeners (Ref. 10) are compared with the proposed criteria in Fig. 11. F11-T1 is under dominant shear and its strength is essentially equal to that of a panel without the longitudinal stiffener. F11-T2 falls into the area where the two criteria have discontinuity and tend to give a too conservative prediction due to the non-utilization of the post-buckling contribution of the longitudinal stiffener.

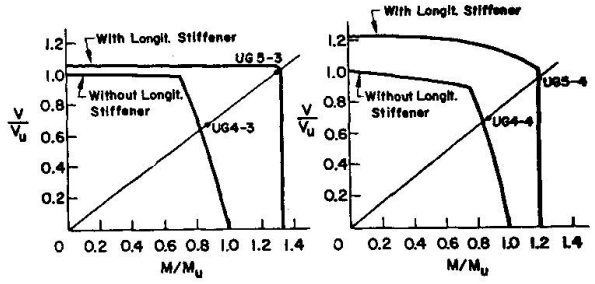

Figure 12

Two pairs of panels, one with and the other without a longitudinal stiffener, are compared in Fig. 12 (from Ref. 11). In all four panels, the capacity was limited by the strength of the compression flange. For the range of high shear and high moment, the interaction diagrams indicate a dramatic increase of the panel strength (about 44%) when the longitudinal stiffener is introduced into the panel.

5. CONCLUDING REMARKS

The following conclusions can be drawn from this investigation:

1) The interaction curve between moment and shear consists of two portions: web failure which occurs under dominant shear and flange failure which occurs under dominant moment.

2) The panel strength for the web failure mode may be computed as a sum of the shear strengths of the individual web subpanels (buckling and post-buckling strengths) and the capacity of the plastic mechanism formed by the flanges and longitudinal stiffener (frame action).

3) The force in a flange for the flange failure mode has contributions from the bending moment and a component of the force due to a partially developed tension field.

4) When the longitudinal stiffener is inadequate, the failure load may be conservatively assumed to be the higher one of the following: (a) the ultimate strength of the panel as if it had no longitudinal stiffener or (b) the strength developed by the panel at the point when the longitudinal stiffener column fails.

5) A comparison of the theory with the results of twenty tests gives an average correlation of 4%. Thus, the presented theory provides a reliable

means of determining the static ultimate strength of longitudinally stiffened steel plate girder panels subjected to shear, bending, or a combination of shear and bending.

6) In application, the method requires some iterative operations and, thus, is not readily suitable for manual calculations. However, the numerical computer output of a program based on the method can be used to develop simple design formulas. Such a development was very successful for transversely stiffened plate girders (9).

Among many aspects of the behavior of longitudinally stiffened plate girders which need further investigation are the following:

1) Tests on composite girders are needed to check whether the proposed approach is applicable to them since the concrete slab acting together with the top girder flange may make a greater contribution to the girder strength than given by the frame action.

2) More work is needed to establish design criteria for transverse stiffeners.

REFERENCES.

1. Basler, K., and Thürlimann, B., "Strength of Plate Girders in Bending", J. ASCE, Vol. 87 (ST6), Aug. 1961.

2. Chern, C., and Ostapenko, A., "Ultimate Strength of Plate Girders under Shear", Fritz Engrg. Lab. Rept. No. 328.7, Lehigh Univ., Aug. 1969.

3. Chern, C., and Ostapenko, A., "Bending Strength of Unsymmetrical Plate Girders", Fritz Engrg. Lab. Rept. No. 328.8, Lehigh Univ., Sept. 1970.

4. Chern, C., and Ostapenko, A., "Unsymmetrical Plate Girders under Shear and Moment", Fritz Engrg. Lab. Rept. No. 328.9, Lehigh Univ., Oct. 1970.

5. Cooper, P. B., "Strength of Longitudinally Stiffened Plate Girders", J. ASCE, Vol. 93 (ST2), Apr. 1967.

6. Kollbrunner, C. F., and Meister, M., "Ausbeulen", Springer-Verlag, Berlin, 1958.

7. Ostapenko, A. and Chern, C., "Strength of Longitudinally Stiffened Plate Girders", Fritz Engrg. Lab. Rept. No. 328.10, Lehigh Univ., Dec. 1970.

8. Ostapenko, A., Yen, B. T., and Beedle, L. S., "Research on Plate Girders at Lehigh University", Final Report, 8th IABSE Congress held in New York, Sept. 1968, IABSE, Zurich.

9. Ostapenko, A., Chern, C., and Parsanejad, S., "Ultimate Strength Design of Plate Girders", Proc. of the Conference on Developments in Bridge Design and Construction, held in Cardiff, Apr. 1971. To be published by Crosby Lockwood & Son, Ltd., London, Nov. 1971.

10. Patterson, P. J., Corrado, J. A., Huang, J. S., and Yen, B. T., "Fatigue and Static Tests on Two Welded Plate Girders", WRC Bulletin 155, New York, Oct. 1970.

11. Schueller, W., and Ostapenko, A., "Tests on a Transversely Stiffened and on a Longitudinally Stiffened Unsymmetrical Plate Girder", WRC Bulletin 156, New York, Nov. 1970.

NOTATION

In general, subscripts "1" and "0" refer to subpanels "1" and "0", respectively. Subscript "y" means yielding, "u" - ultimate, "f" - compression flange, "w" - web. Definition is given here only for the symbols which are not in common usage and are not defined in the text or in the figures.

A_{fc} area of the compression flange

$A_{\ell s}$ area of the longitudinal stiffener = $2c_s \times d_s$ for a two-sided stiffener

$I_{\ell s}$ moment of inertia of the longitudinal stiffener about the vertical axis of the girder cross section

c_s width of the longitudinal stiffener on each side

d_s thickness of the longitudinal stiffener

ε_{ys} yield strain of the longitudinal stiffener

ρ averaging coefficient of the tension field stress in the elastic triangular portions; it is assumed to be equal to 0.5 for ordinary welded steel girders

φ_c optimum inclination of the tension field force in a panel under combined loads

SUMMARY

The static ultimate strength of longitudinally stiffened plate girder panels subjected to any combination of shear and bending is determined for symmetrical, unsymmetrical, homogeneous and hybrid girders. The panel strength is obtained as a sum of the ultimate strengths of the two web subpanels and of a frame formed by the flanges and the longitudinal stiffener. The average deviation of the theory from test results is 4%.

RESUME

Les auteurs déterminent la charge de ruine statique des poutres à âme pleine munies de raidisseurs longitudinaux, soumises à une combinaison quelconque de flexion et de cisaillement; la méthode s'applique aux poutres symétriques, asymétriques, homogènes et hybrides. La charge de ruine d'un panneau se compose de la résistance limite des deux sous-panneaux d'âme et de celle du cadre formé par les membrures et le raidisseur longitudinal. La différence moyenne entre la théorie et les essais atteint 4 %.

ZUSAMMENFASSUNG

Die Traglast statisch belasteter längsversteifter Blechträger unter Biegung und Querkraft wird bestimmt. Die Methode ist für symmetrische und unsymmetrische Träger anwendbar, die aus einer oder mehreren Stahlgüten zusammengeschweisst sein können. Die Gesamttraglast setzt sich aus den Tragfähigkeiten der zwei von der Längssteife gebildeten Stegfeldern und des aus den Flanschen und der Längssteife geformten Rahmens zusammen. Die durchschnittliche Abweichung der theoretischen Ergebnisse von den experimentellen beträgt 4%.

Leere Seite
Blank page
Page vide